1-1-2011

New insights into the mechanism of dna replication on unmodified and benzo[a]pyrene modified templates using surface plasmon resonance

Richard George Federley
Wayne State University,

NEW INSIGHTS INTO THE MECHANISM OF DNA REPLICATION ON UNMODIFIED AND BENZO[A]PYRENE-MODIFIED TEMPLATES USING SURFACE PLASMON RESONANCE

by

RICHARD G. FEDERLEY

DISSERTATION

Submitted to the Graduate School

of Wayne State University,

Detroit, Michigan

in partial fulfillment of the requirements

for the degree of

DOCTOR OF PHILOSOPHY

2011

MAJOR: CHEMISTRY (Biochemistry)

Approved By:

_____

Advisor Date

_____

_____

_____

DEDICATION

This work is dedicated to those that helped me to succeed throughout my education; in particular my Mother and Father, Sisters, and most of all my Wife.

ACKNOWLEDGEMENTS

There are many whom guided me throughout this undertaking, but foremost I must thank Dr. Louis J. Romano, who provided me all the tools, support, friendship, and advice required to become a scientist. Dr. Romano provided me intellectual freedom to pursue my own ideas, and provided an excellent atmosphere where my thoughts could be expressed freely and were welcomed with great appreciation. I have greatly enjoyed working in his lab, and I will forever be thankful for the wonderful experience he has provided. In addition, my committee members; Dr. Christine Chow, Dr. Peter Andreana, and Dr. Phillip Cunningham, have provided excellent questions and support during this project.

A large amount of appreciation and gratitude also goes to the members of the Romano Lab, both past and present. Radoslaw Markiewicz has been a wonderful friend, and we have shared many insightful discussions. Kyle Vrtis has accompanied me on some interesting adventures such as scuba diving, which helped to relinquish thoughts of laboratory experiments gone sour. Ashley Floyd has been a good friend and we have told many tales. Also, the past lab members Dr. Thomas Christian, Dr. Alexandra Gorgevska, Dr. Venkataramana Vooradi, Dr. Asad Ullah, Dr. Jessica Back, Dr. Jeanne Deslich and Dr. Joshua Gill helped to instruct me in several protocols, and provided me with the prior foundations upon which to base my research. For all of their help I am grateful.

I also give sincere gratitude to my family for their steadfast support. My mother has unquestionably supported me in all my efforts, instilling within me confidence in all my decisions. My father paved the road for my life by expressing his love for learning by

constantly seeking out something new to explore. My sisters Tiina and Jaana, and their families have also provided love and support throughout the years.

Lastly, my greatest gratitude goes towards my wife Jannah. Jannah has been the pillar upon which my life stands. The days when I was down, she lifted me back up. Simply put, she is my life and the reason I strive to do better. I could not have done this without her and I cannot thank her enough.

TABLE OF CONTENTS

LIST OF TABLES

LIST OF FIGURES

LIST OF ABBREVIATIONS

(-)-*anti*-B[a]PDE	7(S),8(R),9(R),10(S) absolute configuration
(+)-*anti*-B[a]PDE	7(R),8(S),9(S),10(R) absolute configuration
3-HPA	3-hydroxypicolinic acid
AAF	*N*-acetyl-2-aminofluorene
AF	*N*-2-aminofluorine
ALEX	alternating laser excitation
B[a]P	Benzo[a]pyrene
B[a]P-N^2-dG	Benzo[a]pyrene adduct at N^2 position of guanine
BPDE	Benzo[a]pyrene diol epoxide
ddNTP	2'3'-dideoxyribonucleoside 5'-triphosphate
dG-C8-AAF	*N*-(2'-deoxyguanosin-8-yl)- *N*-acetyl-2-aminofluorene
dG-C8-AF	*N*-(2'-deoxyguanosin-8-yl)-2-aminofluorine
DNA	deoxyribonucleic acid
DNA Pol I	*E. coli* DNA polymerase I
dNTP	2'-deoxyribonucleoside 5'-triphosphate
E. coli	*Escherichia coli*
E_{max}	Maximum effect at infinite substrate concentration
FRET	Förster resonance energy transfer
FWHM	full width at half maximum
HPLC	high performance liquid chromatography

k_d	Dissociation off rate
K_D	Dissociation constant
KF	truncated *E. coli* DNA polymerase I
KF(exo$^-$)	exonuclease free *E. coli* DNA polymerase I
MALDI-TOF	matrix assisted laser desorption time of flight mass spectrometry
NTP	either a ribo- or 2'- deoxy-nucleoside 5'-triphosphate
PAGE	polyacrylamide gel electrophoresis
PAH	Polycyclic aromatic hydrocarbon
PCR	polymerase chain reaction
R_{max}	Maximum response
RNA	ribonucleic acid
rNTP	ribonucleoside 5'-triphosphate
SDS	sodium dodecyl sulphate
S_f	Selectivity factor
smFRET	single molecule Förster resonance energy transfer
SPR	Surface plasmon resonance
TLS	trans lesion synthesis
Tris-HCl	tris-hydroxymethyl aminomethane hydrochloride
WC	Watson-Crick (ie., G:C and A:T base pairs)

CHAPTER I: INTRODUCTION

Since the pivotal discovery of DNA in 1953 by Watson and Crick, the fundamental mechanism of DNA replication by DNA polymerase has been intensely investigated (*1*). Despite a lengthy and rich history, packed with discovery and driven by theories, the full mechanistic details of DNA replication remains uncertain. Researchers have argued the minimal reaction scheme from various standpoints, quarrelling over which step is rate limiting and even disagreeing upon fundamental questions such as what drives nucleotide selection (*2-4*). The minute mechanistic details of replication are justifiably a worthy topic for debate, for errors produced by incorrect replication can lead to a variety of genetic disorders, most notably the generation of cancerous cells. A thorough understanding of the mechanism of DNA replication builds a framework upon which the process of mutagenesis can be investigated.

The mechanism of DNA polymerases can be further complicated by the presence of DNA adducts such as benzo[a]pyrene (B[a]P), *N*-acetyl-2-aminofluorene (AAF), and *N*-2-aminofluorene (AF) within the templating strand (*5*). DNA adducts interfere with replication by triggering the polymerase to misread the template, causing mismatches to be inserted or deletion products to be formed (*6, 7*). Carcinogen-induced replication errors are uniquely defined by the structures of these adducts, giving rise to various effects depending upon the chemical makeup of the particular adduct involved. B[a]P is of particular importance because of the ubiquitous distribution within the environment and its direct link to cancer (*8, 9*).

This research focuses on identifying what happens during the selection of a dNTP and how this selection process fits into the mechanism of DNA replication. In addition, the effects of positioning a benzo[a]pyrene adduct on the template is used to investigate how this carcinogenic adduct may produce errors during replication, and how the benzo[a]pyrene may perturb the native mechanism of DNA polymerase action.

I. DNA Polymerase

A. Structural Overview

E. coli DNA polymerase I was first discovered by Arthur Kornberg in 1957, resulting in the rewarding of a Nobel prize in 1959 (*10*). *E. coli* DNA polymerase I plays a role in the repair of damaged duplex DNA and the processing of Okazaki fragments in *E. coli* (*11*). This polymerase consists of a multi-domain architecture housing not only the 5'-3' polymerization activity required for DNA replication, but also 3'-5' and 5'-3' exonuclease activities. The 3'-5' exonuclease, or proofreading activity, allows greater fidelity to be achieved by removing incorrectly incorporated nucleotides from the growing DNA primer strand resulting in another opportunity to incorporate the correct base before continuing on with synthesis. The 5'-3' exonuclease does not directly function in increasing fidelity but instead is involved with processing of Okazaki fragments by the excision of RNA primers situated on the lagging strand.

A very useful proteolytic digest of DNA polymerase I produces a truncated enzyme termed Klenow fragment, named after the researcher Hans Klenow who first discovered this useful derivative (*12, 13*). Klenow fragment is unique in that it houses the

5’-3’ polymerase activity required for DNA synthesis and the 3’-5’ exonuclease proofreading activity, but is devoid of the 5’-3’ domain responsible for the excision of RNA primers. In addition, a single D424A point mutation within Klenow fragment’s 3’-5’ exonuclease domain almost abolishes the exonuclease activity, making this polymerase an excellent choice for DNA synthesis studies without the complication of exonuclease action (*14*). Klenow fragment has been a model enzyme for the study of DNA replication for the last four decades, and the solution of the crystal structure in 1985 by Ollis *et al.* aided in providing a structural overview of DNA polymerase enzymatic domains (*15*).

The crystal structure of Klenow fragment revealed a two domain architecture; a smaller 200 amino acid N-terminus forming the 3’-5’ exonuclease domain, and a larger 400 amino acid C-terminal domain folding to form the polymerization domain. The general shape of the Klenow fragment polymerization domain, being akin to a human right hand, has proven to be strikingly universal among DNA polymerases. Later crystal structures of the analogous Klenow fragment portion of thermophilic *Thermus aquaticus* DNA polymerase I, called Klentaq1, showed a close homology to Klenow fragment with a nearly identical C-terminal fold (Figure 1) (*16*). The polymerase domain can be further subdivided into three subdomains consisting of the fingers, thumb, and palm, all of which form a cleft of approximately 20-24 Å wide and 25-35 Å deep (*15*). Based on previous biochemical studies identifying catalytically important residues in Klenow fragment, the active site of the C-terminal polymerization domain was mapped to the base of the cleft within the palm of the enzyme, with the 3’-5’ exonuclease active site located about 35 Å away. The cleft was noted to be of the approximate size to bind DNA, but it would not be

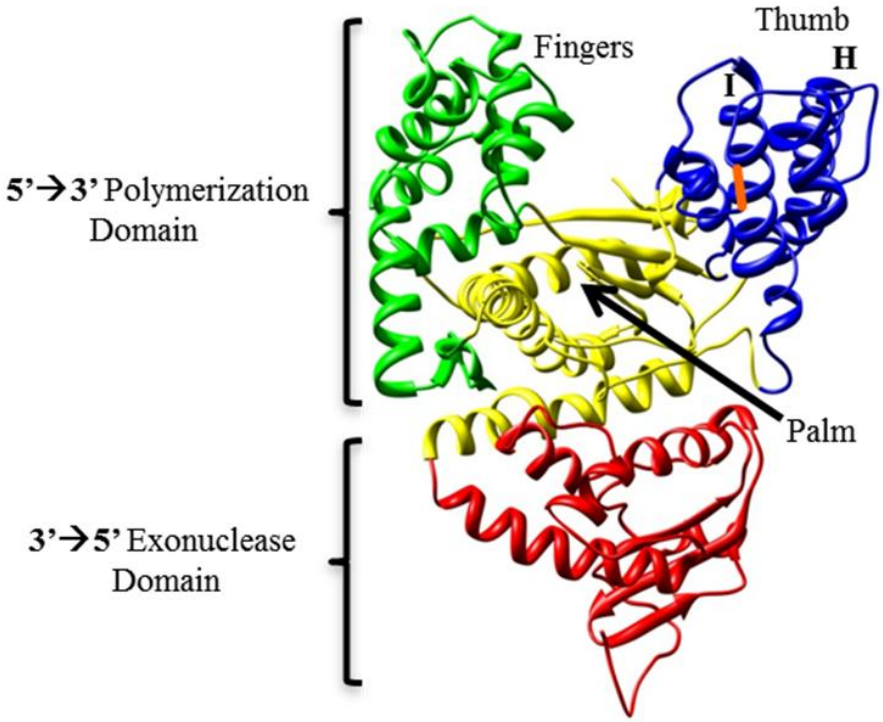

Figure 1. Structure of Klentaq2. Structure of Klentaq in the absence of DNA (PDB #1KTQ). The overall structure of polymerases resembles that of a human right hand forming palm (yellow), fingers (green) and thumb (blue) domains. The palm domain houses the active site residues responsible for the 5' to 3' polymerase activity, and the 3' to 5' exonuclease domain (red) allows excision of misincorporated bases. The H1H2 Loop is disordered and missing from the structure (ends connected with orange line).

until 1993 when Beese *et al.* published a co-crystal structure of Klenow fragment bound to duplex DNA that the orientation and structure of the duplex within the enzyme would be known (*17*).

B. Open Binary Complex

The co-crystal structure of Klenow bound to duplex DNA gave the first glimpse into the arrangement of the DNA within the polymerase and evidence of the first conformational change that takes place within the enzyme (*17*). In this structure, the DNA was situated within the polymerase at right angles to the cleft containing the active polymerase site, however the 3' primer terminus was melted from the template and situated within the exonuclease site in an editing complex. Despite being in an editing complex, the authors modeled the primer strand at the polymerase active site and concluded that the primer could alternate between the exonuclease and polymerase sites, without dissociation of the enzyme. Interestingly, Beese *et al.* noted in their modeling that some distortion of the DNA duplex terminus or protein would be required in order to achieve binding at the polymerase site and that this distortion of the DNA would make the equilibrium between single-stranded and double-stranded DNA more sensitive to mismatches. Irrespective of the mode of binding, many important observations were noted from this structure and further confirmed in later crystal structures of Klentaq (Figure 2A) (*18*).

One such observation was the small DNA-induced closing motion the thumb region undergoes upon formation of the binary complex. This region of the thumb, residues 558 to 637 in Klenow fragment, executes a shift (12 Å at the N-terminus of helix

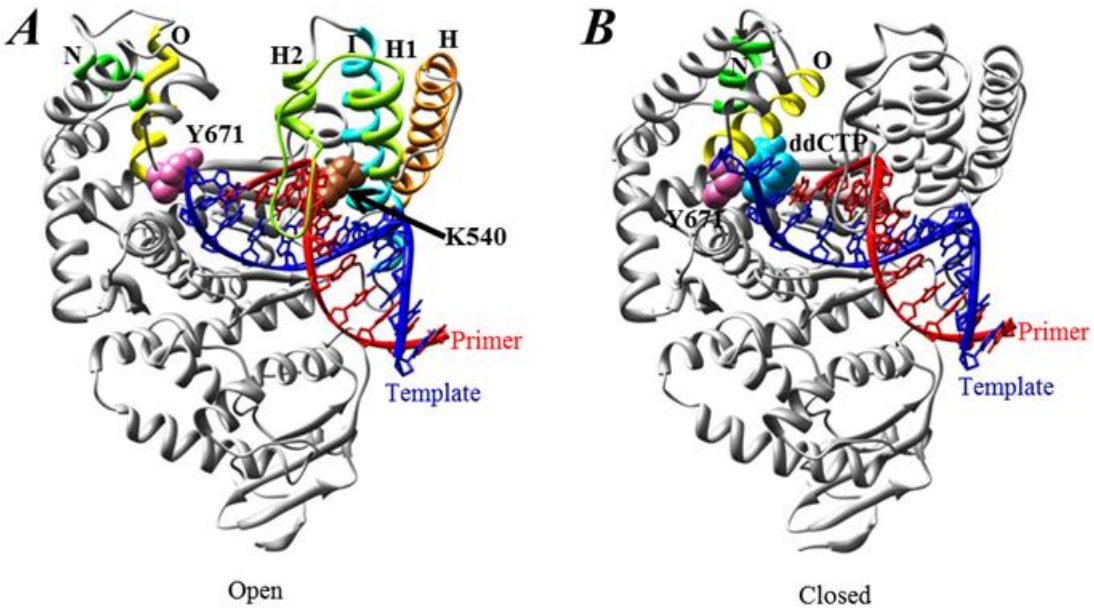

Figure 2. Open binary and closed ternary structures of Klentaq2. (A) Klentaq open binary complex (PDB #4KTQ) [10]. The DNA is situated in the cleft formed between the fingers, thumb, and palm domains. The Y671 residue (pink) is stacked on top of the template (dark blue). K540 (brown) makes non-specific interactions with the minor groove to aid in holding the polymerase bound to the DNA. Helices I (cyan) and H (orange) make small movements relative to their positions in the open complex, and the H1H2 loop (light green) now becomes visible in the structure. The remainder of the colors are as follows; primer (red), H1 and H2 helix (light green), O helix (yellow), N helix (green). (B) Klentaq closed ternary complex (PDB #3KTQ) [10]. A correctly base pairing ddCTP (light blue) is located within the active site inducing a large conformational change of the O (yellow) and N (green) helices (compare with positions in (A)). Y671 is now flipped out of its stacking arrangement with the -1 template base and the n templating base forms Watson-Crick base pairs with the ddCTP.

I) towards the 3'-5' exonuclease domain to form direct contacts with the DNA (*17*). Chemical modification studies also showed that Lys635 (Lys540 in Klentaq), which is a highly conserved residue among the Pol I family, is directly involved in DNA binding (*19*). In addition to the thumb, extensive contacts are formed between the enzyme and the DNA, however virtually all contacts are non-specific in nature forming interactions with the phosphate backbone of the DNA, or to the universal hydrogen bond donors and acceptors of the minor groove. This is important to ensure that the polymerase will bind all DNA equally, irrespective of the sequence. The small closing movement of the thumb upon DNA binding proved to be the first of at least two conformational changes to take place.

The initial description of Klenow fragment in terms of a hand, and specifically the naming of the subdomains as fingers and thumb, proved to be somewhat serendipitous due to their anthropomorphic motions upon forming a binary complex, and as was later shown, a catalytically competent ternary complex.

C. Ternary Complex Formation

In order to successfully replicate DNA, an active ternary complex must be formed with the proper geometric alignment of the polymerase catalytic residues, the metal ions, the primer-template DNA duplex, and the correctly chosen dNTP. The first crystal structure solutions for the ternary complexes were of Rat DNA polymerase β, Klentaq1, the replicative DNA polymerase of bacteriophage T7, and *Bacillus stearothermophilus* DNA polymerase I (*18, 20-22*). These structures revealed a great deal of information regarding the location of dNTP binding and catalytically active residues, a large

conformational change in the protein, and a two metal ion mechanism for nucleotidyl transfer. Despite the wide breadth of organisms these polymerases were obtained from, all exhibited the now stereotypical polymerase architecture of a human right hand and share a similar geometry of the polymerase active site. What follows is a general culmination of information for most observed structures.

i. Conformational Change

The ternary complex is defined by binding of a dNTP into the polymerase cleft alongside the DNA. The incoming dNTP is aligned within the active site by interactions of the non-bridging oxygens of the phosphate moiety to positively charged residues along and near the O helix, placing the phosphate moiety roughly parallel to the O helix. These phosphate interactions are suggested as the primary recognition segment of the incoming dNTP, which is based upon crystal structures of binary complexes of Klentaq1 with all four dNTPs, showing the phosphates of all four dNTPs aligned in similar positions (*23*). However, the base and ribose moieties were in slightly different orientations for the four structures. Most interestingly, the formation of the ternary complex in the presence of the next correct dNTP for base-pairing with the first single stranded template base is accompanied by a large conformational change in the fingers of the polymerase (Figure 2B). In the case of Klentaq this change is an inward rotation of the O helix by approximately 46° (41˚ in T7) towards the primer-template (*18, 21*). The formation of the closed ternary complex has the effect of clamping down the dNTP into the active site, effectively sealing off the crevice formed by the thumb, palm and fingers, resulting in the

proper geometric alignment of catalytic residues to complete a nucleotidyl transfer reaction.

Further elaboration by Dzantiev and Romano showed that the closed tertiary complex could only be observed in the presence of the next correct nucleotide and not in the presence of incorrectly base-pairing nucleotides (*24*). Using a tryptic digestion analysis they showed that trypsin was capable of cleaving Klenow fragment near the active site of the polymerization domain in its open form. However upon incubation of Klenow fragment with a correctly base-pairing dNTP the cleavage was inhibited, presumably due to the conformational change of the enzyme protecting the region near the active site from proteolytic cleavage. Further, a correctly base-pairing ribonucleotide substrate also did not trigger this conformational change as evidence by the formation of trypsin cleavage products. This suggested that only a correctly base-pairing dNTP could conform to the close fitting active site of the polymerase and any deviation from the ideal active site geometry would not allow the conformational change to take place. Indeed, the crystal structures of the closed ternary complexes showed the dNTP situated in a tightly surrounded environment as it stacks between the 3' base of the primer strand and residues of the O helix (*21*). The dNTP binds such that it can form a Watson-Crick base pair with the first single-stranded templating base. The dNTP is further co-ordinated and positioned by interactions to two metal ions located within the active site.

ii. Reaction Mechanism

The alignment of the dNTP in the closed conformation allows a two metal ion mechanism for the nucleotidyl transfer to occur. The two metal ions, positioned

approximately 3.6 Å apart, are octahedrally coordinated by all three phosphates of the dNTP, the highly conserved side chain residues of the enzyme, and two water molecules (Figure 3A and 3B). Metal ion A functions to lower the ribose's 3'OH affinity for its hydrogen. This makes the attack on the α phosphate of the dNTP by the primer's 3' O^- possible. Metal B serves to support the leaving of the pyrophosphate and together both metals stabilize the negative charge of the pentacovalent transition state. It appears that all polymerases studied to date, as well as enzymes such as HIV-1 reverse transcriptase, utilize this same two metal ion mechanism for nucleotide addition (*25*).

iii. DNA Conformational Changes

Similar to the changes within the enzyme during binding, the DNA undergoes several changes from its typical solution based linear B-form duplex structure (*18, 20-22*). The DNA in the ternary complex remains held in place by the small conformational change of the thumb. This maintenance of the closed thumb conformation ensures that despite continued dissociation and re-association of incoming dNTPs during the selection process, the transient binary DNA-Pol complex remains relatively stable and the propensity for dissociation during these transient events does not increase dramatically. The polymerase-DNA- interactions are almost exclusively non-specific in nature, binding to the non-sequence specific minor groove while providing no interactions to the sequence specific major groove, with the small exception of those bases located near the active site. Despite the wide breadth of organisms the polymerases were obtained from, the DNA is mostly B-form yet transitions to A-form DNA as it nears the active site (*18, 20-22*). The B-form DNA has an ordered spine of water molecules along the minor

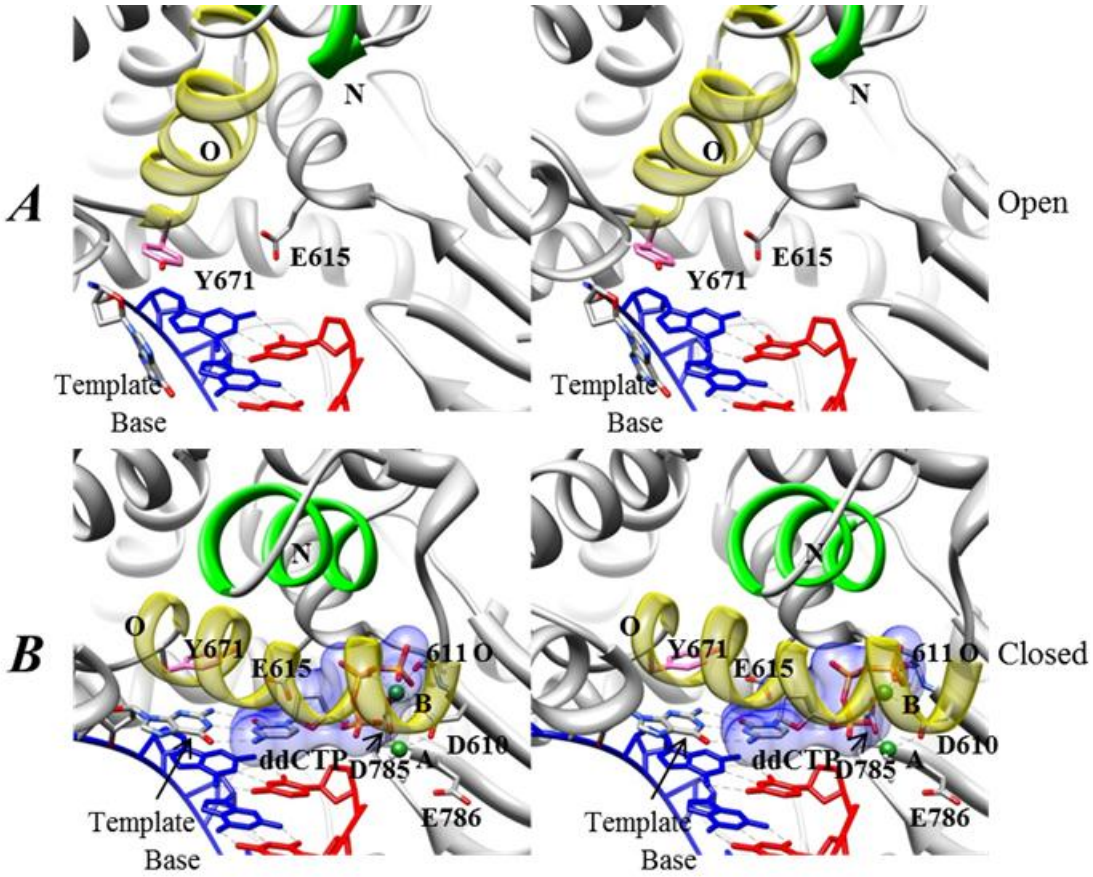

Figure 3. Stereoview of Klentaq active site in the open binary and closed ternary conformations from the same view point [10]. (A) Open conformation (PDB #4KTQ): The O (yellow) an N (green) helices are in an open conformation allowing incoming dNTPs to reach the active site. The templating base (colored by element) is flipped out and Y671 (pink) occupies a stacked arrangement with the template (dark blue). (b) Closed conformation (PDB #3KTQ): The O and N helices have undergone a large conformational change and closed off the nucleotide binding pocket, which a ddCTP (colored by element with blue space filling) now occupies. The Y671 residue has flipped away from the template allowing the templating base to form a Watson-Crick base-pair with the ddCTP. The position of E615 allows screening of rNTPs via a steric clash with what would be a 2'OH of an incoming rNTP. The metal ions A and B (green spheres) form interactions with the phosphates of the ddCTP, and Klentaq residues D610, 611 O, D785, and 2 waters (grey spheres). The missing binding partner of metal A is hypothesised to be the missing 3'OH of the dideoxy-terminated primer terminus. (cross-eyed viewing).

groove interacting with the N3's of purines and O2's of pyrimidines (*22*). Both proper A-T and G-C base pairs display the correct N3 and O2 along the minor groove required for this interaction, whereas misincorporations will cause a disturbance in these interactions, possibly providing a mechanism by which misincorporations can be detected upstream of the active site. These highly ordered water molecules are intentionally disrupted along the minor groove as it nears the active site, giving rise to A-form DNA and a widening of the minor groove with a decreased helical twist in this region. The DNA is further contorted forming a slight "S" shape, with the first bend being induced by interactions with the palm domain, and the second from interactions with the closed thumb (*21*).

As the conformational change from the open to closed ternary complex occurs, another interesting movement takes place regarding the templating base and an aromatic residue at the base of the O helix (Tyr766 in Klenow Fragment, Tyr671 in Klentaq, Tyr530 in T7). In both the open binary and open ternary complexes, the templating base is twisted almost 90° away from the nucleotide binding site (Figure 3A), and in its place the aforementioned Tyr671 of the O helix is stacked on top of the template of the terminal base pair (*18*). At first glance this appears to be illogical since the template base must be base-paired with the incoming nucleotide to direct its proper selection. However, this unique positioning of the templating base in the open conformation is thought to allow an incoming dNTP to "preview" the template prior to reaching the full depth of the binding pocket, and has thus been coined the preinsertion site (*26*). This preview in the preinsertion site may facilitate selection of a correct dNTP early on in the incorporation process. Upon binding of a correct dNTP to the complex, the conformational closing

movement of the O helix induces a movement of the tyrosine side chain out of its stacking arrangement on the template, allowing the flipped out templating base to rotate back into its typical stacking arrangement with the template (Figure 3B) (*18*). The exchange of positions of the tyrosine side chain with that of the templating base in the closed conformation allows the templating base to form its typical Watson-Crick hydrogen bonding alignment with the incoming dNTP. Given a correct fit, the subsequent alignment of catalytic residues takes place and phosphodiester bond formation can ensue.

D. Mechanism of Polymerization

i. Walk Through of the Mechanism

The minimum polymerization mechanism (Figure 4) highlights various states the polymerase is known to undergo upon the route to catalysis (*27, 28*). The initial step, and the only step that would not require repetition during a bout of synthesis, is the formation of a binary complex where the polymerase initially binds the DNA. For polymerases that contain exonuclease domains, such as *E. coli* DNA polymerase I and T7 DNA polymerase, the polymerase may bind the DNA at either the polymerase domain (E_P) or at the exonuclease domain (E_e). Templates that contain several mismatches, as well as some properly base paired segments with certain sequences are known to cause a larger extent of binding to the exonuclease domain than to the polymerase domain (*29-31*). However, certain polymerases such as bypass polymerase eta (Polη) and DNA polymerase IV (Dpo4) are devoid of exonuclease domains, and in these instances would lack the portions of the mechanism related to exonuclease function (*32-34*).

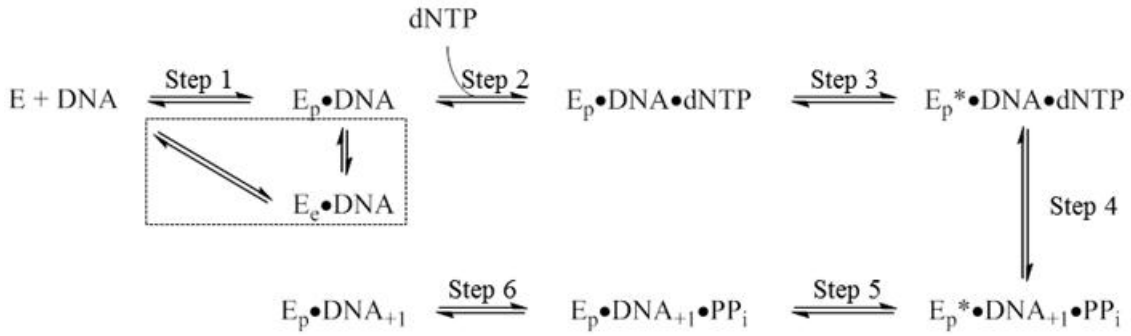

Figure 4. Linear schematic of DNA replication. Step 1) Enzyme forms a binary complex with DNA by binding at either the polymerase site or the exonuclease site. Some polymerases are devoid of exonuclease function and would subsequently exclude the boxed in region of the mechanism. In KF-DNA binding experiments using non-extendible primers everything after step 1 will be measured as DNA binding. Step 2) Nucleotides bind the complex to form a ternary complex in an open conformation. Step 3) If a correct dNTP is present in the polymerase active site a conformational re-arrangement involving closing of the fingers domain to form a ternary closed conformation is induced. Steps 4-6) Catalysis ensues and product is formed. Polymerase re-opens and releases the pyrophosphate, followed by translocation to the next templating base.

Once the DNA is positioned within the polymerization active site, the addition of a dNTP first forms a ternary complex appears to be in an open conformation (*18*). If the bound dNTP is capable of forming a WC base pair with the templating base the polymerase then undergoes a conformational change to a closed ternary complex (*18, 20-22, 24, 35, 36*). Following phosphodiester bond formation, the polymerase returns to the open conformation, pyrophosphate is released, and the polymerase transitions along the DNA to the next templating base. The polymerase, once again in an open binary complex, may then begin the selection process once again to find the next correct dNTP.

ii. dNTP Selection

The successful proliferation of cells requires that DNA polymerases must not only have a very rapid catalytic rate while maintaining incredible accuracy, but also must be able to vary their specificity depending on which of the four bases is at the templating position in the active site. In essence the polymerase must recognize four types of substrates, differentiating between them in order to reject incorrectly pairing dNTPs and catalyzing incorporation for correct dNTPs. The statistical reality of this process is that during the incorporation of a properly paired nucleotide, the polymerase must be able to cope with the binding of incorrectly pairing dNTPs multiple times prior to finding the correctly pairing dNTP. DNA polymerases have clearly evolved the ability to repetitively and precisely accommodate these four different Watson-Crick (WC) base-pairing arrangements, minimize the possibility of catalyzing the incorporation of incorrect WC base-pairing dNTPs, and in each case reject rNTPs that are present at significantly higher concentrations.

Selection of a proper nucleotide is no trivial matter considering this onslaught of correctly base-pairing ribonucleotides and mismatched deoxyribonucleotides that must be rejected in order to find the correctly matching substrate. Utilizing a FRET-based stopped flow and chemical quench assay, Joyce *et al.* studied the mechanism by which each of these incorrect substrates are selected against during the process of replication (*2*). In this assay a fluorophore donor was positioned on a mobile portion of the fingers of Klenow fragment and a fluorescence quencher was positioned on the DNA. This allowed monitoring of a change in position of the fingers relative to the DNA and the formation of a correctly paired ternary complex. A concentration-dependent decrease in fluorescence was seen in the presence of the next correct dNTP, indicating that fingers closing was occurring. Mispairing dNTPs as well as mispairing rNTPs showed little fluorescence change, suggesting that they are selected against early on in the process, prior to fingers closing. This implied that a large discrimination against mispairing nucleotides (dNTPs and rNTPs) occurs directly in the open conformation.

Addition of a correctly base-pairing rNTP caused the conformational change to a closed complex to become significantly hampered, yet still occur to a marginal extent. This reduction in conformational change had previously been identified as a direct clash between the 2'-OH of the incoming ribonucleotide and the steric gate side chain Glu710 of Klenow fragment (Glu615 of Klentaq, see Figure 3) (*37*). Similarly, based on their crystal structure of T7 DNA polymerase, Doublie *et al*. postulated that the corresponding Glu480 residue along with Tyr526 forms a hydrophobic pocket that would preclude the 2'-OH of ribonucleotides (*21*).

Taken together these data indicate that the selection of a correctly paired nucleotide substrate occurs first, followed by a selection against ribonucleotides. This specific order for the stepwise selection of a proper substrate provides a more efficient pathway for replication. By initially constraining downstream processing of a substrate to only correctly base-pairing molecules, six of the eight possible substrates will be selected against. This provides an efficient first step to screen out as many incompatible substrates as possible, thereby limiting downstream processing of incompatible substrates. In essence only one incorrect substrate (the correctly pairing ribonucleotide) of the initial eight nucleotide substrates will see further unnecessary processing. Conversely, if the ribonucleotide was selected against first, four of the eight substrates (all dNTPs) would need to be screened for in downstream processing prior to catalysis, and any additional time spent in their processing would be wasted three out of the four times. Overall, the conformationally-induced changes in the thumb upon binding DNA, and the large changes in the fingers, function to grip the DNA and dNTP substrate respectively. This provides a means for testing the nascent base pair for correct alignment and ensuring that only compatible dNTPs are incorporated.

Although numerous studies have focussed on what happens when a correctly paired dNTP is placed within the polymerization active site, few have examined the process by which the polymerase rejects an incorrectly paired dNTP. A recent study has identified a novel state that forms when a polymerase binds an incorrect dNTP (*38*). In this analysis, it was shown that E. coli DNA polymerase I (Klenow fragment) (KF^1) formed an intermediate when bound to a mispaired dNTP that could not be classified as

either an open or closed complex, but instead appeared to be a previously unobserved state. Prior studies had also alluded to the possibility for the formation of this open mispaired dNTP bound ternary complex but did not include it in the polymerization mechanism (*27, 29, 39, 40*).

E. Polymerase Dynamics

Recently a new picture regarding the conformational dynamics of polymerases has begun to emerge. Single-molecule assays allow the direct monitoring of individual molecules and can reveal properties that are otherwise masked by ensemble averaging of large populations of molecules. Non-synchronous fluctuations that appear in fleeting moments of time go unseen in ensemble averages yet become obvious when viewed at the single molecule level. Single-molecule FRET (smFRET) experiments where a FRET donor was positioned on the template of a duplex DNA strand, and a FRET acceptor was positioned on Klenow fragment, allowed the direct visualization of DNA synthesis as it proceeded through incorporation of three nucleotides (*41*). The movement of the DNA to the exonuclease domain, as well as the movements during synthesis, could also be viewed. As expected, discrete steps in the FRET traces were observed for each nucleotide incorporation event. Further, a few individual molecules were noted to have the primer transition directly from the polymerization site to the exonuclease site, and visa versa, without dissociation of the binary complex. This correlated well with the proposition made during the modeling of the crystal structure in 1993 by Beese *et al* (*17*). In Addition, following each incorporation event the polymerase appeared to move one nucleotide further downstream than was necessary to place the following nucleotide in

the preinsertion site. This was immediately followed by a return back to the expected FRET level for the ensuing preinsertion site. This transient drop was routinely observed in the presence of the next correct nucleotide and was never observed in the presence of an incorrectly base-pairing nucleotide. The ubiquitous nature of this novel step led the authors to conclude that this was indeed an integral step in nucleotide incorporation and that it might be involved in checking for proper base pair formation. Movement to this site might be part of the routine proofreading process that results in movement of a misincorporation to the exonuclease domain. This transitioning process to the exonuclease domain was observed when experiments were performed using mismatched primer-template termini (*41*). Alternatively, it was also suggested that the transient state could represent an equilibrium between the preinsertion and insertion complexes, or it could represent a further conformational rearrangement that is part of the polymerase mechanism. Regardless, the smFRET based discovery of this novel motion of the polymerase shows new dynamics previously unobserved in bulk biochemical experiments.

Further demonstration of the lively dynamic nature of these enzymes comes from new evidence regarding the continual conformational changes that polymerases undergo during nucleotide incorporation and the identification of yet another conformational state (*38*). Santoso *et al.* utilized alternating-laser excitation (ALEX) smFRET with both members of the FRET pair placed on Klenow fragment to directly monitor conformational changes of the polymerase in real time. More specifically, one fluorophore was positioned on residue 744 of the fingers domain of Klenow fragment,

and the other on residue 550 of the thumb. Using a femtoliter observation volume where individual molecules diffuse freely, the conformational changes of the enzyme could be accurately tracked. Observations of Klenow fragment bound to DNA in a binary complex revealed that despite the lack of dNTP, the enzyme was found to occupy both the open and closed states, with the open conformation existing 66% of the time. The large occupancy of polymerases in a closed binary complex is a fascinating proposition and adds an active quality to the crystal structure snapshot of the binary complex published almost two decades previously (*17*). Upon addition of the next correctly base-pairing dNTP the closed conformation dominated 84% of the time (*38*).

Addition of incorrectly base-pairing dNTPs revealed a third conformation of the enzyme that was distinct from the open and closed complexes identified previously. Similarly, addition of rNTPs also showed the formation of a third state. Despite the similarities observed in the third conformational state observed with incorrect dNTPs and rNTPs the authors advocate that they cannot be the exact same state, because as noted earlier the rejection of an incorrectly base-pairing dNTP occurs at a different step along the reaction pathway than does the rejection of rNTPs. Regardless, the third state is thought to more closely resemble an open KF-dNTP complex where the interactions of the triphosphate moiety induce a subtle rearrangement of the residues along the O helix, yielding the third FRET state. This process would allow the complementarity of the templating base with the incoming dNTP to be tested in the open conformation. Provided a good fit is obtained the polymerase would then move the pair to the active site via

rearrangements of the O-helix as the closed conformation is formed, whereas mispairing nucleotides would be rejected in the open conformation.

More striking than the identification of the novel third conformational state was the observations that the unbound enzyme was found to be continually fluctuating between various conformational states despite the lack of a DNA template or dNTPs (*38*). These conformational transitions were incredibly rapid, occurring in the low millisecond range. The ability of the polymerase to continually sample its conformational states in the absence of substrate further exemplifies the dynamic nature of this enzyme.

II. Carcinogenesis

Many exogenous compounds have been identified in the environment that can alter the genetic makeup of organisms by inducing mutations in their genomes. The accumulation of such mutations within the genome can lead to successive proliferation of cells that are lacking the normal restrictive processes that govern their replication. This unrestricted proliferation is known as cancer. The mechanism by which a correct nucleotide is chosen is clearly a complex process even under ideal conditions. However, DNA is under constant assault from both endogenous and exogenous agents that alter the DNA template by modifying the bases, resulting in distortions in the DNA structure or changes in the base electrostatics. Due to their disrupting nature, DNA damage can act as roadblocks to DNA polymerases or result in nucleotide misincorporations and generation of frameshifts.

A. Benzo[a]pyrene

i. Brief History of Benzo[a]pyrene

Arguably one of the most well studied compounds belonging to the polycyclic aromatic hydrocarbons (PAHs) is benzo[a]pyrene (B[a]P) (Figure 5). The carcinogenic effects of B[a]P were indirectly first investigated in 1775 by Sir Percival Pott who demonstrated a direct correlation between exposure to soot by chimney sweeps, and their incidence of scrotal cancer (*42*). Over 100 years would pass before Bell discovered a link between exposure to similar compounds as soot, such as coal tar, paraffin, and oil, with a heightened incidence of cancer (*43*). Despite this result, it was not until the early 1920s that this link was solidified by experiments showing the formation of epithelial tumors on the backs of mice by directly applying coal tar (*44*). It was then a short while later in the early 1930's when isolation and purification methods for compounds had developed sufficiently that investigations began by Cook *et al.* to determine which compounds in coal tar were responsible for these mutagenic consequences (*45*). Cook *et al*. discovered that B[a]P was the carcinogen responsible for inducing the tumor growth found on mouse skin exposed to coal tar, cementing B[a]P as a representative carcinogen that would be intensely studied in the years to come.

The link between B[a]P and its ability to induce mutations is now conclusively established by being identified as a causative factor in many human epithelial cancers such as skin, lung, bronchus and colon cancer (*46*). Since the first establishment of this link in the 1930s, a plethora of studies have been directed at investigating the specific carcinogenic action of B[a]P.

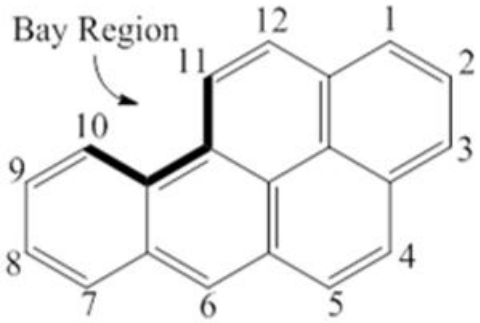

Figure 5. Structure of benzo[a]pyrene (B[a]P) and numbering scheme. Defining bonds of bay region are indicated by darkened lines

ii. Environmental Sources

B[a]P is considered by many to be the ultimate environmental carcinogen both due to its ubiquity in the environment, being found in waterways, oceans, soil, the atmosphere, and throughout the food chain, and also due to its potent ability to induce mutations (*47, 48*). Various PAHs, including B[a]P, can be formed from virtually all carbon based sources including coal, tar, crude oil, gasoline, most organisms, and also produced in many foods (*47*). The chief natural sources of B[a]P are from volcanic eruptions and forest fires, with some of the largest anthropogenic sources being combustion of fossil fuels, coke oven emissions and transportation emissions (*47, 49*). These sources chiefly expel B[a]P into the atmosphere where widespread distribution is achieved, and exposure is virtually unavoidable. Rain water then transfers the carcinogen to the soil and sediment where 82% and 17% respectively of B[a]P is found (*50*).

Despite B[a]P's abundance in the environment, 97% of human exposure is via the food chain, where B[a]P is present in many foods that utilize some type of combustion in their cooking or processing, such as charcoal broiled meats, cereals, tea, and smoked foods, resulting in an average daily exposure of approximately 2.2 micrograms (*9, 50-53*). Despite the environmental prevalence of B[a]P, some sources of B[a]P are easily preventable, such as avoiding the direct exposure from cigarette smoke where an individual is exposed to approximately 20-40 ng of B[a]P/cigarette (*54*). When a comparison is made between the mutational hotspots found in human lung cancers, and the regions that are largely modified with B[a]P metabolites, there is an overlap

indicating that B[a]P is most likely at least partially responsible for the generation of lung tumours in smokers (*8*).

iii. Metabolic Activation of B[a]P and DNA Adduction

It is now known that B[a]P itself is actually not carcinogenic and possess little reactivity, but instead requires metabolic activation to highly reactive epoxides and diol epoxides to induce its mutagenic action (*55*). Once B[a]P has entered the body, the hydrophobic molecule is altered by several enzymes in an effort to make the molecule more hydrophilic, and hence expedite its excretion from the body. This is the body's normal response to rid foreign compounds from the body by making them more readily excreted in the urine. Unfortunately, the process that normally provides hydrophobic molecules a one way ticket out of the body results in the metabolic activation of B[a]P, forming four major benzo[a]pyrene diol epoxide (BPDE) stereoisomers, designated (+/-)-syn and (+/-)-*anti* (Figure 6).

The dire consequence of this metabolic pathway is that the diol epoxides produced are very electrophilic, and hence readily reactive. Although the electrophilic hydroxyl and epoxide groups do allow B[a]P to become more soluble in aqueous solutions, and hence aid in expediting its removal from the body, they also become more reactive with other compounds, in particular DNA. In 1964, it was discovered that in order for a chemical to be mutagenic, it must specifically be able to bind to DNA (*56*). The metabolic activation of B[a]P directly achieves this due to the creation of the electrophilic epoxide, allowing the BPDE to be the site for nucleophilic attack by the electron rich exocyclic amines of purines, such as the N^2 of guanine and the N^6 of

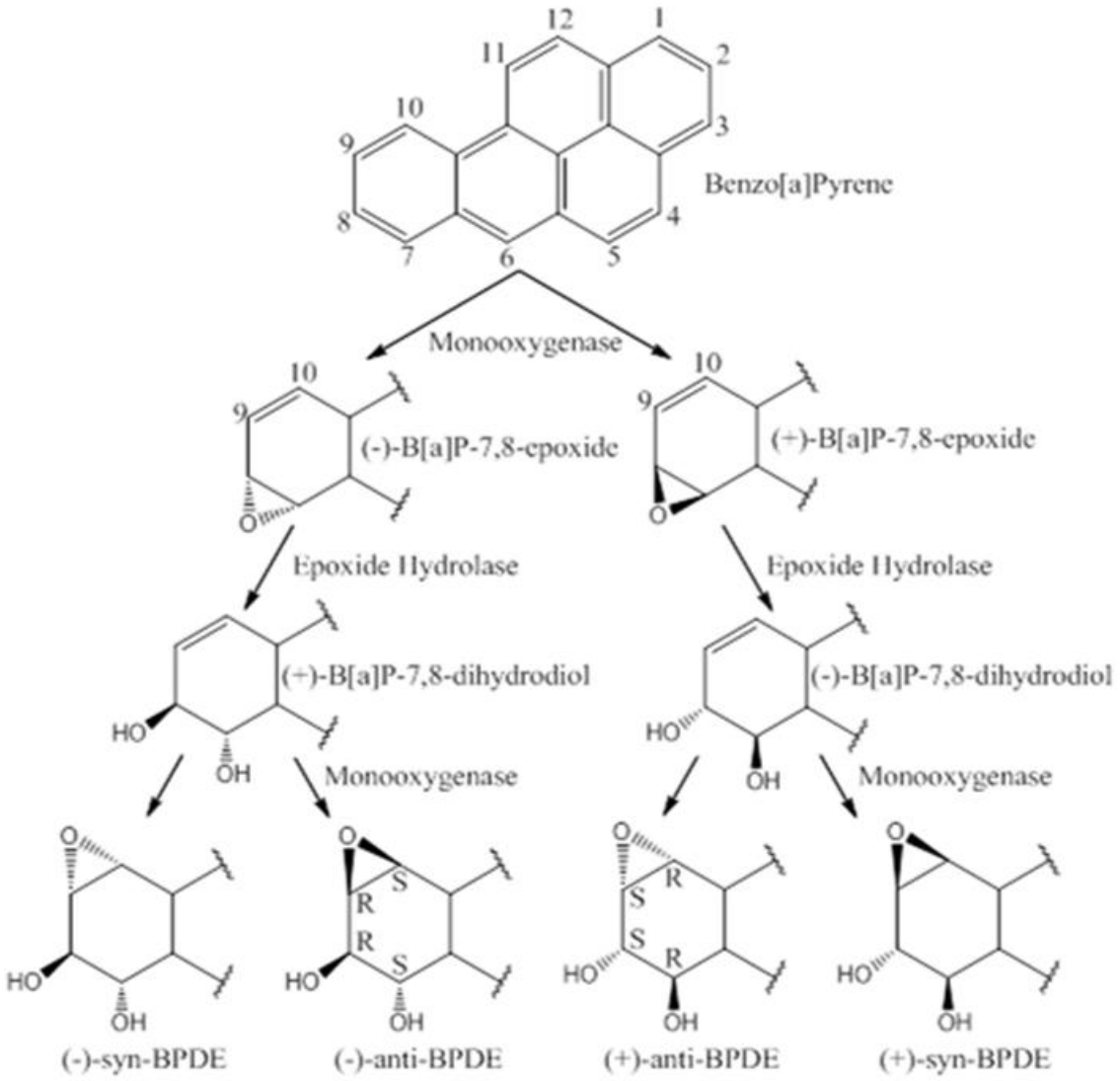

Figure 6. Metabolic activation of benzo[a]pyrene by monooxygenases and epoxide hyrolases to yield 4 benzo[a]pyrene diol epoxide stereoisomers.

adenine. This metabolic activation from a hydrophobic to an electrophilic molecule allows the BPDE to be converted into a molecule capable of adducting DNA, and thus revealing its carcinogenic potential. Of the four major BPDEs formed, studies have shown that the *anti* isomers are the more active compounds in mammalian systems, possibly owing to their much longer half life in aqueous solutions (*46*).

To establish a covalent bond with DNA the BPDE is first thought to non-covalently interact with duplex DNA by intercalating between two adjacent base pairs (*57*). Once posed within the DNA duplex and stabilized by the formation of hydrophobic interactions, the epoxide is free to react with the DNA. Of the assortment of possible reactions, the predominate reactions of BPDE with DNA is the N^2 of guanine performing a nucleophilic attack at the C10 position of the *anti* BPDEs (*58*). Reactions also take place with the N^6 of adenine, and marginally with N^7, however these adducts do not have the same biological relevance that the guanine adducts possess (*59*). The cis or trans opening of the (+/-)-*anti* epoxide ring results in the production of four adducted B[a]P-DNA stereoisomers designated (+)-cis, (-)-cis, (+)-trans and (-)-trans (Figure 7). Although these DNA adducts only differ in stereochemistry, their mutagenic properties are quite diverse.

iv. DNA B[a]P Structures in Duplex DNA

The mutagenic properties associated with each stereoisomer can be attributed to the varying conformations that each adopts in a DNA segment. The structures that are formed in both duplex DNA and those found at a primer template junction are dramatically different from one another, also varying with the identity of the B[a]P

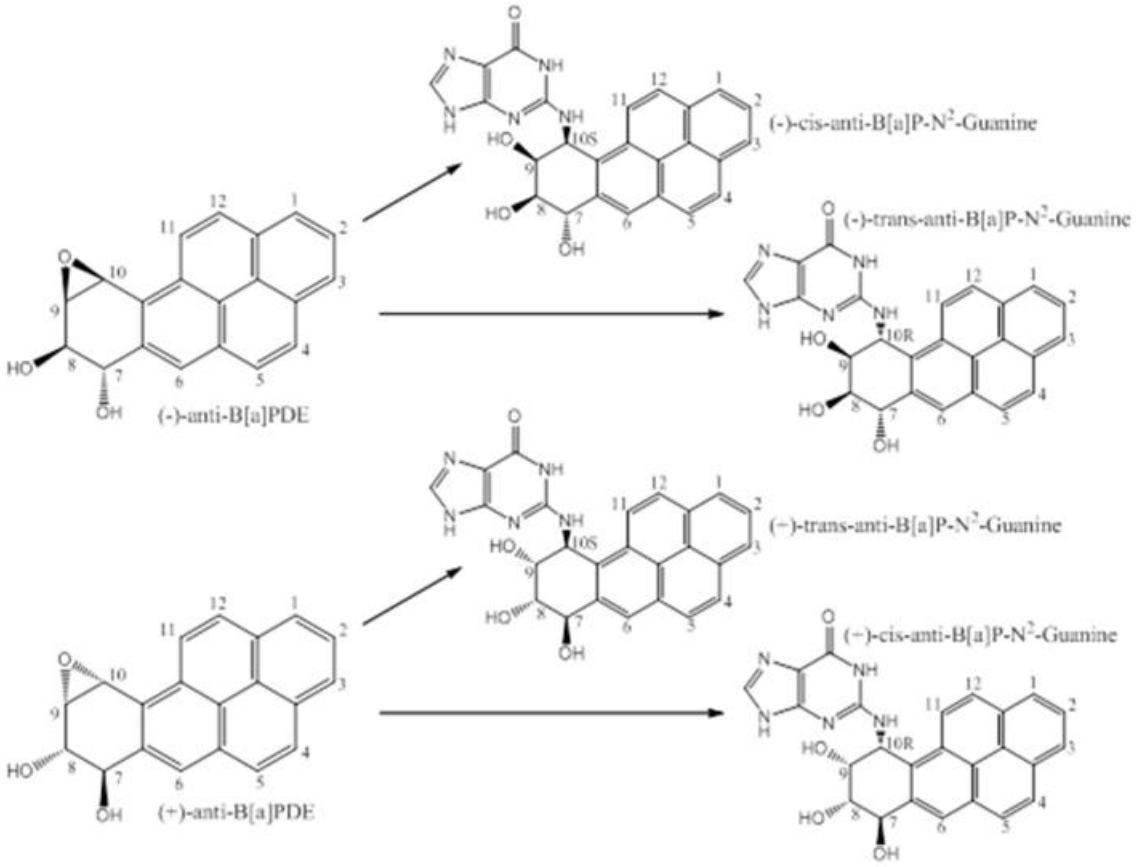

Figure 7. Binding of activated *anti*-benzo[a]pyrene diol epoxide isomers to the N2 position of a guanine base. This process forms four stereoisomers. The isomers are abbreviated to: (–)-cis, (-)trans, (+)-trans, and (+)-cis.

isomer, and these structures may hold clues for the mutagenic properties that each isomer exhibits. For instance, the (+)-trans isomer adopts a conformation in double stranded DNA with the pyrenyl moiety stacking on the ribose of the opposite strand, along the minor groove pointing towards the 5' end of the adducted template strand. However, the (–)-trans isomer has the pyrenyl moiety pointing towards the 3' end while stacking with the ribose of the opposite strand along the minor groove (Figure 8) (*60*). Thus, the similarities of the trans isomers are that they adopt a conformation where the pyrenyl moiety stacks with a ribose of the opposite strand either 3' or 5' of the adduct. In contrast, the cis isomers form a base displaced intercalative structure which is markedly different from that of the trans isomers. More specifically, the (+)-cis isomer has the pyrenyl ring pointing towards the major groove as it intercalates in the duplex and forces the modified guanine into the minor groove, with the partner cytosine displaced into the major groove. Similarly, the (–)-cis isomer also has the pyrenyl ring intercalate, with the partner cytosine being pushed towards the major groove. However, here the pyrenyl ring points to the minor groove and the modified guanine is displaced into the major groove. Overall, the major conformations of the trans stereoisomers in duplex DNA has the modified guanine remain within the duplex and the B[a]P residue stack along the minor groove, whereas the cis stereoisomers have the B[a]P intercalate while the modified guanine is displaced out of the helix.

These structures that form are further complicated by variations in sequence identity surrounding the adduct. For instance, when the sequence is switched from a CGC context seen above, to a TGT sequence, the NMR structure was not able to be solved, and

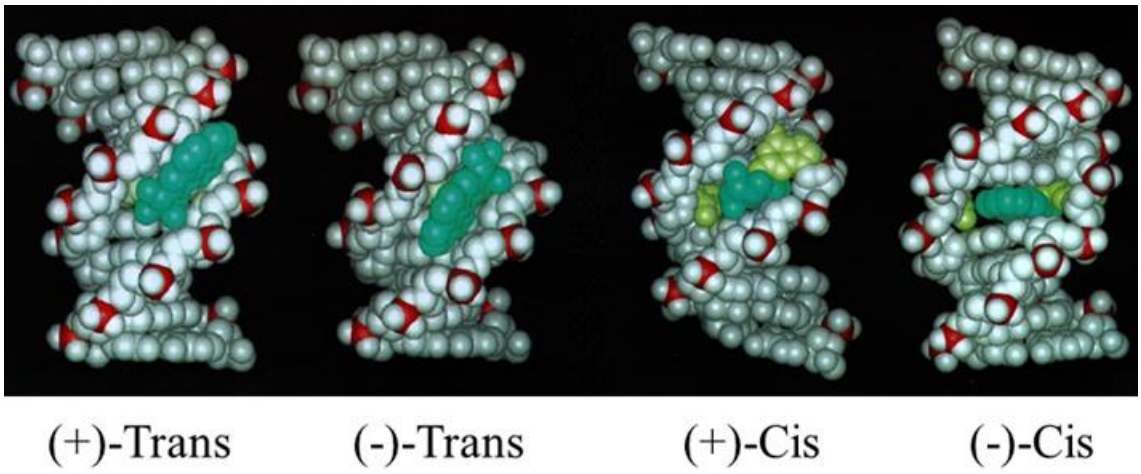

Figure 8. Duplex DNA structures containing four isomers of B[a]P adducts. The B[a]P moiety is in varying conformations for the different adduct isomers, resulting in a different mutagenic profile for each isomer. Figure adapted from Geacintov et al., Chem Res Toxicol, 10(2): 111-146 (1997).

this was attributed to fluctuations in adduct conformations. Molecular modeling studies have further investigated this and have shown that up to 16 conformations with similar stability can exist in the TGT context (*61*).

v. DNA B[a]P Structures in Primer-Template Junctions

Within the primer template junction the conformation of the B[a]P adduct is yet again different, however here the adduct has primarily been shown to stack with the terminal base of the primer strand (Figure 9). Due to the various conformations adopted by the four isomers, the effects of an adduct during replication which is positioned at a primer template junction is dependent upon which isomer is present. This can be seen in the complexity of the mutational spectrum produced by B[a]P adducts, yielding substitutions, frameshifts, insertions, and deletions in *E. coli* (*7*). Presumably, this complex mutational spectrum is dependent on the varying conformations of the different B[a]P stereoisomers at a primer template junction, within the active site of the DNA polymerase, the types of polymerases involved, and the sequence context surrounding the adduct. For instance, within the same primer template junction a (-)-trans isomer has been shown to cause a greater disturbance to the overall structure of the region, as compared to a (+)-trans adduct. This region of deformation extended three base pairs into the duplexed region 3' of the adduct.

vi. B[a]P and Polymerase

Klenow fragment has been widely utilized to study replication across from various adducts including B[a]P. One main reason Klenow fragment has been the choice for investigation is chiefly due to its capability to replicate across from and past a B[a]P

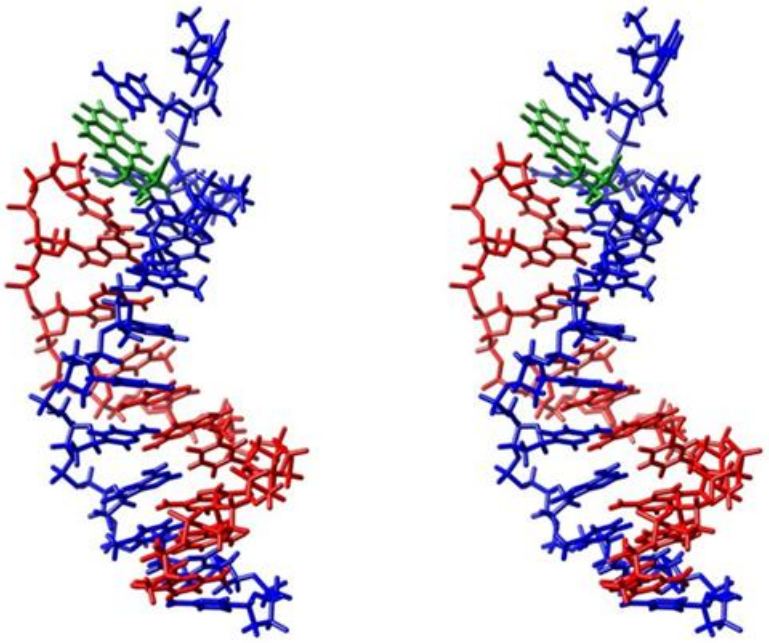

Figure 9. Stereoview of a (+)-trans-anti-B[a]P-N2-dG adduct in a primer-template junction across from a cytosine (cross eyed viewing). The B[a]P adduct (green) is base stacked with the terminal base of the primer (red). Template is colored blue. PDB#1AXO.

adduct positioned in a primer template junction (*3*). It is thought that when KF encounters an adducted B[a]P on the template strand, the polymerase will attempt to incorporate a nucleotide that causes the least amount of local distortion. The nucleotide that causes the least amount of distortion may vary with various adduct conformations. Consequently, the polymerase will often incorporate the incorrect nucleotide across from the adducted guanine, presumably due to steric clashes within the polymerase active site. Many studies have shown that an adenine is the most easily incorporated nucleotide, which coincides with the most common mutation, a G→T transversion (*62*). Nevertheless, the nucleotide that is most favored for incorporation may not necessarily be the nucleotide that is required for bypass and extension from the lesion, and the preferred nucleotide for incorporation also changes with a change in the sequence context surrounding the B[a]P lesion (*63*).

B[a]P has also been shown to exhibit inhibitory effect on the conformational change of the polymerase when it is positioned within the templating position. Both the (+)-trans and the (+)-cis isomer inhibit the switch from the open complex to the closed ternary complex (*64*). Moreover, the addition of the next correct nucleotide, cytosine, causes an increase in the KF's propensity to dissociate from the DNA. This is exactly the opposite effect as seen with an unmodified primer template.

Regardless of KF's inability to form a stable closed, ternary complex in the presence of B[a]P adducts, replication past these adducts does transpire. The formation of -1 to -6 deletion products are possibilities, depending on the sequence context surrounding the B[a]P adduct, as well as the sequence of the downstream template bases

(*63*). In the instance of frameshift mutations, translesion synthesis is thought to happen via a slipped displaced frameshift intermediate. In this mechanism, the 3' nucleotides of the primer base pairs with nucleotides along the template downstream of the adduct, generating a nucleotide bulge in the template strand. This bulging of the template strand may help facilitate the bypass of strongly blocking adducts such as the (+)-trans isomer of B[a]P. Despite extensive study, the molecular mechanism by which each isomer generates mutations, and the mechanism by which frameshift mutations are generated has yet to be determined.

B. AAF and AF

One class of DNA damage that has been well-studied is that formed when experimental animals are treated with *N*-acetyl-2-aminofluorene (AAF). This compound, originally patented as an insecticide, has been shown to induce the formation of tumors in a variety of organs and was subsequently never introduced to market (*65*). Metabolic activation and reaction of these compounds with DNA results in the attachment of the AAF or the related AF counterpart to the C8 position of guanine as the major DNA adducts.

i. AAF-DNA Structure

Structural, biochemical, and theoretical studies all indicate that the dG-C8-AF structure causes much less distortion in duplex DNA compared with the dG-C8-AAF adduct. NMR experiments show that the guanine bearing the AAF adduct rotates from an *anti* to *syn* conformation (Figure 10) in the double stranded DNA helix so that the fluorine moiety becomes inserted into the helix (base displacement model) (*66*). This

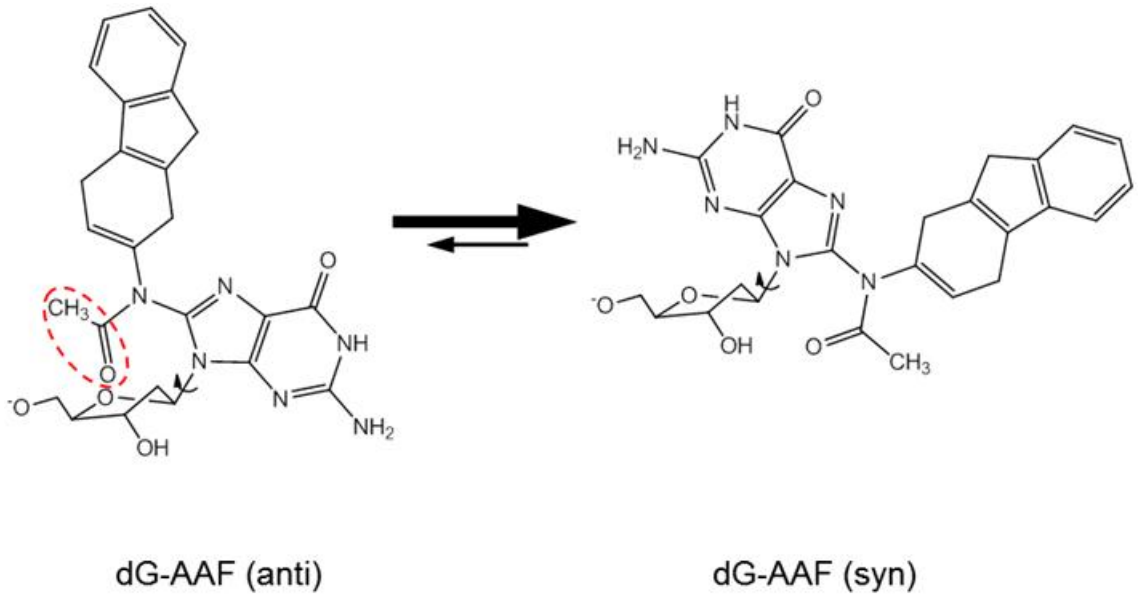

Figure 10. Conformations of a dG-C8-AAF adduct. Native DNA favors the *anti*-conformation that allows Watson-Crick base pairs to form with the opposing strand while a dG-C8-AAF in the *anti* conformation results in a steric clash between the acetyl moiety (dashed circle) and the ribose. This causes the conformational equilibrium to shift towards the more favorable *syn* conformation. dG-C8-AF adducts differ from dG-C8-AAF adducts by having a smaller hydrogen in place of the circled acetyl moiety. This avoids the steric clash and allows both the *syn* and *anti* conformations to be sampled more equally.

contrasts with the dG-C8-AF adduct that can adopt interchangeable conformations: (i) in the major structure the fluorene remains outside the helix (outside binding model) (ii) while the minor conformation has the fluorene ring stacked within the helix (*67, 68*). These different conformations presumably are related to the differences observed in the biological properties of these two adducts. Utilizing primer extension assays, numerous studies have shown that a dG-C8-AAF adduct at the templating position poses a strong block to DNA synthesis by high-fidelity polymerases, whereas a dG-C8-AF adduct in the same sequence is more easily bypassed (*69*). When the adducts are positioned on the template downstream single stranded region at the +1 and +2 templating positions[3], little to no effect from either adduct is noted. However, positioning of the adduct at the postinsertion site (position -1) or in regions of the DNA upstream of the postinsertion site (at the -2 and -3 positions relative to the insertion site) also leads to diminished synthesis (*70*). This indicates that the specific placement of the adduct within the polymerase active site was guiding its behaviour (*70, 71*).

ii. KF Binding to AAF-DNA

It is interesting to note that despite the block posed by the presence of the dG-C8-AAF adduct, gel shift binding experiments utilizing Klenow fragment showed that polymerase binding to the AAF modified template was an order of magnitude greater than to native DNA (*69*). In addition, unlike native DNA where addition of a correctly base-pairing dNTP induces a tighter binding, the identity and presence of any dNTP had little to no effect on this already strengthened binding. To remedy this counterintuitive discovery Dzantiev and Romano postulated that the AAF moiety was interacting with

hydrophobic amino acid residues located within or near the active site of the polymerase. This interaction was thought to strengthen the binary DNA-polymerase complex and also preclude binding of a dNTP within the active site. Further, the authors postulated that the adduct may block the conformational change seen in the presence of the next correctly base-pairing nucleotide, thereby removing any further energetic contribution that the dNTP would bestow upon the complex.

A subsequent paper by the same authors explored more directly the conformational change of Klenow fragment in the presence of these two adducts (*71*). Utilizing the same tryptic digestion assay discussed above for unmodified DNA, it was shown that the conformational change typically induced by the presence of the next correct dNTP was in fact inhibited by the presence of the dG-C8-AAF adduct, as predicted. The tryptic digestion band indicative of the open conformation was maintained despite the presence of any dNTP. However, this was only observed when the adduct was in the templating position. When the dG-C8-AAF adduct was moved one nucleotide to the +1 templating position (the preinsertion site), the dNTP-induced conformational change was again observed. Conversely, placement of a dG-C8-AF adduct in the templating position (insertion site) only partially inhibited the conformational change to a closed ternary complex. This difference was attributed to the dissimilar conformations that each adduct adopts within the polymerase active site and further strengthened the proposition that the AAF adduct was inducing interactions within the polymerase-DNA complex in a way that precluded the conformational changes necessary for competent nucleotide binding (*71*).

Picking up on this line of investigation, in 2003 Lone and Romano utilized a Klenow mutant, Y766S, to focus on the specific interactions responsible for the effect of the AAF adducts on this inhibition (*72*). In the native protein the tyrosine at position 766 is located at the base of the O helix near the junction of the fingers and palm domain and is thought to function in maintaining active site geometry. This tyrosine stacks with the templating base in the open conformation and swings away during formation of the closed complex (similar to Figure 3B), (see more detailed description under the DNA Polymerase section). Mutations at this position have been shown to both increase the rate of insertions of incorrect nucleotides and reduce the ability to extend from these misincorporations (*73*). Under identical conditions, the wild-type Klenow fragment predominantly stalled one nucleotide prior to the dG-C8-AAF adduct, incorporating across from the adduct approximately 20%, and extending past the AAF adduct to yield 6% full extension. Interestingly the Y766S mutant showed a higher (40%) incorporation across from the AAF adduct, but gave only 1% full extension (*72*). In addition, the Y766S mutant showed a 16-fold higher V_{max}/K_m for incorporation of a correct dC across from the dG-C8-AAF adduct and also displayed a much greater propensity to misincorporate nucleotides on unmodified DNA. Together this illustrated the importance placed upon the tyrosine residue for discrimination of a correct base pair and also shows that the Y766S mutation allowed the accommodation of the AAF-C8-dG lesion, possibly because of a more open active site that allows improper base pairs to form during synthesis (*72*).

iii. Polymerase Conformational Change and AAF

Using gel shift analyses and the tryptic digestion assay, the ability of the Y766S mutant to undergo a conformational change was examined (*72*). Similar to wild-type, the Y766S mutant showed an increased binding to native DNA in the presence of the next correct dNTP. The binding of the mutant polymerase to a dG-C8- AAF adduct was also increased, again similar to wild-type. However, where the wild-type showed no further increase in binding strength to dG-C8-AAF containing primer-templates in the presence of a correctly pairing dCTP, the mutant polymerase did show increased binding. In fact, the presence of any nucleotide appeared to increase the binding strength of the mutant, indicating a possible conformational change was occurring. This was confirmed utilizing the tryptic digestion analysis in which it was shown that the presence of dCTP caused protection of the cleavage site whereas other dNTPs reduced cleavage, indicating a conformational change was taking place despite the presence of the dG-C8-AAF adduct (*72*). The ability of the mutant Y766S to undergo a conformational change even in the presence of a bulky dG-C8-AAF adduct is indicative of the more open active site and the importance the tyrosine residue plays in this conformational transition. Interestingly, the Y family of bypass polymerases that specialize in synthesis past bulky adducts also display a markedly open active site (*32*). It is thought that this open nature better accommodates lesions by reducing the propensity of steric clashes, although at the expense of reduced fidelity.

iv. AAF and AF Binary Crystal Structures

It has long been thought that the conformations adopted within the active site by various DNA adducts will account for the array of biological effects and mutagenic consequences that the adducts display (*65, 74*). Direct evidence for the predicted mechanism of inhibition of the conformational change for wild-type Klenow fragment in the presence of dG-C8-AAF, along with the increased binding affinity to these substrates, came in the form a crystal structure published in 2004 (*75*). Dutta *et al.* were successful in obtaining functionally relevant crystal structures of bacteriophage T7 DNA polymerase bound to DNA duplexes containing either a dG-C8-AAF or dG-C8-AF at the templating position. The crystal structure of the dG-C8-AAF adduct has several key features that correlate with the aforementioned results obtained by Romano *et al*. First, the polymerase complex with dG-C8-AAF modified DNA is in a distorted open conformation and no nucleotide is bound to the complex despite the fact that crystals were growth in the presence of ddCTP (Figure 11). The modified nucleoside is in a *syn* conformation, flipped out of the active site and bound to the surface of the fingers. The AAF moiety is positioned in a hydrophobic pocket behind the O helix stacking alongside Phe528, which is usually buried within the fingers (Figure 12). Further stabilizing the position of the AAF moiety are hydrogen bonds between the adducted guanine's N2 and N7 with Asp534 and Arg566, respectively. The AAF interactions with the O helix pushes the helix towards the active site, forcing Tyr530 (analogous Tyr766 of Klenow fragment and Tyr671 of Klentaq) partially into the nucleotide binding site (*75*). The positioning of the AAF and its various direct interactions with the polymerase, as well as the inability to

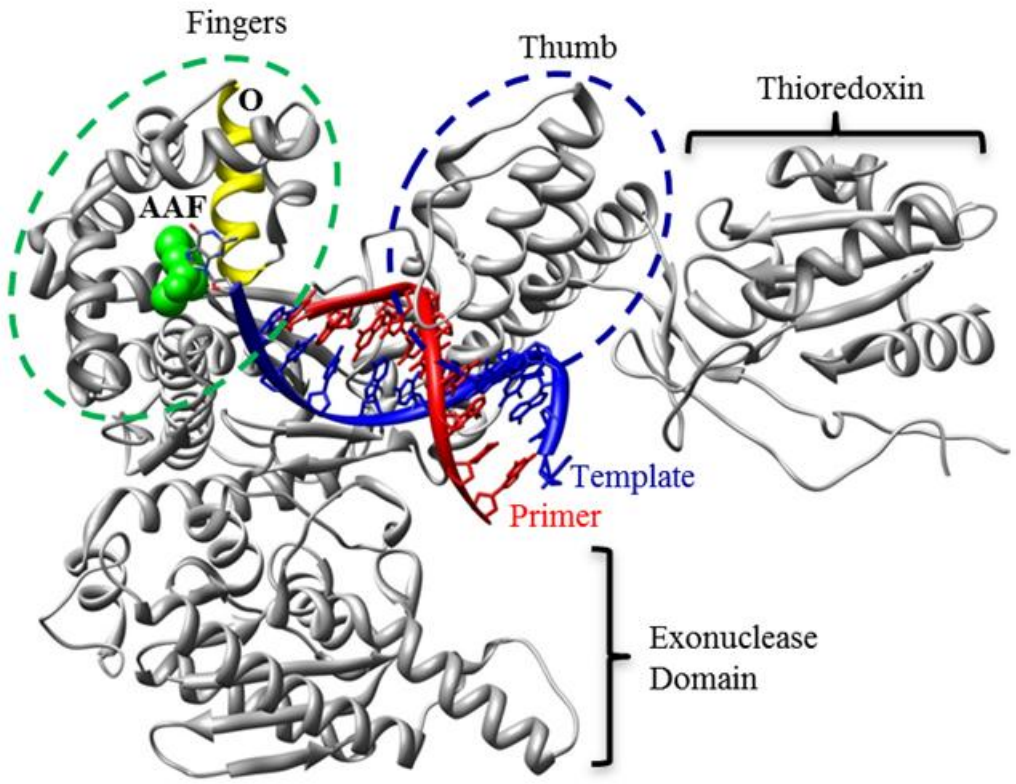

Figure 11. Structure of bacteriophage T7 polymerase bound to a DNA primer-template containing a dG-AAF adduct at the templating position (PDB# 1X9M). The overall shape of T7 polymerase resembles a human right hand forming fingers (green circle), thumb (blue circle), and palm (not highlighted). T7 also contains thioredoxin, a processivity factory, in addition to the polymerase and exonuclease domains. The AAF adduct inserts behind the O helix, locking the helix in a distorted open conformation, inhibiting the binding of dNTPs.

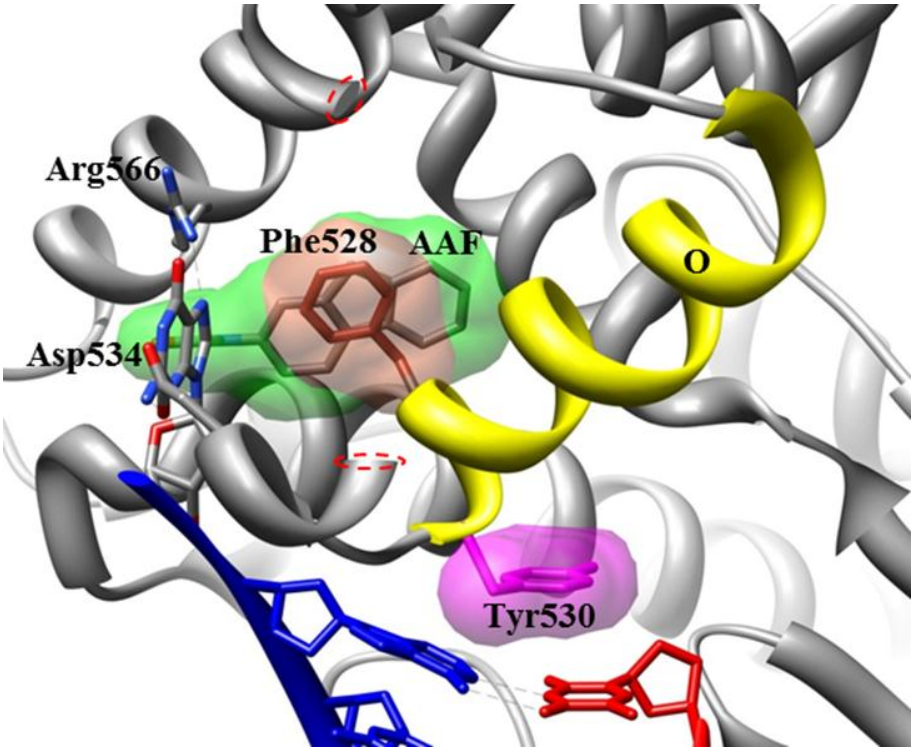

Figure 12. Close-up view of active site of bacteriophage T7 bound to a DNA primer-template containing a dG-AAF adduct at the templating position (PDB# 1X9M). The AAF moiety (grey with green space filling) is inserted into a hydrophobic pocket behind the O helix stacking with a flipped out Phe528 (brown, with brown space filling), which is buried in the native structure. The adducted guanine is in an anti conformation placing the hydrogen bond acceptors and donors away from the nucleotide binding position. This position is further stabilized by hydrogen bonds to Arg566 and Asp534. The AAF moiety pushes the O helix forward, causing Tyr530 (pink with pink space filling) to stack on top of the DNA, occupying the nucleotide binding site which occludes a dNTP from binding. Residues 537-557 have been removed for simplified visualization (ends are circled red).

bind nucleotide due to the positioning of Tyr530, explain why the adduct places a strong block on replication as well as its increased binding affinity. This also confirms the previous experiments performed using Y766S that showed that the presence of the smaller serine allowed the conformational change to a closed ternary complex to occur.

The crystal structure containing the analogously positioned dG-C8-AF adduct showed similar conformations as the AAF adduct, but with a few significant differences. The AF residue was not positioned in the same hydrophobic pocket as its AAF counterpart, but instead the electron density of this moiety was either of poor quality or absent (*75*). Despite limited quality of the electron density around the AF adduct, it could be established that the AF moiety was also not binding to the active site of the polymerase. This is indicative of a fluctuation between various conformations, possibly a transition from *anti* to *syn* conformations. The amino acid residues forming the hydrophobic pocket of the AAF complex were oriented in more native-like positions within the AF containing structure. Also, the important Tyr530 was found to occupy the binding site of the template base in the closed ternary complex. The authors modeled the positions of the AF adduct in both *syn* and *anti* conformations of the nucleoside (*75*). The *anti* conformation was shown to be able to form a closed complex with no significant steric clashes with the AF adduct. However, the *syn* conformation was shown to place the AF adduct stacked in the active site. This stacking arrangement will effectively compete with the stacking arrangement of guanine in the alternative *anti* conformation. The positioning of the adducted guanine in the *syn* conformation would not allow base-pairing

with an incoming nucleotide and would subsequently stall synthesis when in this conformation.

A paper published by Hsu *et al.* in the same year was successful in crystallizing thermophilic *Bacillus* DNA polymerase I fragment in the presence of an AF and AAF adduct, and provided direct visualization of the effects of a dG-C8-AF adduct (*76*). *Bacillus* DNA polymerase I fragment has the ability to catalyze nucleotide addition within the crystal, allowing snapshots to be taken of the adducted guanine within the pre- and postinsertion sites (*20*). Capture of a dG-C8-AF adduct within the preinsertion site showed the adducted template base within the preinsertion site in a *syn* conformation, with the fluorene moiety also buried within the confines of the same site. The presence of the adduct induced a perturbation of the O1 helix, yet the O helix maintained its position in an open conformation. The remainder of the protein and the DNA was unaltered by the presence of the dG-C8-AF adduct. This showed that prior to incorporation of a dCTP the dG-C8-AF was positioned within the preinsertion site, whereas the catalytic site, the O helix, and postinsertion site remained unaffected and presumably capable of performing the transfer of the template base from the preinsertion site to the insertion site. The relatively ordered structure allows nucleotide incorporation to occur opposite the dG-C8-AF adduct, albeit to a reduced extent relative to unmodified DNA.

After a dCTP had been incorporated within the complex, the dG-C8-AF adopts an *anti* conformation, placing the AF moiety within the major groove while the dG forms cognate Watson-Crick hydrogen bonds with the dC within the postinsertion site. The polymerase is able to accommodate this structure because the adduct is solvent exposed

within the major groove, unlike what would occur if its placement was into the minor groove where many interactions between the DNA and the polymerase are found. This conformation is similar to the outside model that places the AAF moiety outside the duplex DNA helix (*67, 68*). This structure also showed a much greater degree of distortion that ultimately affects DNA replication. The dG-C8-AF:dC induces distortions to the template that relocate the *n*-1 template base causing perturbations to the minor groove, the O and O1 helicies, and placing the AF moiety obscuring the preinsertion site to the next template base. This conveniently explains the ability of polymerases to incorporate across from an AF adduct, yet exhibit difficulty in extending further. Conversely, the dG-C8-AAF adduct-containing structure in the pre- and postinsertion sites were indistinguishable, and hence a dCTP was absent from the postinsertion structure. In both structures the protein was in an open conformation with an empty pre-insertion site as the AAF-adducted guanine is somewhat disordered and placed over the preinsertion site. The duplex DNA, as well as the protein's catalytic, pre- and postinsertion sites were undisturbed. Again, this inability to perform incorporation could presumably be due to the inability of an dG-C8-AAF adduct to adopt an *anti* conformation. In general, the observed crystal structures Dutta *et al.* (*75*) and of Hsu *et al.* (*76*) correlated well with the previous results and provided further support for the premise that the effects of these adducts are related to the conformations that they adopt within the polymerase active site. However, the crystal structures of Dutta *et al.* and Hsu *et al.* show that the conformations adopted by the adducts are also dependent upon the polymerase they are bound to, yet still correlate well with the previously observed results.

v. AAF and AF Sequence Context Effects

The stark difference in the mutagenic properties of AAF and AF adducts are further influenced by the sequence of bases surrounding the adduct. AAF's ability to induce frameshifts is targeted to repetitive sequences such as the *Nar*I restriction recognition sequence (5'-$G_1G_2CG_3CC$-3') (*Nar*I sequence reviewed in (*77*)) (*78*). In bacteria, when an AAF adduct is positioned at G_3 a dinucleotide GC deletion is produced, while an AF adduct at this same position does not yield the deletion product (*78, 79*). The dinucleotide deletion is thought to be induced via a slipped displaced structure where during synthesis the primer is capable of misaligning with the template within the polymerase active site. These misaligned looped out structures are further stabilized by Watson-Crick base-pairing of adjacent nucleotides, allowing the polymerase to skip the nucleotides in proximity to the adduct. Gill and Romano explored this possibility utilizing primer extension analysis and gel shift binding assays of various primers along the *Nar*I restriction recognition sequence (*80*). By positioning various primers along the AAF modified template and examining which nucleotide best complemented binding of Klenow fragment, along with the ability to extend the substrate, it was shown that the formation of a GC dinucleotide bulge was induced. Interestingly, where the AAF adduct previously had caused a significant increase in binding to non-*Nar*I sequences, an AAF adduct positioned at G_3 of the *Nar*I sequence showed no increase in binding affinity over the unmodified *Nar*I sequence. In fact, both the binding of Klenow fragment to AAF modified and unmodified *Nar*I sequences showed decreases over non-*Nar*I sequences (*80*). This indicated that a possible different conformation with the AAF modified *Nar*I

sequence existed within the polymerase active site than had previously been noted in the non-*Nar*I sequence of the T7 or *Bacillus* fragment crystal structures. Similar to non-*Nar*I sequences modified with AAF, the addition of nucleotides did not enhance Klenow fragment binding. However, the presence of dGTP, dATP, or dTTP did decrease the binding affinity. This was indicative of a destabilizing effect these nucleotides had on the complex, presumably due to an incorrect base pair match.

Taken together, these results indicated a specific two-step mechanism for formation of the dinucleotide deletion (Figure 13). The first step has a dCTP be incorporated across from the AAF modified base, followed by a structural rearrangement that places the AAF modified base along with the upstream 3'C in a dinucleotide bulge. The primer's 5' upstream guanine and the cytosine initially incorporated across from the adduct now base pair downstream of the templates adducted guanine. This two-step mechanism also suggests that the frameshift extension product could be generated *in vivo* by two different polymerases, one better suited for incorporation across from the bulky AAF adduct followed by another more suited for extension from the adduct (reviewed in (*81*)). This two enzyme stepwise mechanism has been postulated for both bacterial and eukaryotic polymerases and provides a mechanism to reconcile the different properties required of a polymerase for replicative DNA synthesis, and the specialized niche of performing replication in proximity to bulky DNA adducts. This process is exacerbated by specific sequences such as *Nar*I that preferentially adopt structures to induce frameshift mutations after incorporation of a nucleotide opposite the adducted base.

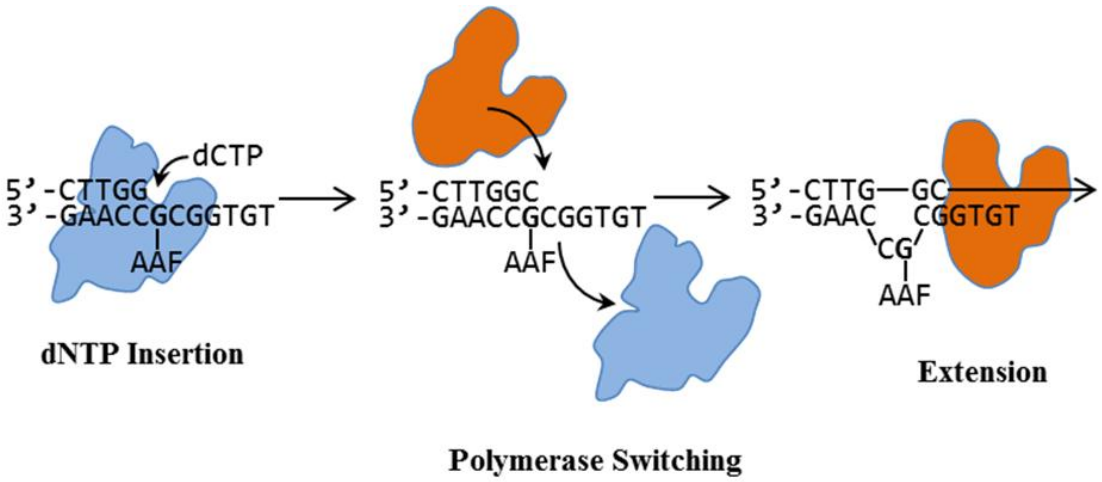

Figure 13. Mechanism for bypass of a dG-C8-AAF adduct in the NarI sequence. A polymerase more suited for incorporation across from the adduct places a proper dCTP:G base pair at the adducted position followed by incorporation, then dissociation of the enzyme. A subsequent rearrangement of the DNA to form a 2 nucleotide budge ensues, allowing a possible second polymerase to perform extension from this slipped structure, resulting in a -2 deletion frameshift product.

C. Bypass Polymerases

i. AF and AAF

A class of polymerases capable of performing nucleotide incorporation in the presence of such distorting adducts as AF and AAF are the bypass or translesion synthesis (TLS) polymerases (*82*). TLS polymerases are characterized by their open active sites that are capable of accommodating bulky lesions and the DNA distortions they produce. For example, yeast Polη (γPolη) has a more open active site caused by stubby fingers and thumb domains, as well as an additional polymerase associated domain (PAD) (Figure 14). γPolη belongs to the Y-family of polymerases and also contains a little finger domain that is unique to this class of polymerases. The more open active site allows Polη in both humans and yeast to correctly synthesis past a *cis-syn* thymine-thymine UV-induced dimer (*83*). Unlike the solvent-excluded tight constraints of replicative polymerases, the active sites of Y-family polymerases are solvent exposed and thus capable of accommodating many distorting lesions. However, the open active site comes at the cost of low fidelity, orders of magnitude lower than replicative polymerases (*84, 85*). Bypass polymerases typically also do not possess high processivity, indicative of their brief role in synthesis past a lesion then allowing a more precise replicative polymerase to continue synthesis (*86*).

Prakash and co-workers were the first to present evidence that γPolη was capable of undergoing a conformational change step prior to chemistry occurring (*87*). Utilizing pre-steady state kinetics and measuring the elemental effect of a sulfur substituted for an oxygen at the α-phosphate of the nucleotide they showed that γPolη undergoes an

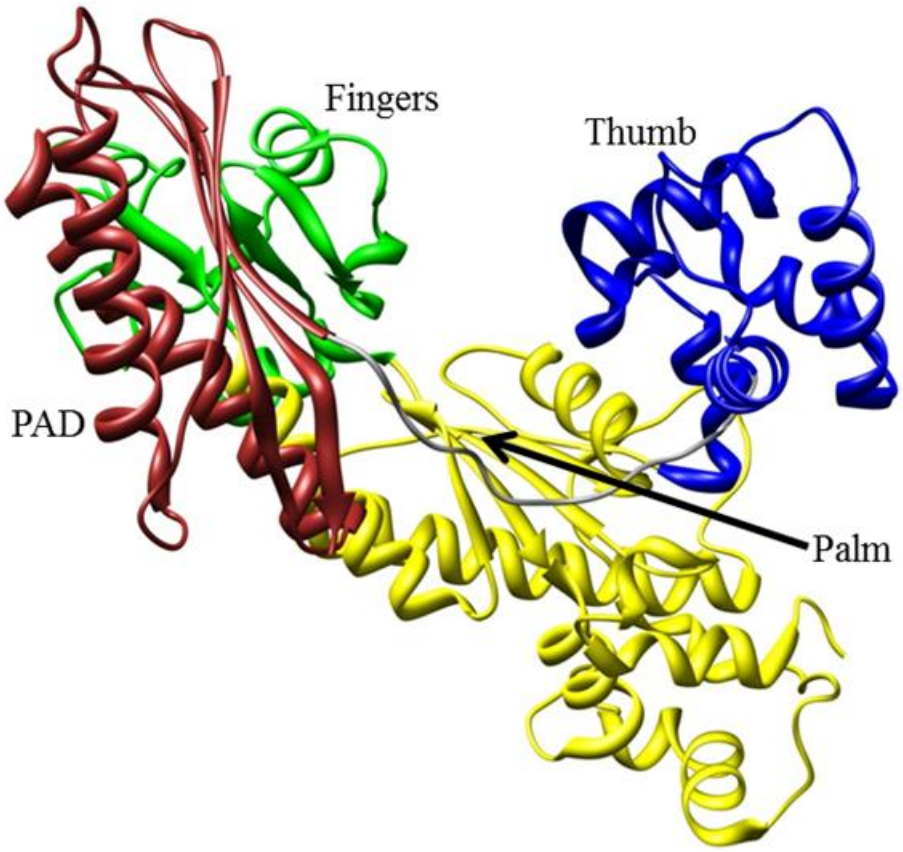

Figure 14. Structural overview of the TLS yeast polymerase eta (PDB# 1JIH, molecule A). γPolη contains stubby fingers (green) and thumb (blue) domains, a palm (yellow) domain, as well as a polymerase associated domain (PAD, (brown)). The open nature of the active site allows two nucleotides to be accommodated during synthesis, as well as bulky carcinogenic adducts and DNA distorting lesions.

induced fit mechanism for nucleotide incorporation. γPolη poorly discriminates between correct and incorrect nucleotides both at the initial nucleotide binding step and during the induced conformational change. A more direct FRET based method was used to visualize the global conformational dynamics of another similar Y family polymerase, Dpo4, in a paper published by Xu and co-workers (*88*). Here FRET pairs were positioned at various locations around Dpo4 allowing movement of specific locations to be tracked during real time measurements. Assemblage of all movements along with the rates of the corresponding FRET changes allowed the authors to assemble global movements of the enzyme. Upon binding of a correct nucleotide a concerted global rearrangement of all four domains (fingers, little fingers, thumb, and palm) takes place where the little fingers domain moved in opposing directions to the polymerase core domains. The movement was relatively small compared to those of T7, being only a few angstroms, yet form similar fingers and thumb closing motions as mentioned previously for various other polymerases.

On unmodified DNA, gel shift binding assays with γPolη showed increased binding in the presence of the next correct nucleotide (*89*). This is consistent with a dNTP-induced conformational change resulting in a closed ternary complex, just as what had been shown previously for Klenow fragment. Addition of an incorrectly base-pairing dGTP was noted to have a destabilizing effect on the complex, presumably due to an incompatible fit within the enzyme, again similar to that previously observed for Klenow fragment.

Extension assays showed that γPolη is capable of fully bypassing a dG-C8-AF adduct and while incorporation occurred across from a dG-C8-AAF adduct, extension past this position was inhibited (*89*). These results are similar to that observed for the Klenow mutant Y766S, which, similar to γPolη, also has a more open active site. Interestingly, where Klenow fragment was unable to become more stable upon addition of any dNTP across from a dG-C8-AAF adduct, binding was stabilized with γPolη in the presence of dCTP, consistent with the formation of a closed ternary complex. Also consistent with the lack of extension after incorporation across from the AAF adduct, no enhanced binding was observed at this position in the presence of the next correct nucleotide. Despite the structural and behavioral differences between replicative polymerases and lesion bypass polymerases, a common conformational change in the mechanism appears to be shared in this case. It should be noted however that studies of some polymerase such as Dbh have not been able to detect a conformational change (*90*). Although it is conceivable that smaller undetected conformational changes are performing the analogous function as the larger scale rearrangements seen in replicative polymerases or that these motions have yet to be detected.

The open active site of Y-family polymerases is not necessary only to accommodate DNA lesions, but also able to allow various primer-template alignments that may favor the replication of the adducted template. As mentioned previously, the formation of frameshift mutations in the *Nar*I sequence occur via a template misalignment and this misaligned structure must be accommodated within the polymerase active site. A recent crystal structure by Rechkoblit *et al.* of the Y family

polymerase Dpo4 in the presence of an dG-C8-AF adduct shows such a complex and how it can be accommodated and stabilized within the polymerase (*91*).

In this study two molecular structures were obtained in one asymmetric unit of the crystal: 1) a correct alignment with the dG-C8-AF adduct base-pairing with a dC at the -1 position (dG-AF:dC at the postinsertion site) and a typical correctly forming dC:dGTP pair of the adjacent base (5' template side of adduct at position n, the insertion site) (Figure 15A) a misaligned structure with the dG-C8-AF adduct base-pairing with a dC shifted to the -2 position (1 position upstream of the postinsertion site) and the adjacent 5' C of the template looping out (Figure 15B). More specifically, in the correctly aligned molecule 1 the dG containing the AF is in an *anti* conformation and the AF is placed on the major groove side of the duplex within a pocket buried from solvent, and stabilized by interactions to the little finger domain. This is similar to the conformation of the AF adduct in *Bacillus* fragment, with the exception that Dpo4 contains interactions to the little fingers domain that stabilize the adducts position, a caveat that is impossible in *Bacillus* fragment due to the lack of a little fingers domain (*76*). The template C 5' of the adduct (at position 0, the insertion site) is base paired with an incoming dGTP, yet is shifted from its typical stacking arrangement over the postinsertion site base pair, and is instead poised partially over the AF adduct with the dGTP over the center of the postinsertion site base pair. In addition, the next downstream template base (0 position, which would typically be within the insertion site) is flipped out and stacks on top of the AF adduct in alignment with the templating C base and the incoming dGTP at the 0 position (insertion site). In the misaligned structure of molecule 2 the dG-C8-AF: dC base

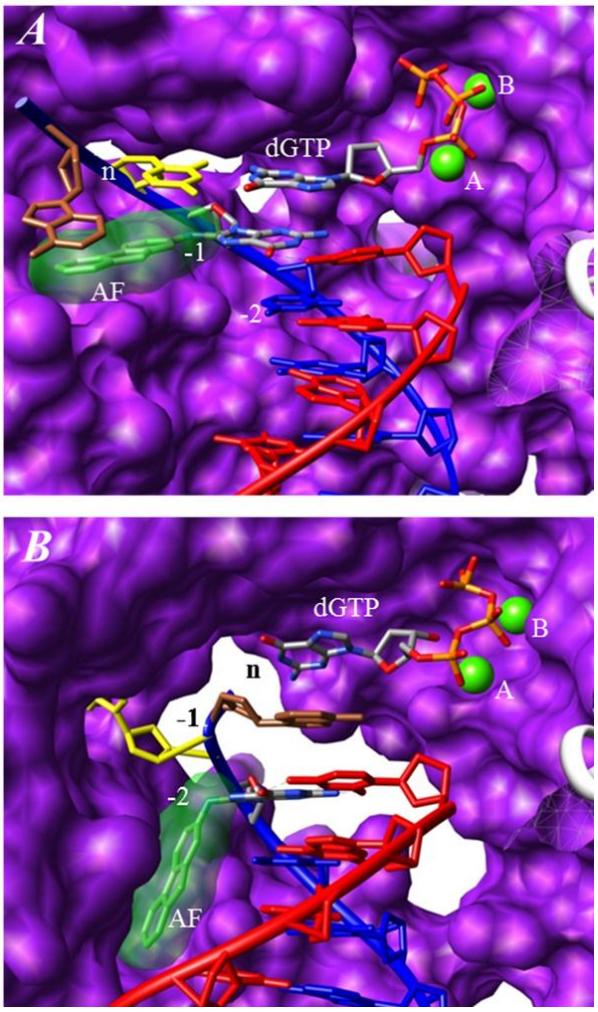

Figure 15. Two structures of Dpo4 ternary complexes in the presence of a dG-C8-AF adducted template. (A) Correctly aligned primer template with the dGTP and corresponding template dC correctly at the 0 position. The adducted dG retains base paring with its corresponding dC while the AF is positioned towards the major groove and stacks in a pocket of the little fingers domain. The +1 templating base stacks on top of the AF adduct and is in alignment with the 0 position. (B) The misaligned structure contains the templating base in a looped out structure. The looped out base slides into a pocket, rotated away from the active site. As a consequence the +1 templating base rotates and stacks on top of the adducted dG base, and the DNA is shifted downwards as the +1 base now occupies the -1 position within the polymerase. The AF adduct is rotated downwards and placed into a hydrophobic pocket within the little fingers domain. The dGTP does not contain any Watson-Crick binding partner as it occupies the 0 position and stacks onto of the template base below.

pair is shifted upstream relative to the polymerase to the -2 position, as the adjacent 5' template C loops out of the helix towards the major groove, stacking with the little fingers domain (Figure 15B). Again, the AF adduct is on the side of the major groove and situated within a pocket on the little fingers. The 0 template base is rotated back into the helix and occupies the post-insertion site (-1 position) as the incoming dGTP stacks on top of it in the insertion site (occupying the n position). Consequently, the incoming nucleotide does not possess a Watson-Crick hydrogen binding partner.

Interestingly, the correctly pairing ternary structure of molecule 1 was poised in resemblance to a binary like state which is incapable of performing catalysis without additional rearrangements. However, the misaligned structure of molecule 2 showed an uncanny resemblance to the ternary complex of Dpo4, with protein-DNA interactions similar to that of the ternary complex. It should be noted however that the misaligned structure of molecule 2, despite being arranged similar to a ternary complex, would also require further rearrangements in order to achieve a catalytic state.

The ability of Dpo4 to not only accommodate the bulky AF lesion but also to stabilize its position by binding to the little fingers domain that only Y family polymerases possess, is indicative of its design for its role in lesion bypass. In addition, Dpo4's ability to further utilize its specialized little finger domain to stabilize primer-template misalignments strengthens its ability to cope with distorting lesions, albeit at the expense of increasing mutagenicity. This paper also shows that misaligned structures are not only stabilized by the Watson-Crick base-pairing of the misaligned structure, but also,

and possibly more so by direct interactions of the polymerase with the misaligned complex (*91*).

III. MALDI-TOF MS

A. Theory

The ability to measure the masses of molecules greatly aids in the physical characterization of samples. Matrix-assisted laser desorption ionization time-of-flight mass spectrometry (MALDI-TOF MS) obtains mass spectra by ionizing a sample and accelerating the ions over a fixed distance to a detector, where the relative ion abundance along with the time of flight, are used to calculate the mass spectrum based upon the mass to charge ratio (*92*).

The ionization process is achieved by co-crystallizing sample with a suitable matrix. The matrix is typically a low molecular weight compound that readily absorbs the laser light in the UV region. The matrix functions to increase the ionization and vaporization processes of the sample by absorbing pulsed laser light. The absorption of this energy ionizes and vaporizes matrix which carries the sample into the vapour phase and transfers charge to the sample (*93*). The now charged sample is accelerated through a field-free drift tube using electric and magnetic fields. The time required to traverse the distance from the source to the detector is related to the mass and charge of the sample species. For two samples with the same given charge, the sample molecules having larger mass will take longer to reach the detector. Similarly, for two samples of the same given mass, the sample molecules having the smaller charge will take longer to reach the

detector. Thus, based upon the time of flight a mass to charge (m/z) ratio of a particular species can be determined.

B. Use in Biological Systems

MALDI-TOF mass spectrometry is able to accurately determine masses of a wide range, making it useful for biological studies. Large molecules such as proteins and nucleic acids are routinely examined by MALDI-TOF MS in order to rapidly ascertain an accurate mass of the molecule. In addition to this type of simple characterization, MALDI-TOF MS can also be used for more sophisticated characterizations such as sequencing by exonuclease digestion (*94, 95*), sequencing by a Sanger type method (*96, 97*), single nucleotide polymorphism (SNP) analysis (*98, 99*), analysis of DNA-protein interactions (*100, 101*), and identification of covalently bound carcinogenic adducts (*102-104*).

An important factor in the analysis of biomolecules by MALDI-TOF MS is the method used to prepare the sample for analysis. It is well-established that the matrix used plays a crucial role in both the vaporization and ionization process and utilizing the proper matix can greatly improve results (*105*). For DNA analysis, the most common matrix used is 3-hydroxypicolinic acid (3-HPA) because of its ability to give good vaporization and ionization with low levels of fragmentation. Various other matrices, such as 3-hydroxycoumarin, have also been shown to give promising results when used with DNA (*106*). The addition of additives such as sugars to the sample has aided in improving mass resolution by preventing the transfers of excess laser energy to the DNA molecules (*107*). Other research efforts have focused on techniques for spotting of

samples onto the MALDI plates and in this regard various methods have been developed to maximize the concentration of matrix and sample while still providing high-quality crystal growth (*108, 109*).

A second area of research focuses not on the matrix and sample preparation but instead on the support where the sample is spotted prior to laser ionization. Most commercial systems use steel plates because of their high durability, evenness of the surface, and ease of cleaning the surface following use. Several methods have been developed to achieve higher resolution or better spotting properties, including Teflon coatings to anchored gold particles (*108-110*), sheets of Parafilm (*111*), and paraffin wax (*112*). Despite the advantages these hydrophobic coatings may confer, each suffers from numerous drawbacks. The Teflon-coated gold surface is difficult to prepare and very expensive. Methods that used Parafilm sheets placed on top of a steel plate are often not compatible with the strict tolerances of the sample chamber in commercial instruments and further suffer from the reliance on the use of internal standards because of the unevenness of the Parafilm layer thickness.

IV. Surface Plasmon Resonance

A. History

One method that has grown widely in use over the last two decades for investigating the binding of various molecules and proteins is surface plasmon resonance (SPR). SPR is capable of measuring, in real time and label free, the binding of an analyte to a ligand. SPR was first indirectly observed in 1902 by Wood, whom noted varying

light and dark bands in the reflected light when he reflected polarized light through a diffraction grating placed on the surface of a mirror (*113, 114*). An interpretation of these results would follow shortly in 1907, described by Lord Rayleigh, and then built upon from 1936 to 1941 by Fano (*115-117*). Despite the first published observations in 1907 by Wood, a complete physical description of the results would not be purposed until 61 years later, in 1968, by Andreas Otto, and in the same year by Kretschmann and Reather (*118, 119*). They noted that the phenomena observed and reported prior could be explained by the excitation of surface plasmons. Briefly after this explanation was purposed, Leidberg *et al.* had come up with a method to utilize this phenomenon to investigate the binding of biomolecules, specifically immunoglobulin's, while designing a laboratory experiment for undergraduate students to explore surface plasmons (*120*). This informal experiment directly paved the road for the upcoming development of commercial Biacore systems that are available today.

B. Physical Description

When p-polarized light is reflected off of a surface at varying angles great than the critical angle, such that total internal reflection occurs, the energy of the reflected photons typically will not vary with a change in the angle of reflection. However, the following will described that if surface plasmon resonance is possible at the interface of two mediums, then the reflected light intensity will vary with a change in angle of the reflected light, and a minimum will form at the angle that generates plasmon resonance.

To begin, surface plasmons can be found at the interface between a metal and a dielectric medium. At this interface, a charge density wave can exist due to the free

conduction electrons found in the metal. It should be noted that some authors describe this charge density wave an electromagnetic wave that is strongly bound to the interface of the two materials. The undulating nature of this wave allows a resonance to be established upon proper excitation. The excitation of these surface plasmons can occur when the energy and momentum of an incoming photon matches that of the charge density wave on the surface of the metal (*121*).

Due to the overlap of these coordinated waves, the result is a transfer of energy from the photon to the charge density wave on the metal surface via an evanescent wave. However, the energy and momentum of the incident photon, and consequently the energy of the evanescent wave, will vary with varying angles of total internal reflection. Thus, only angles of reflection that cause the energy and momentum of the evanescent wave, generated by the incident photon, to coincide with that of the charge density wave will cause resonance to take place. This can be seen in Figure 16A, with angle θ_b. In this example the incident light from θ_a and θ_c do not generate an evanescent wave capable of establishing resonance, however θ_b does. This causes a decrease in the reflected light intensity at this particular angle of reflection, due to the transfer of energy from the incident photon to the metal surface. If the reflected light intensity (reflectance) is plotted as a function of the angle of incidence, this event is registered as a sharp decrease in the reflected light intensity at a particular angle of reflection. This can be seen in Figure 16C, where the center of the dip (θ_b) corresponds to the angle that gave rise to the highest level of plasmon resonance.

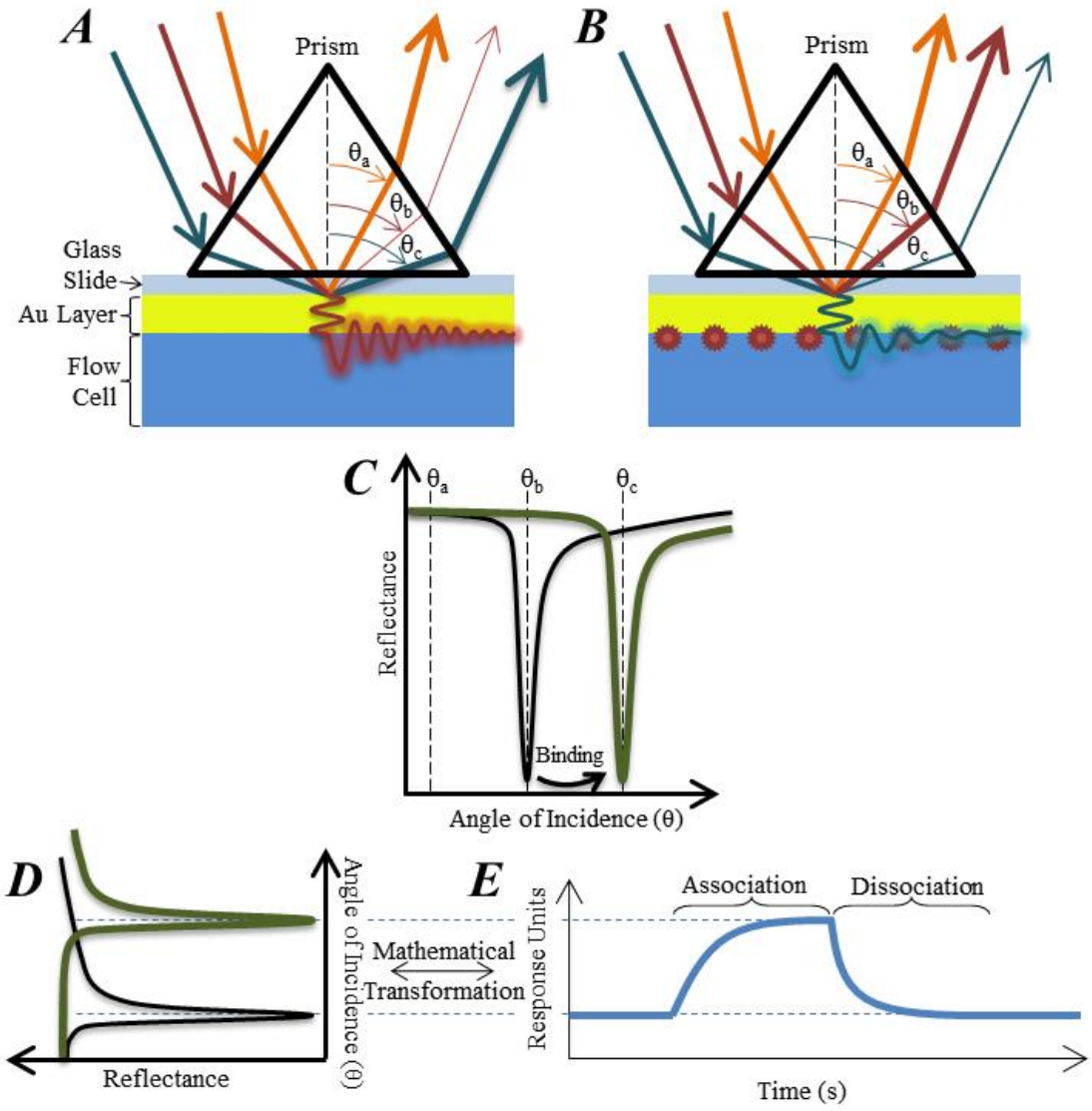

Figure 16. Principles of SPR. (A) Light at varying angles is reflected off a gold surface to produce an evanescent wave. A low mass at the surface will result in θ_b transferring energy to the plasmons and consequently having a weaker reflected light intensity. (B) An increase in mass (binding of red spheres) will cause light reflected at θ_c to now be of lowest intensity. C) Plots of the intensity of reflected light vs. angle of incidence shows the shift in the minimum reflectance upon binding of the biomolecules. Black line represents reflectance in figure A and green line represents reflectance in figure B. (D) Figure C rotated 90°. (E) The shift in angle in D is converted to response units by a mathematical transformation. This shift in the minimum reflectance is monitored in real time allowing direct observation of association and dissociation of biomolecules in what is termed a sensorgram.

The charge density wave, and its ability to resonate, is influenced by mass accumulation near this region. An accumulation of mass will cause the need for an evanescent wave of different energy and momentum in order to establish plasmon resonance, and hence a different angle of incident light will be required (Figure 16B). This accumulation of mass has the effect of shifting the dip in the reflectance as seen in Figure 16C. This shifting of the minimum reflectance can be monitored in real time and is expressed on a sensorgram where the shift in the minimum reflectance is plotted as response units (RU) on the Y axis, and it's real time change is monitored along the x axis (Figure 16E and E). A response unit is merely a mathematically transformed unit of the shift in reflectance, where the angle change generated from a mass change of approximately 1ng/mm on the surface (0.001˚) corresponds to a signal of 1000 response units.

C. Use for Biological Systems

The ability of surface plasmon resonance to monitor a change in mass on its surface opens the door to many biological studies. By covalently linking one molecule to the surface, binding can be visualized by flowing the other over the surface and monitoring any changes in the refractive index. This provides a direct means to monitor in real time the binding kinetics of biomolecules.

Several facets of SPR Biacore machinery provides benefits beyond those obtained for more classical binding experiments such as gel shift, anisotropy or circular dichroism. Because SRP allows the re-use of the same surface, and consequently the same substrate, very direct comparisons can be made between binding of different ligands. For example,

attachment of a potential target to the sensor surface followed by flowing of various antibodies over the same surface can identify which antibody sample has the highest affinity to the desired target. This allows rapid screening of large numbers of biosamples to identify potential binding interactions.

In addition, the multiple flow cells of the instrument allow the same ligand to be flowed over multiple covalently bound surfaces concomitantly, again allowing more direct comparisons between noted binding activities between various substrates. For example, if mutant and wild type proteins show small changes in binding to their targets, both of the proteins can be immobilized onto adjacent flow cells. During an injection of sample the same sample is flowed over both surfaces which will allow a sensitive comparison of the binding parameters of the two proteins.

SPR is also a very sensitive method for visualizing binding, and thus requires low levels of sample to be immobilized onto the sensor surface. This is beneficial when using limited quantities of precious sample. The immobilized sample is required in very low levels, and only one immobilization procedure is required for each experiment. However, the amounts of required sample that will be injected and flowed over the surface can be quite high, especially if high flow rates are used.

CHAPTER II: EXPERIMENTAL PROCEDURES

I. Materials

A. DNA Oligonucleotides

Unmodified, biotinylated, and fluorescein labelled DNA oligonucleotides (Figure 17A-F, and 17J-L) were purchased from either Midland Certified Inc. (Midland, TX), or MWG Operon (Huntsville, AL). All DNA was purchased as either GF grade desalted oligonucleotides or reverse phase HPLC purified, and further purified and verified as described under methods.

B. Protein

DNA polymerase I Klenow fragment of *Escherichia coli* was overexpressed and purified from a strain provided by Dr. Catherine Joyce of Yale University (New Haven, CT) as described in (57). The Klenow fragment used carries a D424A mutation that greatly reduces the 3'-5' exonuclease activity of the enzyme, yet does not affect its polymerase activity. Purification of the enzyme was graciously performed by Asad Ullah and Radoslaw Markiewicz.

C. Other Materials

Terminal deoxynucleotidyl transferase, 2'-deoxyribonucleotide 5'-triphosphates (dNTPs) and 2',3'-dideoxyribonucleotide 5'-triphosphates (ddNTPs) were purchased from USB Corp. The instrument used for all SPR biosensor experiments was a Biacore 2000 (Uppsala, Sweden). Carboxymethylated dextran 5 (CM5) research grade sensorchips and the amine coupling kit containing *N*-ethyl-*N*'-[3-(diethylamino)propyl]carbodiimide (EDC), *N*-hydroxysuccinimide (NHS), and 1 M

A	22mer Primer	5'-CAC GAA AAC GAC GGA ACG GTA T
B	28mer Primer	5'-CAC GAA AAC GAC GGA ACG GTA TCT ATG G
C	Biotin 17mer Temp	5'-(p)GTT CCG TCG TTT TCG TG-Biotin
D	Biotin 28mer Temp	5'-CCA TAG ATA CCG TTC CGT CGT TTT CGT G-Biotin
E	28mer Unmod Temp	5'-CCA TAG ATA CCG TTC CGT CGT TTT CGT G
F	11mer Temp	5'-CCA TAG ATA CC
G	23ddG Primer	5'-CAC GAA AAC GAC GGA ACG GTA TC
H	23ddC Primer	5'-CAC GAA AAC GAC GGA ACG GTA TT
I	23ddT Primer	5'-CAC GAA AAC GAC GGA ACG GTA TG
J	21mer Standard	5'-CAC GAA AAC GAC GGA ACG GTA
K	17mer Standard	5'-(p)GTT CCG TCG TTT TCG TG
L	21mer Unknown	5'-GGA GAG TGA TTG GTA GTG TGG
M	BP Mod 11mer Temp	5'-CCA TAG ATA CC (BP)
N	BP Mod 28mer Temp	5'-CCA TAG ATA CCG TTC CGT CGT TTT CGT G (BP)
O	BP Mod 16mer Temp	5'-TCT GCT TCC CCT CCT T (BP)
P	BP Mod 18mer Temp	5'-TCT CTG TCC CCT CCT TTT (BP)

Figure 17. List of DNA oligonucleotides used in this study. A, B, G-I were also used with a 5' end labelled fluorescein.

ethanolamine hydrochloride were also purchased from Biacore. Streptavidin was obtained from Sigma. All other general reagents were obtained from Fisher, Sigma-Aldrich, or VWR.

II. Methods

A. Unmodified DNA Studies

i. DNA Purification

All synthetic DNA oligonucleotides utilized in this study are shown in Figure 17. DNA was extensively purified via several rounds of reverse phase HPLC until a single peak was obtained on HPLC and confirmed via matrix assisted laser desorption ionization time of flight mass spectrometry (MALDI-TOF MS) analysis (method described under MALDI-TOF). A Thermo Fisher Scientific C18 column containing 5 µm particles was used on a Varian ProStar (Palo Alto, CA) with a Varian ProStar photo diode array (PDA) detector. Buffer A was 0.1 M triethylamine acetate (TEAA), pH 7.0, and buffer B was a 70% mixture of buffer A and 30% mixture of acetonitrile. Both buffers were degassed prior to running the HPLC, and subsequently degassed prior to a run if not used for longer than 24 hours. The column was pre-equilibrated at 10% buffer B for 10 minutes, then 14% buffer B for an additional 15 minutes prior to each run. A gradient of 14%B → 45%B over fifty minutes gave good separation of failure sequences. Minor adjustments to the starting percentage of buffer B from 1-4% and of the ending percentage of buffer B from 1-10% were performed, depending on oligonucleotides length and presence or absence of hydrophobic moieties such as biotin or a carcinogenic

adducts, in order to achieve optimum separation yet retain good peak resolution. Nevertheless, a 14%B → 45%B over fifty minutes proved to be adequate for most oligonucleotides used.

ii. Dideoxy Termination of Primers

Dideoxy terminated primers were obtained by 3' extension of the 22mer primer (Figure 17A) with a ddNTP using terminal deoxynucleotide transferase (TdT). This produces a primer lacking the 3'OH required for extension. Concentrations of oligonucleotides were determined using Abs_{260} and the calculated molar extinction co-efficients (*122*). Approximately 10 nmols (final concentration of 10 uM) of the 22mer primer was incubated with an excess of the appropriate ddNTP in 200 mM potassium cacodylate buffer, pH 7.0, 4 mM MgCl2, 1 mM 2-mercaptoethanol, and approximately 50-100 units of terminal deoxynucleotide transferase. The reaction was allowed to proceed for 6 hours at 37 ˚C which achieves near 100% completion. Following incubation the mixture was heated in boiling water for 5 minutes to terminate the reaction. This process was repeated to generate three different primers where the 3' terminal nucleotide was either a ddC, ddT, or ddG (Figure 17G, H and I respectively). The products were then directly purified via reverse phase HPLC as described above (refer to Unmodified DNA Studies, DNA Purification), and the products were analyzed by MALDI-TOF MS as described below (refer to sections MALDI-TOF Instrument Setup and Sample preparation and Spotting).

iii. Annealing Duplex DNA

Oligonucleotides were annealed by incubating a 3-5 fold excess of template in the appropriate buffer for 2 minutes in a water bath at 95°C. After 2 minutes the water bath was removed from the heat source and allowed to slowly cool to room temperature, typically taking approximately 1.5-2 hours. Duplexes for use in the SPR, containing either a terminal T:G mismatch, a correctly base paired C:G, or a terminal G:G mismatch at the -1 position (Figure 18 A, B, and C, respectively) were formed by mixing a 5 μM primer : 1 μM template ratio in HSM buffer (10 mM HEPES, pH 7.4, 150 mM NaCl, 10 mM MgCl2, and 0.05% P40), heating to 95 ˚C for 2 minutes then allowing to slowly cool to room temperature over 1.5-2 hours.

iv. Extension Assays

Extension assays were performed using a novel method in which fluorescein labelled primers were utilized in place of radiolabelled ^{32}P primers. Primers used are identical to the primers listed in Figure 17, however they are 5'-end labelled with fluorescein. Reactions were done with either a constant concentration of Klenow fragment varying the reaction time, or they were completed with a constant time and the concentration of Klenow fragment was varied. DNA was annealed in KB buffer (50 mM Tris, pH 7.5, 10 mM $MgCl_2$, 1 mM DTT, 0.05 mg/mL bovine serum albumin) so the final concentrations loaded per lane contained 200 fmols of labelled primer, and a 4-fold higher concentration of the template. After annealing, all four dNTPs were added to a final concentration of 400 uM. The reactions were initiated by adding the indicated amount of Klenow fragment and allowed to proceed for the indicated time. Reactions

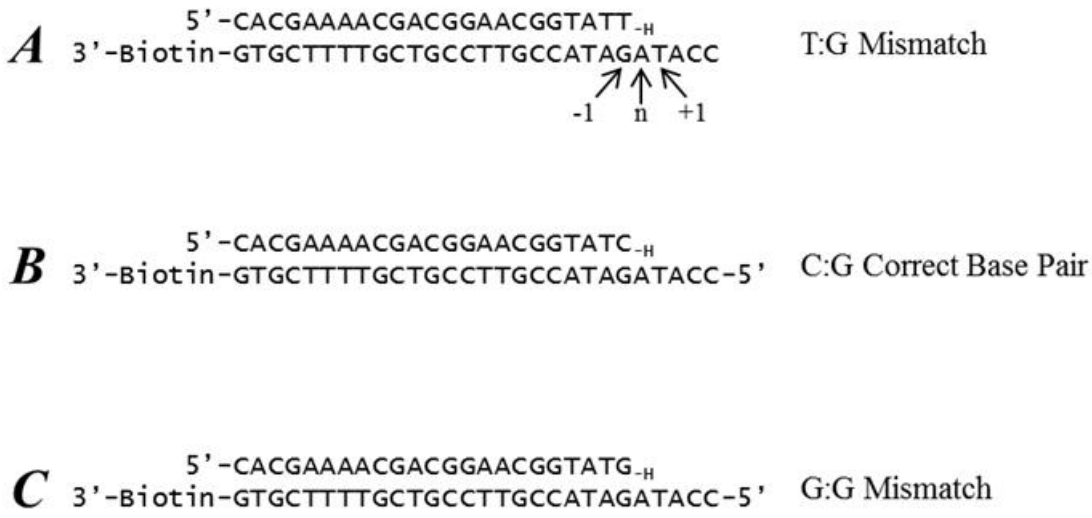

Figure 18. DNA Primer-template duplexes used in SPR experiments. Primer strands are dideoxyterminated at the 3' end to prevent extension. Template stands are 3'-biotinylated to allow capture onto streptavidin coated flow cells for SPR experiments. (A) Duplex containing a T:G mismatch at the primer terminus. This mismatch is positioned at the -1 position (post-insertion site) of the polymerase. (B) Correctly paired primer-template. (C) Mismatched primer-template with a G:G mismatch at the primer terminus.

were quenched by removing 10 uL aliquots at the indicated time and placing into 30 uL of bromophenol blue loading buffer (10 mg bromophenol blue, 10 mL formamide, 10 mM EDTA). Products were resolved by 20% PAGE and directly imaged using a Typhoon scanner.

v. Amine Coupling of Streptavidin to CM5 Sensorchip

The SPR biosensor instrument utilized for all experiments was a Biacore 2000 (Uppsala Sweden) in conjunction with a carboxymethylated dextran 5 (CM5) research grade sensorchip. Prior to amine coupling of the streptavidin, the dextran matrix of the chip was conditioned. To do so HBS-EP buffer (0.01 M HEPES, pH 7.4, 0.15 M NaCl, 3 mM EDTA, 0.005% P20) at a flow rate of 100uL/min, with a system temperature of 25 ˚C was flowed over the chip and three separate 10 µL portions of 10 mM NaOH were repeatedly injected, flowed by three separate 10 µL portions of 500 mM NaCl. All solutions and buffers were sterile filtered and degassed prior to use.

Streptavidin was bound to the sensorchip using the amine coupling kit and the Biacore Immobilization wizard within the accompanying Biacore control software. The flow rate was set to 5 µL/min of HBS-EP buffer (0.01 M HEPES, pH 7.4, 0.15 M NaCl, 3 mM EDTA, 0.005% P20), and the system temperature was kept at 25 ˚C. The immobilization was completed one flow cell (FC) at a time, starting with FC 4 and progressing towards FC 1, in order to achieve precise control over binding levels. The amine coupling kit contains 0.2 M N-ethyl-N'-[3-(diethylamino)propyl]carbodiimide (EDC), 0.05 M N-hydroxysuccinimide (NHS), and 1 M ethanolamine hydrochloride. A 35 µg/mL solution of streptavidin in 10 mM sodium acetate buffer, pH 5.0, was first

injected, and the relative slope governed by the rate of binding of the streptavidin to the sensor surface was calculated. Slopes of approximately 300 RU/min gave good results. The carboxymethylated dextran (CMD) layer of the sensorchip was then activated by injecting a 1:1 mixture of NHS and EDC. Following, repeated injections of the streptavidin solution were performed until the appropriate level of binding was obtained, which in most instances was set to 1000 RU in each individual flow cell unless otherwise indicated. The amount of streptavidin bound is calculated by taking the baseline signal prior to injecting streptavidin and subtracting this value from the baseline signal after the streptavidin injection is complete. This iterative process of injecting streptavidin and calculating the amount bound is repeated until the intended level of binding is reached. Once the intended level of binding is reached, a 1 M solution of ethanolamine is injected to quench any reactive NHS esters left over. The sensor surface was then washed with HBS-EP buffer to remove any non-bound streptavidin from the surface, and the process was repeated for the next flow cell.

vi. Duplexing and Binding of Unmodified DNA to the CM5 Sensorchip

Primer-template duplexes were annealed in HMS buffer (10 mM HEPES, pH 7.4, 150 mM NaCl, 10 mM $MgCl_2$, and 0.05% P20) by incubating a 5 µM : 1 µM mixture of primer to template. The excess of primer ensures that during duplex formation all template is annealed. It is of importance to note that this is the opposite ratio that is used for extension reactions and gel shift binding assays, where the primer must be limiting. The oligonucleotides mixture was then placed in a boiling water bath, and the bath was immediately removed from the heat source and allowed to cool slowly to room

temperature to anneal the DNA duplexes as indicated above (refer to Annealing Duplex DNA). A small portion of the resulting solutions were then diluted either 500 or 1000 fold to obtain 10-5 nM : 2-1 nM mixtures to be used for binding to the CM5 sensorchip. 10 nM : 2 nM concentrations allow relatively quick increases in binding levels whereas the 5 nM : 1 nM allowed precise control when adjusting the final amount of DNA bound to the matrix.

DNA templates contain a biotin modification at the 3' end, so capturing of the duplexes onto the sensor surface, which is now modified with streptavidin, is performed by simply flowing the DNA duplex over the sensor surface. Binding was accomplished at a flow rate of 5 μL/min of HSM buffer (10mM HEPES, 150 mM NaCl, 10 mM MgCl2, and 0.05% P20) at a temperature of 25 ˚C. Small quantities of 5-50 uL of diluted duplex mixtures of the appropriate primer and template were injected into the appropriate FC, followed by rinsing with HSM buffer. Binding levels were determined by subtracting the baseline level before injection with the baseline level after injection. This was repeated until DNA reached an immobilization level of approximately 15-100 RU, depending on the particular experiment. This process was then repeated with the remaining flow cells leaving FC 1 containing no DNA and only streptavidin, to serve as a reference flow cell to correct for non-specific binding and any bulk changes in the refractive index during injections of polymerase. For any particular experiment, DNA binding levels within each flow cell of the chip are within 5% of each other to allow direct observation of polymerase binding levels on each substrate.

vii. Dialysis of KF

KF solutions were prepared by dialyzing stock 33.5 µM KF using a Pierce Slide-A-Lyzer MINI eppendorf dialysis tube (Rockford, Il), having a 10 kDa cutoff membrane. The dialysis tube was placed into a distilled and filtered 1L water bath for 20 minutes to aid in the subsequent removal of glycerol. The dialysis tube was then placed into 1.5 L of 4 ˚C Tris buffer (50 mM Tris base, pH 7.44, 10 mM $MgCl_2$, 150 mM NaCl, 0.05% P20). The stock KF was then added into the dialysis tube and allowed to equilibrate for 6 hours. 6 hours of dialysis ensured the removal of all contaminants from the KF storage buffer (including glycerol), and was completed each time KF solutions were to be used on the SPR. To obtain the final concentration of KF in the dialysed solution the UV-VIS Abs_{280} was measured, and the concentration was calculated using an extinction co-efficient of 58,800 $Mol^{-1} \bullet cm^{-1}$.

viii. DNA Polymerase Binding Experiments

Three different DNA primer templates were immobilized previously onto three flow cells of the sensorchip so that KF binding to 3 various DNA constructs could be concomitantly examined. KF solutions, ranging from 0-600 nM were prepared from the dialysed KF, in Tris buffer or HMS buffer as indicated. These solutions contained either no nucleotide, or 0.4 mM of either dATP, dTTP, dGTP, dCTP, rUTP, or rATP. An automated method on the Biacore was written to simplify repeated injections of these various solutions. The flow rate was set to 35-50 µL/min, and 25-35 µL of sample was injected followed by a 170-1000 second dissociation in which only Tris buffer was flowed over the sensorchip, or buffer containing the same dNTP used for injection with

KF followed by a short time (~100 sec) in which only buffer was injected. This resulted in greater than 99% of polymerase falling off. This omission of a regeneration procedure ensured that the DNA substrate remains unchanged over several injections. The injections of sample were completed randomly to aid in removing any build-up or hysteresis type effects from previous injections, and repeated in triplicates. For experiments depicted in Figure 37 and 38 the concentration of NaCl within the Tris buffer was varied as indicated. The sensorgrams for all injections were collected in real time at a data rate of 60 Hz.

ix. Nucleotide Selectivity Assay

Twenty-five µL injections of 100 nM Klenow fragment solutions containing either dATP, dTTP, dCTP, or dGTP at a range of concentrations from 0 to 1 mM were injected at a flow rate of 50 µL/min in HSM buffer at 25 ˚C, followed by dissociation using only HSM buffer until greater than 99% of the polymerase had dissociated. For this experiment it is imperative to choose an enzyme concentration that is near the dissociation constant, allowing either an increase or decrease in binding to be observed. This omission of a regeneration procedure ensures that the DNA substrate remains unchanged over several injections. Samples were injected randomly, and repeated in triplicates unless otherwise noted. The sensorgrams for all injections were collected in real time at a data rate of 60 Hz.

x. Equilibrium Data Analysis

Data was analyzed by two methods; an equilibrium type method, where the equilibrium level obtained for injections of KF at various concentrations is plotted to

obtain a dissociation constant, and a direct method where the dissociation phases of the sensorgrams were fit to various equations to obtain off rates.

For the equilibrium method, Real-time sensorgrams were first reference-subtracted from flow cell one, which contains only streptavidin bound to the surface, and no DNA. The reference-subtracted average response at equilibrium was then plotted as a function of KF concentration ([KF]). This data is then fit to a rearranged form of the 1:1 Langmuir binding equation (eqn. 1).

$$RU = \frac{R_{max}}{1 + \left({K_D}/{[KF]} \right)} \quad (1)$$

Here R_{max} represents the theoretical maximum signal obtainable when the chip has reached full binding capacity, K_D is the dissociation constant, and RU is the response in response units. Data was fit using a non-linear regression least squares approach. Solver, an add on for Microsoft Excel, or Scrubber 2 (Biologics Inc., Australia) was utilized for the fitting of Equation 1 to the data by minimizing the residual differences between calculated data points and actual data points by varying the R_{max} and K_D. The RU values were then converted to % bound by taking the RU obtained for each data point and dividing it by the calculated R_{max} to obtain plots of % bound versus KF concentration. Theoretical R_{max} values were calculated based upon the known levels of DNA bound. The calculated R_{max} was compared to the theoretical R_{max} based upon known levels of bound DNA to verify its accuracy and reduce errors caused by multiple polymerases concurrently binding the same primer-template. The experimentally determined R_{max} values agree well with the theoretical R_{max} values. Tables depicting dissociation constants

are the average of three data fits, and the errors reported are the standard errors associated with each non-linear regression fit of the data.

To obtain dissociation rates for the various complexes, the data was modeled to single or double exponential decay Equation 2 or 3.

$$RU = R_{o1} * e^{-(k_d * t)} + R_\infty \quad (2)$$

$$RU = R_{o1} * e^{-(k_{d1} * t)} + R_{o2} * e^{-(k_{d2} * t)} + R_\infty \quad (3)$$

Again Microsoft Excel Solver, or Scrubber2 (BioLogic Software, Australia), was used to fit the equations to the data by minimizing the residual differences between calculated data points and actual data points. A modified version of equations 2 and 3 were used to fit the data, and also accurately determine the beginning of dissociation by utilizing a logic function in conjunction with Equations 2 and 3 to yield Equations 4 and 5.

$$RU = If(t \geq 0, R_{o1} * e^{-(k_d * t)} + R_{\infty,} R_{eql}) \quad (4)$$

$$RU = If(t \geq R_{o1} * e^{-(k_{d1} * t)} + R_{o2} * e^{-(k_{d2} * t)} + R_\infty, R_{eql}) \quad (5)$$

Here, t represents time, and if the time is before the beginning of the dissociation a linear equation with no slope is fit to the equilibrium level. At time 0, the beginning of the dissociation, the equation for either a single or a double exponential takes over and is fit to the remainder of the data where $t \geq 0$. R_{o1} is the initial response that will decrease as a function of the off rate k_{d1}, and R_{o2} is the initial response that will decrease as a function of the off rate k_{d2}. R_∞ is the response at infinity, and R_{eql} is the equilibrium response prior to the beginning of dissociation. Data fit using Scrubber was globally fit to multiple dissociation curves obtained for various concentration of enzyme injected. Errors represent standard deviation for three triplicate measurements.

xi. Nucleotide Selectivity Data Analysis

The average Klenow fragment equilibrium binding levels achieved in the absence of dNTPs were subtracted from the average equilibrium binding levels achieved in the presence of various concentrations of dNTPs. This provides a method for directly looking at the effects the addition of dNTPs has on KF-DNA binding. The results were plotted as a function of dNTP concentration. The baseline of this plot, or 0, would reflect a dNTP that does not affect the binding of Klenow fragment to DNA, giving the same binding levels as a binary KF-DNA complex; an upwards trend (positive values) would indicate that the included dNTP contributes to a higher level of binding, further stabilizing the complex; and a downwards trend (negative values) reflect dNTPs that would decrease the stability of the complex below that obtained with the binary KF-DNA alone. For the Y-axis +100% reflects the predicted RU level that would be obtained if all available DNA binding sites were occupied by Klenow fragment, and -100% reflects the binding level if all KF-DNA interactions are inhibited. Plots were fitted to a modified version of the hill equation (equation 4);

$$\text{Selectivity} = \frac{\mathrm{E_{max}} * [\mathrm{dNTP}]}{[\mathrm{dNTP}] + (\mathrm{S_f})} \tag{4}$$

where E_{max} is the maximum effect from addition of the dNTP, $[dNTP]$ is the concentration of dNTP, and S_f is the concentration of dNTP required to achieve half the effect from addition of the dNTP at infinite concentration, or the dNTP concentration required to achieve half of the E_{max}. This assay allows a direct visualization of the effect

inclusion of a substrate, in this case dNTPs, has on the binding of the enzyme, and introduces two parameters that describe this effect.

B. BP Modified DNA Studies

i. Modification of DNA with (-)-trans-anti-benzo[a]pyrene

Prior to oligomer modification with B[a]P, the DNA substrate (Figure 17F) was purified as described above (refer to Unmodified DNA studies, DNA purification) and dried down in a speedvac. A racemic mixture of (±)-*anti*-B[a]PDE (National Cancer Institute Chemical Reference Standard Repository, Kansas City, MO) in a 19:1 THF:TEA mixture was mixed with the oligonucleotides (1 mM) in a 1000:1 ratio, in BP reaction buffer (25 mM Tris, pH 10.87, 300 mM NaCl, 1.5% TEA) and allowed to react at room temperature for 48 hours (*123*). Subsequently the mixture was centrifuged at 10000 RPM for 5 minutes and the supernatant was collected and filtered through 0.45 µm Durapore PVDF filters (Bedford, MA). This is done to remove any unreacted and precipitated benzo[a]pyrene tetrol products. The solution was then diluted 3x with buffer A (0.1 M TEAA, pH 7.0), and HPLC purified on a Thermo Fisher Scientific 250 mm x 4.0 mm Hypersil ODS, 5µm C18 column. Buffer A consisted of 0.1M TEAA, pH 7.0, and buffer B was 65% ACN with 35% buffer A, and a gradient of 16% buffer B to 44% buffer B over 80 minutes was run. The HPLC generates a single large unmodified DNA peak, followed by 4 major B[a]P-N^2-dG modified peaks. Each peak was collected and dried down for anaylsis by circular dichroism (refer to Unmodified DNA Studies, Circular Dichroism) and MALDI-TOF analysis (refer to sections MALDI-TOF Instrument Setup and Sample Preparation and Spotting).

ii. Circular Dichroism

CD spectra were obtained for the oligonucleotides in single stranded form (*60*). DNA previously modified with B[a]P and purified via HPLC was re-suspended in 400 uL of distilled water (approximately 8-12 μM). Spectra were obtained on an Applied Photophysics Chirascan (Leatherhead, United Kingdom). Spectra were scanned from 200 nm to 400 nm at 1 nm steps, 0.75 seconds/datapoint, 10 mm pathlength, 25 ˚C, and averaged over 2-5 replicates. Subsequent analysis was performed on the accompanying Photophysics Chirascan Pro-Data software.

iii. Ligation of Benzo[a]pyrene Modified DNA

The 11mer (-)-*trans*-*anti*-B[a]P-N^2-dG modified oligonucleotide (Figure 17M) was ligated to 17mer biotinylated (Figure 17C) modified oligos using a 28mer scaffolding primer (Figure 17B) to form a full length duplex, and T4 DNA ligase was used to ligate the two template pieces (Figure 19). Specifically, a mixture of 2500 pmols of 28mer Primer, 2500 pmols of Biotin 17mer temp, and 500 pmols of BP Mod 11mer Temp was mixed and annealed in 200 uL of T4 ligation buffer (66 mM Tris-HCl, pH 7.6, 6.6 mM MgCl2, 10 mM DTT, 66 μM ATP). The mixture was annealed by placing in a boiling water bath and the bath was immediately removed from the heat source and allowed to cool slowly to room temperature. Once annealed, the solution was placed into a 16 ˚C bath for 10 minutes, and then 2 uL (2 units) of T4 DNA ligase were added to the solution. The mixture was allowed to incubate at 16 ˚C for 16-24 hours prior to purification.

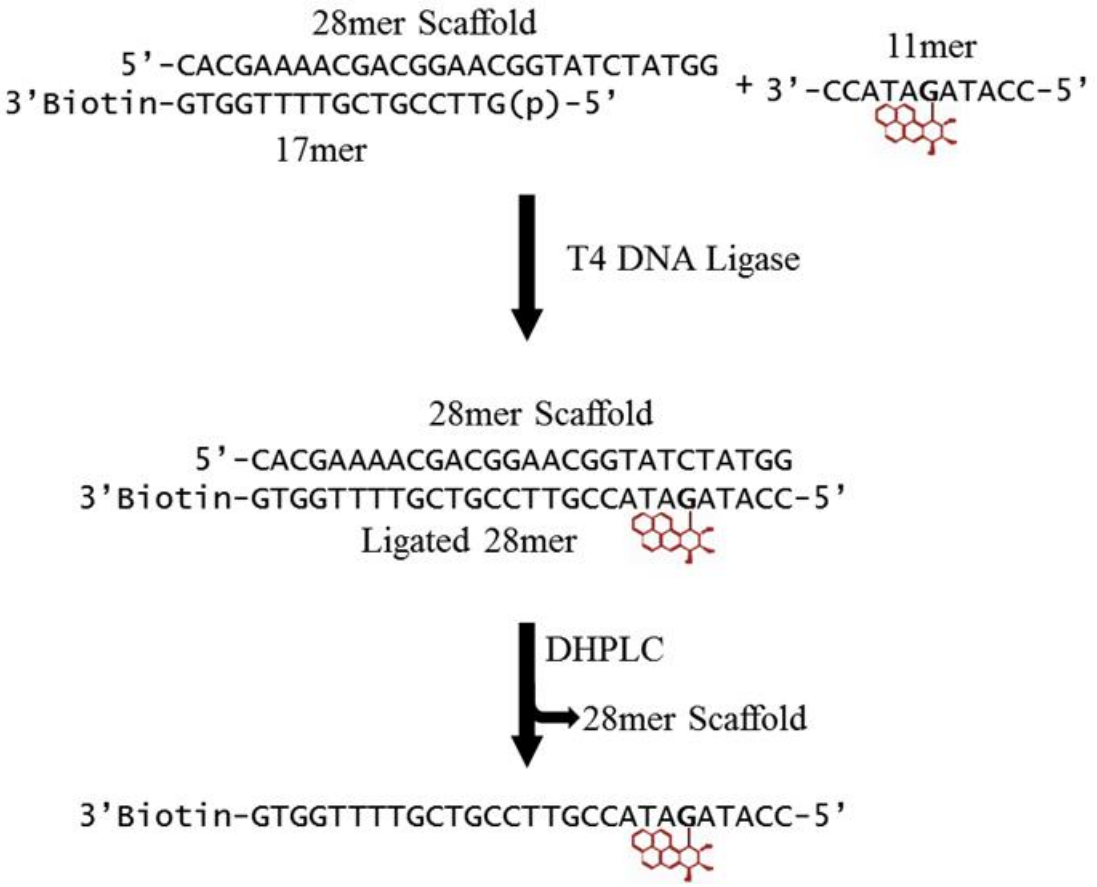

Figure 19. Ligation of (-)-*trans*-*anti*-B[a]P-N2-dG modified 11mer to form a 28mer modified template to be used in SPR experiments. A 28mer scaffolding oligonucleotide serves to hold the B[a]P modified 11mer and the 3'biotinylated and 5' phosphorylated 17mer for ligation. Following ligation a DHPLC protocol is utilized to separate the B[a]P modified 28mer from the 28mer scaffold, remaining 17mer, and any unreacted B[a]P modified 11mer.

iv. DHPLC of Ligation Mixtures

Ligation mixtures were separated out by using a novel denaturing HPLC procedure. A Hamilton PRP-1 (polymeric reverse phase), 10 µm, 100 Å, 4.1 mm x 250 mm column, submerged in a water bath at 74 ˚C was used. The buffer system consisted of buffer A; 0.1 M TEAA, pH 7.0, and buffer B; 30% ACN, 60% buffer A, and a gradient of 27% to 80% buffer B over 80 minutes was run. (-)-*trans*-*anti*-B[a]P-N^2-dG modified 28mer products are easily separated from the remaining oligonucleotides. Products were collected and analyzed by MALDI-TOF MS as described in sections MALDI-TOF Instrument Setup and Sample preparation and spotting.

v. CM5 Chip Preparation with Benzo[a]pyrene Modified DNA

A new sensorchip was coated with 1000 RU of streptavidin using the methods described under the section Unmodified DNA Studies, Amine Coupling of Streptavidin to CM5 Sensorchip. Duplexes containing either a terminal T:G-B[a]P mismatch, a correctly base paired C:G-B[a]P, or a terminal G:G-B[a]P mismatch at the -1 position (Figure 20A, B, and C respectively) were annealed by mixing a 5 µM primer : 1 µM template ratio in HSM buffer (10 mM HEPES, pH 7.4, 150 mM NaCl, 10 mM MgCl2, and 0.05% P20), heating to 95 ˚C for 2 minutes then allowing to slowly cool to room temperature over ~1.5 hours.

vi. DNA Polymerase Binding Experiments

All polymerase binding experiments were done in Tris running buffer (50 mM Tris, pH 7.5, 10 mM $MgCl_2$, 150 mM NaCl, 0.05% P20), at 25 ˚C. KF was dialysed as described under Unmodified DNA Studies, KF Dialysis. KF injections were performed

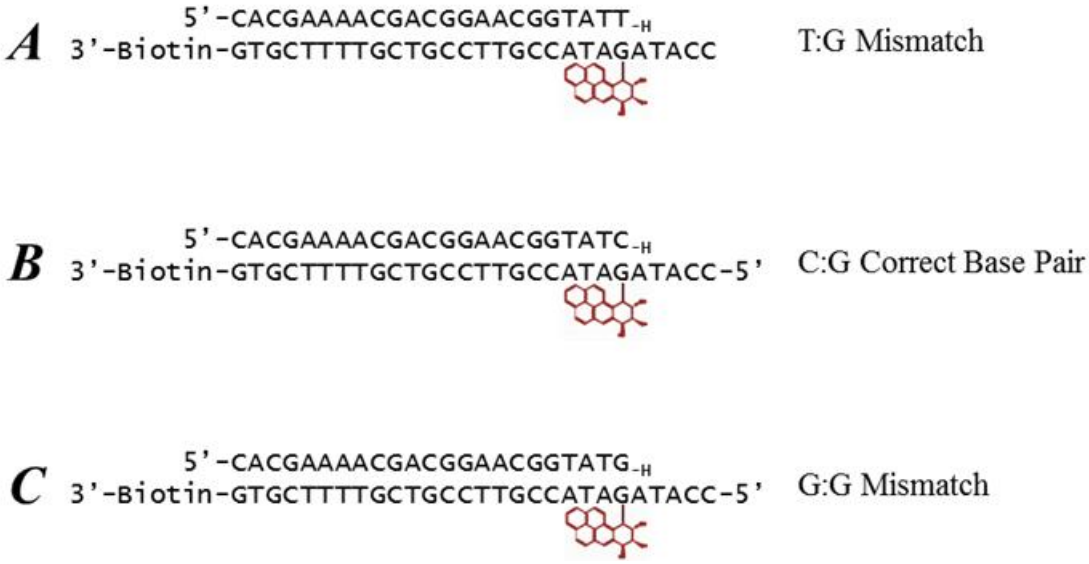

Figure 20. (-)-*trans*-*anti*-B[a]P-N2-dG modified DNA primer-template duplexes used in SPR experiments. Primer strands are dideoxyterminated at the 3' end to prevent extension during injection of Klenow fragment. (A) T:G-B[a]P mismatch positioned at the -1 position. (B) C:G-B[a]P correct base pair positioned at the -1 position. (C) G:G-B[a]P mismatch positioned at the -1 position.

similarly to those described under Unmodified DNA Studies, DNA Polymerase Binding Experiments. 35 µL of Klenow fragment solutions ranging in concentration from 0 to 200 nM, and containing 0.4 mM of either dATP, dTTP, dGTP, dCTP, rUTP, rATP, or no dNTP, were injected at a flow rate of 35 µL/min. Dissociation was accomplished by injecting 170 uL of Tris running buffer containing the same dNTP at 0.4 mM used during the injection. A regeneration procedure was not required as the dissociation with Tris-dNTP was sufficient to remove 99% of bound polymerase. This omission of a regeneration procedure ensures that the DNA substrate remains unchanged over several injections. Samples were injected randomly and repeated in triplicates. Sensorgrams were collected in real time at a data rate of 60 Hz.

vii. Data Analysis

Data analysis was performed as described under Unmodified DNA Studies, Data Analysis.

C. MALDI-TOF

i. MALDI-TOF Instrument Setup

MALDI-TOF mass data was obtained using a Bruker Ultraflex MALDI-TOF mass spectrophotometer. The instrument was operated in the linear positive ion mode with a pulsed ion extraction time of 150 ns. The acceleration voltages were 21 kV and 19.5 kV on ion sources 1 and 2 respectively. The lens voltage was 5 kV. A nitrogen laser (λ = 337 nm) at a frequency of 20 Hz and an energy of 126.7 uJ was utilized. The laser power was adjusted to maximize signal intensity without distorting the baseline surrounding sample peaks. No matrix suppression was used. The plate used for all

experiments was a MTP 384 ground steel target plate (Part No. 209519, Bruker Daltonik, Bremen Germany). Collected MALDI-TOF data was analysed and processed using the accompanying Bruker Daltonik's Flex Analysis software.

Lower molecular weight oligonucleotides (< 10 kDa) were also shot in the reflectron positive mode. Reflectron positive mode gives better mass resolution than linear positive mode, however it should be noted that with larger molecules it becomes increasingly difficult to obtain sensible mass spectra.

ii. Preparation of Parafilm-coated MALDI-TOF plate

A saturated solution of Parafilm "M" (Pechiney Plastic Packaging, Menasha, WI 54952) in hexane was created by cutting up pieces of Parafilm to approximately 5 mm by 5 mm, vortexing them in hexane (approximately 0.125 ml of hexane per 5 mm square) and leaving the solution overnight at room temperature in a sealed container. Small quantities (100-300 µL) of the supernatant were removed and filtered twice through Millipore Ultrafree-MC 0.45 µm centrifugal filters immediately prior to coating the ground steel plate. The filtered solution (20 µL) was pipetted along the margin of the plate (Figure 21A dashed oval region) and immediately spread across the length of the plate using a smoothened straight edge of a plastic ruler while maintaining a very light constant pressure. The layer was left for at least 30 minutes before proceeding with sample spotting. The thin Parafilm layer was then examined under a stereomicroscope to ensure a homogenous layer was obtained and no uneven spots or contaminants were present.

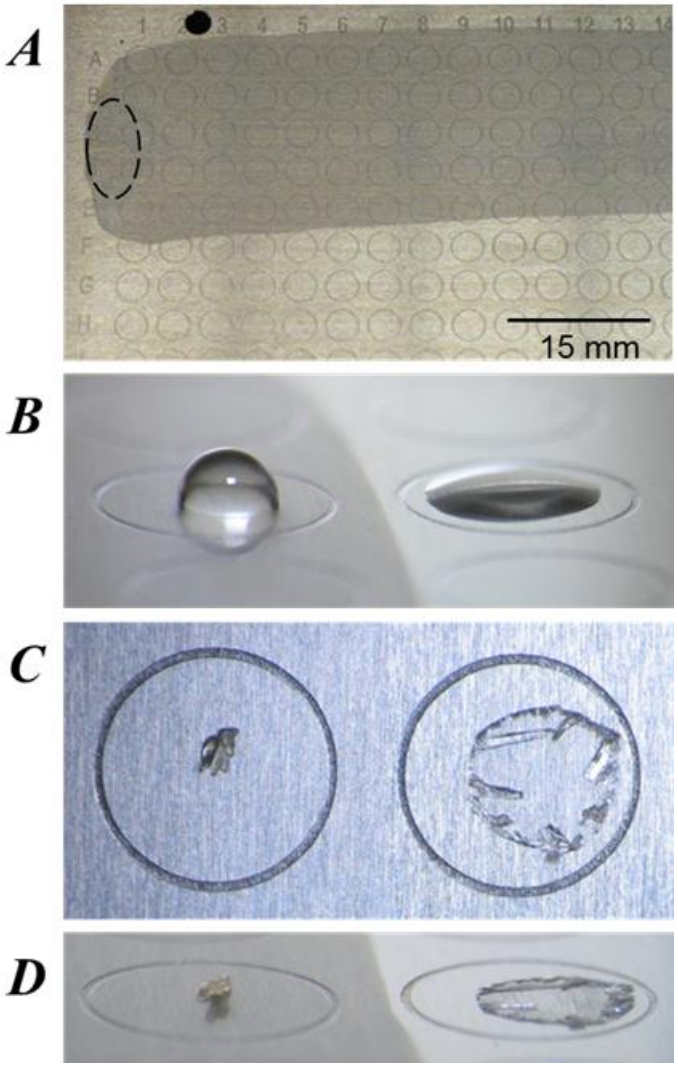

Figure 21. Comparison of thin layer Parafilm coating and ground steel surfaces. (A) Ground steel plate with Parafilm coating. Parafilm coated areas appear darker than uncoated ground steel. Dashed oval region is where initial 20 uL of solution is spotted before being spread across plate to right. (B) 2 uL of 25mM ammonium citrate containing 7.5% acetonitrile (v/v) on both Parafilm and steel (left and right respectively). (C) Top view of crystals on Parafilm and ground steel (left and right respectively). (D) Side view of (C).

iii. Sample Preparation and Spotting

The matrix used for all experiments was 3-hydroxypicolinic acid (3-HPA). A saturated solution of 3-HPA was made in 25 mM ammonium citrate containing 7.5% (v/v) acetonitrile. The saturated solution was then diluted to 75% saturation with the same citrated acetonitrile buffer. The diluted matrix (0.5-1 μL) was then spotted onto the Parafilm or steel surface and allowed to air dry under a vented cover. DNA samples, typically 1-25 pmols, were prepared in filtered deionised water and desalted using C_{18} Ziptips according to the manufacturer's directions. The DNA samples were eluted from the Ziptips using 1 μL of a 50% acetonitrile in water solution and spotted directly onto the matrix previously crystallized on the plate. The samples were allowed to air dry at room temperature under a vented cover and spots were subsequently examined under a stereomicroscope to ensure proper crystallization.

iv. Cleaning the Parafilm-coated Plate

Two options exist for cleaning the sample plate. The first option is to simply run a gentle stream of warm water over the plate for a few minutes until all matrix and sample have been removed. The hydrophobic Parafilm layer will remain intact on the plate as the sample and matrix are washed away and the coated plate can be subsequently reused in this form. The second method entails removal of the Parafilm layer. First the sample and matrix is removed as indicated above and then the Parafilm layer is removed by gently wiping the plate with a Kimwipe soaked with hexane. The Parafilm layer redissolves in the hexane and is easily removed. The plate may then be washed normally as indicated by

the manufacturer and recoated with Parafilm as described above (refer to Preparation of Parafilm-coated MALDI-TOF plate).

CHAPTER III: RESULTS

I. DNA Purification

A. Synthesis of Benzo[a]pyrene Modified 11mer Templates

To study the mechanism by which B[a]P affects polymerization, it is necessary to generate site-specifically modified DNA adducts. The purification of site-specifically labelled B[a]P oligonucleotides of defined stereochemistry is imperative to assigning the observed effects towards a particular isomer and structure. Site-specific modification is also necessary to be able to apply the observed affects towards specific portions of the polymerase mechanism that are affected by that particular stereoisomer. We utilized previously defined methods for the initial reaction of benzo[a]pyrene diol epoxides (BPDE) with short DNA templates that contain only one guanine (*124*).

To generate these site-specific B[a]P adducts, a racemic mixture of the physiologically relevant (+/-)-*anti*-B[a]PDE was reacted with a short 11mer oligonucleotide containing only one guanine residue in the middle of the sequence. The predominant products of this reaction are attachment at the N^2 position. Having the single guanine in the sequence ensures that modification at the guanine will be the major product, and complications from multiple labels will be reduced. However, the sequences used also contain several adenine residues that potentially could have been modified at the exocyclic N^6 position. Even though this reaction does occur, the quantity of this unwanted reaction is relatively low in comparison to quantities of the *anti*-B[a]P-N^2-dG adducts, and the adducted adenine products are quite easily separated from the desired guanine adducts by HPLC.

After the reaction is complete, the reaction mixture was run on an HPLC through a reverse phase C_{18} column. The HPLC allows each isomer to be separated from one another in a single run (Figure 22). Although one HPLC separation is sufficient to separate a significant amount of the products, second and third runs were made on each isolated product to ensure samples pure. According to several studies, the elution profile for the adducts follows the order (+)-*cis*, (-)-*trans*, (-)-*cis*, and lastly (+)-*trans*. In addition, the quantity of the (+)-trans-B[a]P-N^2-dG was greatest followed in quantity by the (-)-*trans*-*anti*-B[a]P-N^2-dG adduct. This is the expected relative quantity of each peak.

After each stereoisomer adduct was collected, circular dichroism (CD) spectra of the two largest peaks, presumably the (+) and (-)-*trans*-*anti*-B[a]P-N^2-dG stereoisomers, were obtained in order to validate the stereochemistry at the C10 position of these adducts. Coinciding with the typical elution profile, the suspected (+)-*trans*-*anti*-B[a]P-N^2-dG adduct exhibited a negative CD spectra at the B[a]P maximum absorbance peaks of approximately 334nm and 350nm, whereas the (-)-*trans*-*anti*-B[a]P-N^2-dG adduct displayed a strong positive CD spectra in these regions (Figure 23). The analysis of the CD spectra confirmed the orientations of all the B[a]P adducts collected (*60*).

B. Ligation to Form 28mer Templates

Subsequent to the validation of the B[a]P isomers, the 11mer oligonucleotides were ligated with 17 mer oligonucleotides using T4 DNA Ligase, generating a 28mer final product (Figure 19). The ligation products were separated using a novel HPLC

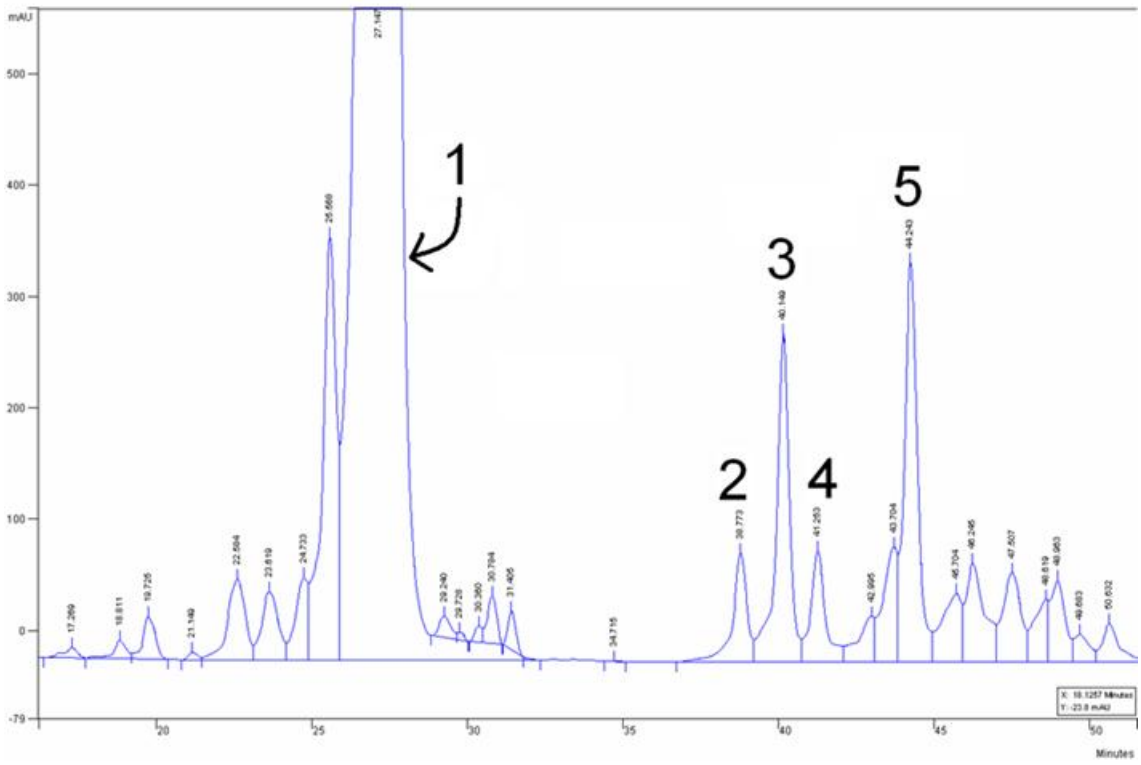

Figure 22. HPLC chromatogram after reaction of (+/-)-anti-B[a]PDE with 11mer oligonucleotide. Peak 1 is unmodified DNA, peaks 2, 3, 4 and 5 are (+)-*cis*, (-)-*trans*, (-)-*cis*, and (+)-*trans* stereoisomers respectively.

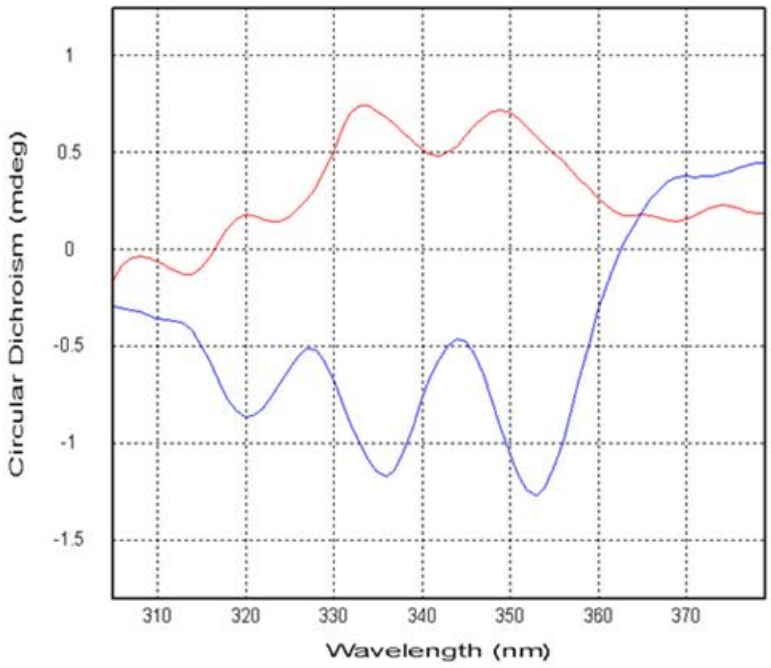

Figure 23. CD spectra of purified B[a]P oligonucleotides. The (-)-*trans*-*anti*-B[a]P-N^2-dG adduct spectra (blue) exhibited a negative CD spectra at the B[a]P maximum absorbance peaks of approximately 334 nm and 350 nm, indicating the C10 position has an S orientation. Conversely the (-)-*trans*-*anti*-B[a]P-N^2-dG adduct spectra (red) displayed a strong positive CD spectra in these regions, indicative of an R orientation of the C10 bond.

protocol employing a PRP polystyrene-divinylbenzene column at a temperature of 70ºC. The high temperature melts DNA duplexes and allows nucleotide separations based on length, permitting any unligated or complement oligonucleotides from eluting with the fully ligated 28mer product. Figure 24 displays a control set of experiments displaying the aforementioned separation. Figure 24A shows an injection of 11mer template (Figure 17F), 17mer biotin template (Figure 17C), and 28mer biotinylated template (Figure 17D). All three oligos are easily separated, with the 28mer template eluting last. Figure 24B shows a duplex mixture of 28mer primer and 28mer biotinylated template. The heating of the column melts the DNA duplex allowing both oligonucleotides to be easily separated. If the column is not heated, the DNA remains partially duplexed and the same level of separation is not achieved (data not shown). Using this method of separation, the ligation mixture for unmodified DNA was first separated (Figure 24C). Ligation was performed with a five-fold excess of the primer excess of 17mer template to ensure that all of the 11mer template would be duplexed. The expected HPLC peaks were obtained and the quantity of 28mer product indicated that the ligation procedure had achieved ~100% ligation.

This method of separation is vastly superior to previous methods in which the ligation products required separation by polyacrylamide gel electrophoresis, followed by a crush and soak procedure where typical loses vastly exceeded 50%. Obtaining product with minimal loss is essential when working with precious samples such as site-specifically B[a]P adducted oligonucleotides.

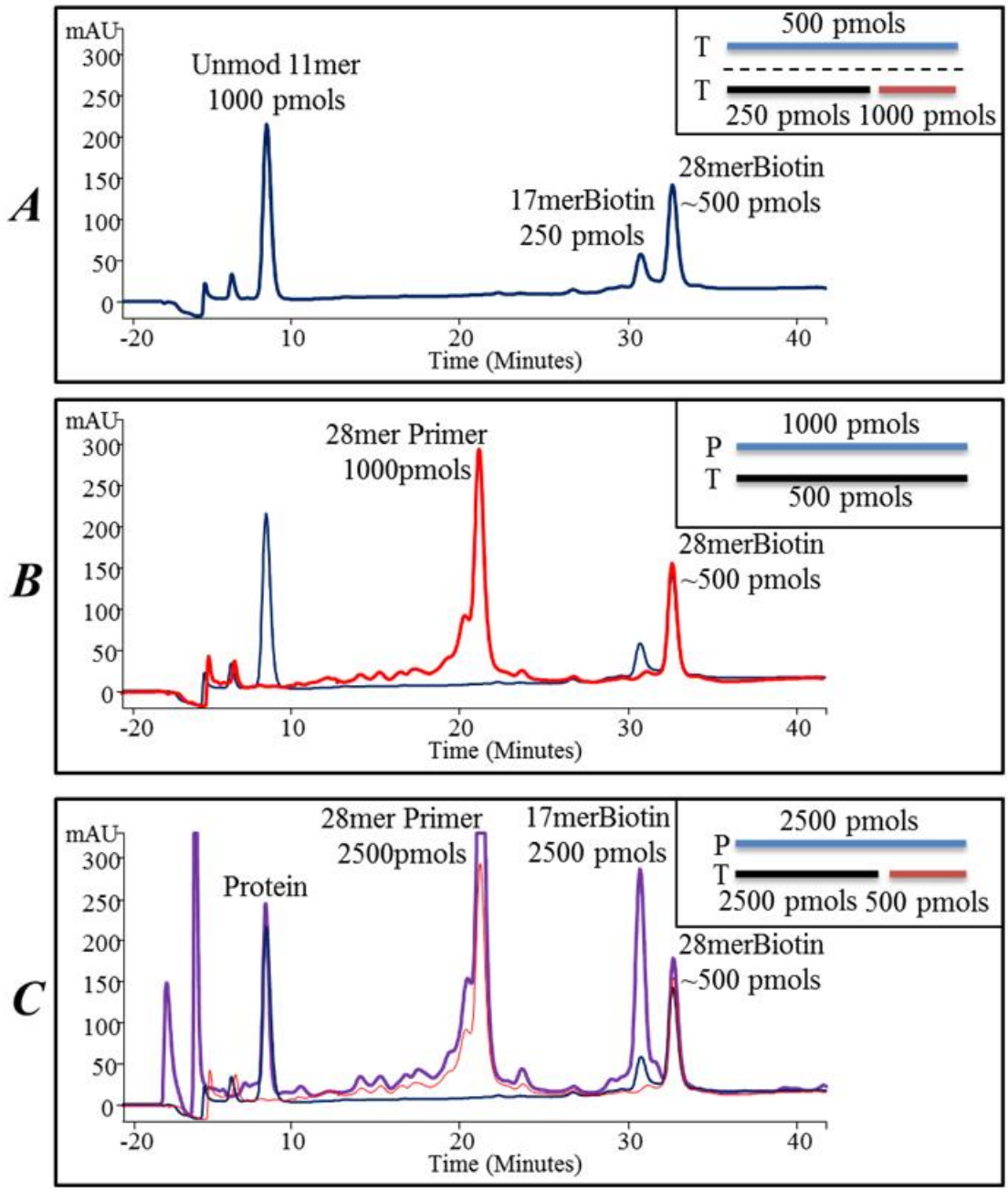

Figure 24. Ligation mixture separation on heated HPLC. (A) Three different template constructs were injected to monitor the elution times. (B) Primer-template duplex is injected (red line). The duplex fully separates. (C) Ligation mixture is injected (purple line). The fully ligated product is easily resolved from the 17mer biotinylated product. Based upon a theoretical maximum of 500 pmols of product the reaction appears to have gone to 100% completion.

The same ligation protocol was then followed to ligate the (-)-trans-B[a]P-N^2-dG adducted 11mer. Here, the separation of the scaffolding oligos is achieved to even a greater degree because the B[a]P-modified template is retained longer on the column than the unmodified templates. In addition, the modified ligated 28mer is retained longer than the unligated modified 11mer. Overall, all oligonucleotides have baseline separation and this new method of purifying the ligation products achieves a high level of purity with minimal loses of sample.

C. Fluorescein Labelled Extension Assays

Having generated site-specifically modified B[a]P-adducted oligonucleotides, as well as having isolated and verified the stereoisomers, extension experiments were done to once again confirm both the position and nature of the adduct. Figure 25A and B show two extension assays, the first with a primer extended across from the adduct, and one with the primer extended one position before the adduct. Under these conditions unmodified DNA is fully extended in one minute, however the presence of the adduct does not allow extension past the adducted template position. If the primer is backed up one position as in Figure 25B, it can be seen that polymerase is capable of incorporating a nucleotide into the primer across from the adduct but unable to extend the substrate any further. This characteristic where a dNTP can be inserted across from the adduct and inhibit further downstream extension, validated the position and identity of the adducted templates. Had the adduct been placed at a different position on the template, or have been a cis isomer, the extension of these two assays would have looked different. Had the adduct been positioned on an Adenine the extension would have occurred up to the

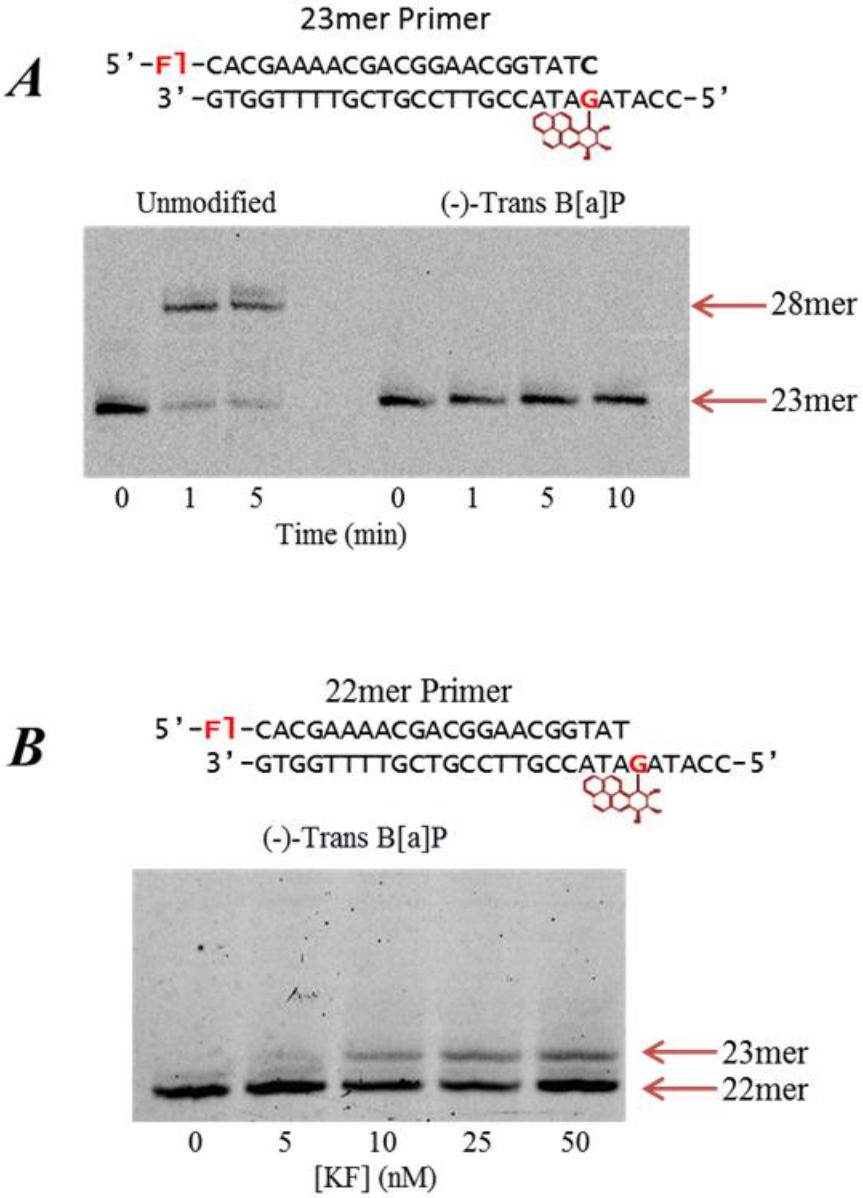

Figure 25. Extension assay of umodified and (-)-trans B[a]P adducted templates. (A) Extension performed with a 23mer primer that extends across from the adducted position and 5 nM KF. Unmodified templates show full extension in 1 min, whereas B[a]P containing templates show no extension. (B) Extension performed with a 22mer primer that ends one position before the adduct. Here polymerase is capable of incorporating a dNTP across from the adduct but further extension is again inhibited.

adducted position. Our extension is blocked at the expected adduct position. Also, had the adduct been a cis isomer, small amounts of extension past the adduct would be expected. Once again, the identity and position of the adducted templates were confirmed by this analysis.

II. MALDI-TOF Method Development

A. Characterization of Hydrophobic Coating and Crystal Formation

To prepare this hydrophobic layer small squares of Parafilm were dissolved in hexane to produce a saturated solution. This solution contains undissolved Parafilm and many very small strands of filamentous particles. Thus it is important to filter the solution through a 0.45 μm centrifugal filter immediately prior to use so the small particles do not create an uneven surface when it is spread on the steel plate.

To achieve a high degree of homogeneity and uniform thickness of the Parafilm layer on the steel MALDI-TOF plate, the short straight edge of a flexible plastic ruler was used to spread the hexane solution. A small amount of the solution (typically ~20 uL) was placed on the peripheral edge of the plate (Figure 21A dashed oval) and spread with the straight edge using a very light but constant pressure. The hydrophobic coating appeared darker grey against the brighter steel surface and the homogeneity of the coating was examined by both a visual inspection and a stereomicroscope examination. The consistency of the pressure as well as the smoothness of the applicator was critical in producing a good quality layer. A 20 μL volume of the Parafilm solution would generally cover 16-20 cm^2 of surface area on the plate (Figure 21A). With minimal practice 75

sample spotting areas could be coated with Parafilm where greater than 80% of the sample area was useful for sample spotting. It is important to carefully inspect the layer for irregularities so that these regions can be avoided when applying the sample spots. Typically, it is best to avoid the region where the 20 µL of Parafilm solution was initially spotted because of its non-uniform appearance.

The effect of the thin hydrophobic surface on the size and shape of the sample spotted onto the steel plate is shown in Figure 21B where equal volumes (2 µL) of a sample-matrix mixture were deposited on the uncoated plate (right sample) and the Parafilm-coated area (left sample). As one would expect, the hydrophobic layer causes the sample to bead up compared with sample spotted onto the steal surface. This results in the sample being concentrated into a much smaller area on the plate.

To further investigate the properties of the Parafilm coating, the contact angle of a water sample on the Parafilm coating was measured by microscopy. Figure 26C shows 2 uL of filtered deionized water placed onto a Parafilm coated area that was dried under argon after application of the Parafilm layer. The Parafilm coated area was dried with argon in order to maximize the contact angle by reducing nucleation sites from water trapped on the surface. With the argon dried Parafilm coated surface the contact angle was measured to be approximately 114º-117º. Comparison of Figure 21B right spot with Figure 26 shows the dramatic difference the hydrophobic coating makes upon the sample. This indicates that the Parafilm coating forms a true non-wetting surface because the measured contact angle was greater than 90º (Figure 26B). This is beneficial because the

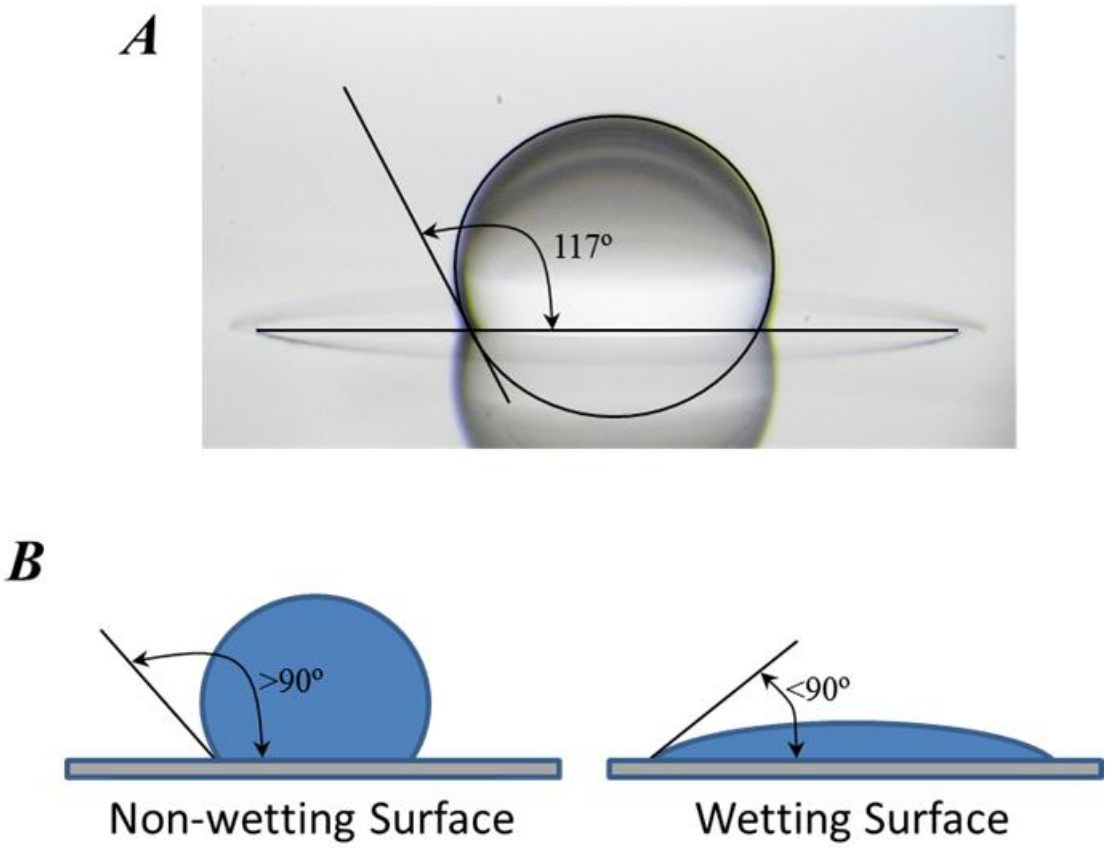

Figure 26. Measurement of contact angle. (A) 2 uL of filtered deionized water on parafilm coated surface gives a contact angle of approximately 117º. (B) Wetting and non wetting surfaces. A non-wetting surface (left) has a contact angle greater than 90º and consequently has a smaller surface area in contact with the surface than a wetting surface (right). In terms of sample crystallization this will result in samples being concentrated into a smaller area upon crystallization.

volume to surface area ratio is maximized by placing hydrophilic buffers on non-wetting surfaces.

Furthermore, because the volume to surface area ratio of the sample spot is higher on the Parafilm coating than on the ground steel the spots dry slower. In addition, the spots on the Parafilm shrink dramatically in diameter as they dry whereas the sample spots on the steel tend to flatten out. The slow drying helps slow crystal growth and helps formation of good crystals on the Parafilm coating. Consequently the crystals can be found throughout the entire area where the spot dried, whereas the crystals found on ground steel tend to be located at the peripheral edge of where the spot dried. The central localization of crystals further helps aid in finding the most beneficial signal. However, because the crystals tend to also grow up away from the plate as well, different signals and consequently different mass spectra can be obtained by shooting a high versus low crystal. Because of this, only the highest mass spectra obtained for a given sample are utilized when adding shots to generate the final mass spectra. The highest masses generated will represent sample that is closest to the Parafilm coating and thus supplies the user with a consistent bases for measurement. This is especially simple to do because of the wealth of usable signal obtained on the Parafilm coated plate.

Shown in Figures 21C and D are the resulting crystals formed after an oligonucleotide and matrix have dried on the Parafilm coating (left) and ground steel (right). As expected the crystals that formed on the hydrophobic surface are in a much smaller area compared with those formed on the steel surface. The side view of the crystals formed on the hydrophobic surface shown in Figure 21D indicates that there can

be some differences in the height of the crystals. As a result different signals and consequently different mass spectra can be obtained by shooting at a high spot versus low spot on the sample. Because of this, if external calibrations are being used, only mass spectra giving the highest masses obtained for a given sample are utilized when adding shots to generate the final mass spectra. It is of importance to note that the laser power should be adjusted slightly over the ionization threshold, and not any higher due to the shift in the m/z location of peaks. The highest masses generated using adequate laser powers will represent sample that is closest to the hydrophobic coating and thus supplies the user with a consistent bases for measurement.

B. Effect of a Parafilm Layer on MALDI-TOF Mass Spectra

We examined MALDI-TOF spectra obtained on the ground steel and the Parafilm-coated plate for DNA samples in the moderately low femto-mol range. Shown in Figure 27 is a direct comparison MS analysis of 93 fmol of three oligonucleotides spotted directly onto a steel plate or the Parafilm coating. From the onset of data collection several differences were noticed between obtaining sample data on the steel versus the Parafilm coating. The steel sample required a significantly longer time to locate usable regions of the sample crystal. On the contrary, crystals on the Parafilm coating proved easy to locate regions that gave suitable spectra. On average, the Parafilm coating was able to give these better results with 66% fewer shots than the ground steel plate. Moreover, the resolution of the spectra obtained on the Parafilm coating was sufficient that the $(M+salt)^+$ peaks, associated with both the internal standards as well as

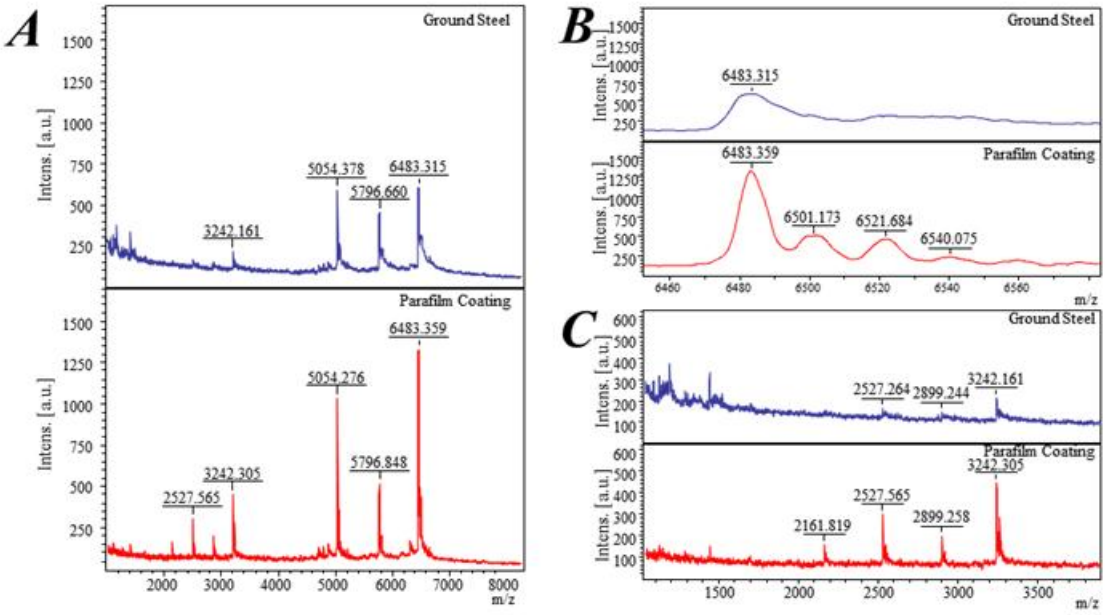

Figure 27. Comparison of MALDI-TOF mass spectra of DNA oligonucleotides on steel and Parafilm-coated steel plates. 83 fmols each of three oligonucleotides, a 16mer, 19mer, and 21mer, are displayed. (A) Top spectrum obtained from a steel plate and represents 40 laser shots. Bottom spectrum utilized a Parafilm-coated steel plate and represents 30 laser shots. (B) Expanded regions from 6400 to 6600 m/z for each spectra shown in A. (C) Expanded regions from 1000 to 3800 m/z for each spectra shown in A.

the unknown sample, were readably identified (Figure 27B). On the ground steel the region of the salt peaks appeared only as a broad hump adjacent to the major peak.

We also note that at these sample concentrations the sample located on the ground steel gives a spectra that lacks useable $(M+2H)^{2+}$ peaks and also has baseline drift in the lower mass range. In contrast, the sample on the Parafilm coating not only displays excellent $(M+2H)^{2+}$ peaks but also an $(M+3H)^{3+}$ peak, which allows calibration through a larger mass range without the insertion of additional internal standards. On the ground steel the additional noise under 1500 *m/z* may pose problems for researchers who wish to extract useful data out of this range while still maintaining useful data in the higher mass ranges (Figure 27C).

Due to the difference in locating usable regions of the crystal that give good signal on the Parafilm layer *vs*. the ground steel surface, we performed an area scan of crystals on both surfaces. The entire crystal surface area was analysed to locate regions of the crystal that gave low and high quality sample signals. Figure 28 shows the results of one such experiment. Regions of the crystal that gave low quality sample signal are displayed in enclosed white areas, and areas that gave high quality sample signal are displayed as black enclosed areas. Figure 28A displays a typical crystal obtained on the ground steel surface. In this case approximately 30% of the crystal area gave some sample signal but only about 1% of the area gave high quality signal. Using the Parafilm-coated plates increases the area giving usable signal to about 50% and increases the high quality signal to about 20%.

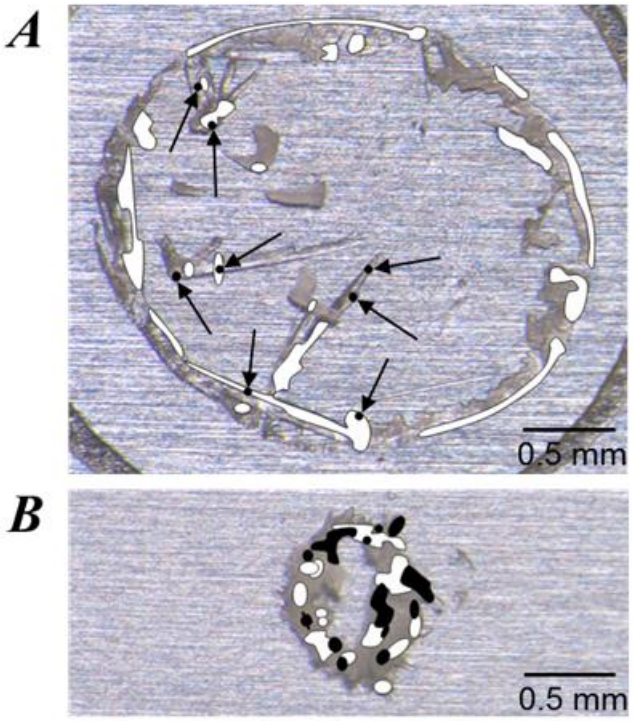

Figure 28. Area scan to locate regions of the crystal that gave high quality MS signals. (A) Crystal formed on ground steel surface: white enclosed areas indicate regions where MS signal could be observed and black areas (indicated by arrows) where high quality MS signals could be observed. (B) Crystal formed on the Parafilm coated surface: white enclosed areas indicate regions where MS signal could be observed and black areas where high quality MS signals could be observed.

C. Effect of a Parafilm Layer on Analysis of Labile Oligonucleotide Adducts

Several oligonucleotides ranging from 16 to 18-mers were modified with benzo[a]pyrene (B[a]P) and examined on the Parafilm-coated plates utilizing 17 and 21-mer oligonucleotides as internal standards. B[a]P has two peak major UV absorbances ranging from 346-355 and 330-336 nm, depending on the isomer of the adduct and the sequence context it is situated within (*60*). Because the nitrogen laser used excites at 337 nm, an absorbance that is close to the absorbance of B[a]P adduct, higher laser powers may cleave the B[a]P adduct from the DNA. The mass spectra obtained were internally calibrated using a quadratic fit to the $(M+H)^+$ and $(M+2H)^{2+}$ peaks of the 17 and 21-mers. A typical spectra for the (+)-*trans*-*anti*-B[a]P adducted 18-mer can been see in Figure 29. The resolution of the peaks was more than sufficient to easily identify the B[a]P modified oligo as well as several associated salt peaks. Four such peaks were identified as $(M+Na)^+$, $(M+K)^+$, $(M+Na+K)^+$ and $(M+2K)^+$ (Figure 29 insert).

As seen in Table 1, all four B[a]P isomeric adducts gave markedly similar spectra results with high mass accuracy as demonstrated by the very low error (< 0.05%) in the calculated masses. The FWHM is also relatively small indicating that the peaks are very narrow, mostly being in the 5-15 Dalton range, while still maintaining a high signal-to-noise ratio.

D. Use of External Standards When Using the Parafilm Layer

We chose to compare the use of external standards on steel and Parafilm-coated plates. In this case, 16 and 21-mer external standards were used to determine the mass of an unknown oligonucleotide. In this experiment it was important to aim at sample

Table I. Summary of four B[a]P adducted 18mer oligonucleotides analyzed using MALDI-TOF MS on a Parafilm-coated plate utilizing internal standards

Oligonucleotide	Calculated $(M+H)^+$ Mass	Measured $(M+H)^+$ Mass	% Error	FWHM	S:N Ratio
(-)-Cis B[a]P 18mer	5621.826	5621.645	3.22E-05	8.8	3776.7
(+)-Cis B[a]P 18mer	5621.826	5621.692	2.38E-05	5.9	3577.9
(-)-Trans B[a]P 18mer	5621.826	5622.122	5.27E-05	10.32	22127.1
(+)-Trans B[a]P 18mer	5621.826	5621.811	2.67E-06	6.562	7086.4

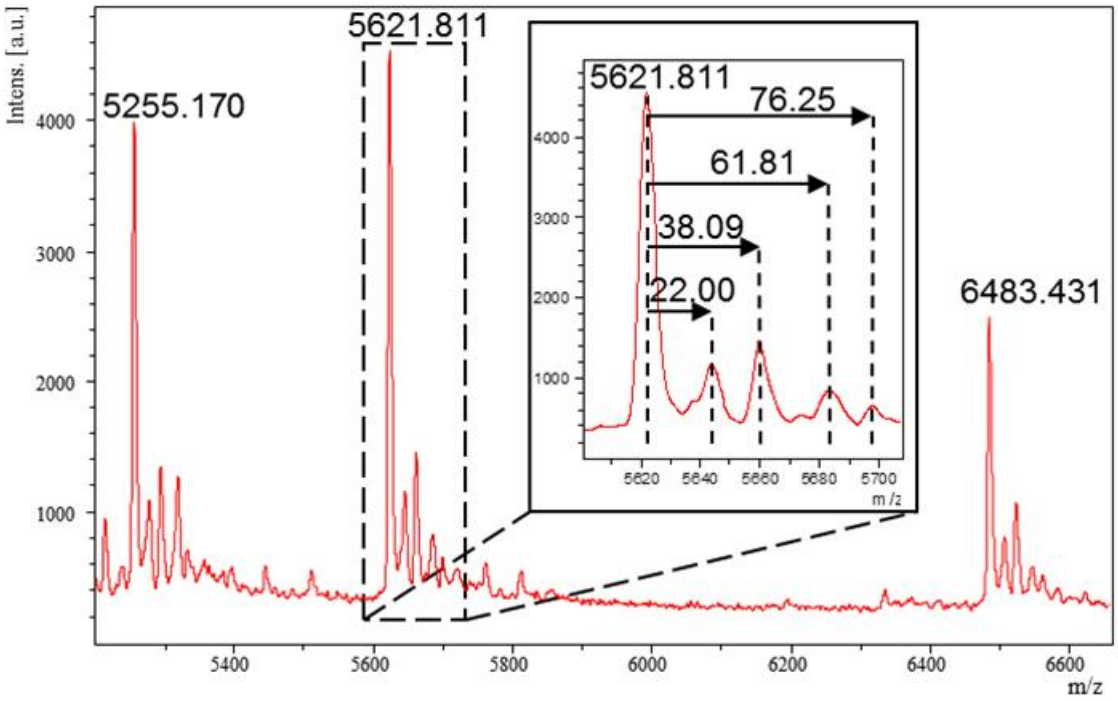

Figure 29. MALDI-TOF mass spectrum of a (+)-*trans*-*anti*-B[a]P-modified DNA oligonucleotide on a Parafilm-coated steel plate. An 18-mer modified with a (+)-*trans*-*anti*-B[a]P adduct was prepared and analyzed as described in the Materials and Methods section using a total of 30 laser shots. A 17-mer and a 21-mer were used as internal standards. The calculated average $(M+H)^+$ mass of the modified oligonucleotide is 5621.826. The spectra was calibrated using the $(M+H)^+$ and $(M+2H)^{2+}$ peaks for the 17-mer and 21-mer (far left and far right peaks respectively). (Insert) Expanded view of the modified oligonucleotide mass range (dashed box). The $(M+Na)^+$, (M+K)+, $(M+Na+K)^+$, and $(M+2K)^+$ peaks are clearly visible.

locations that gave the highest masses for peaks. This was done for both the external standard and the unknown sample in order to minimize variances in TOF due to the crystals height above the surface. Figure 30 displays the mass spectra of the unknown sample after calibration using the external standards. A remarkable similarity can be noted between the mass of the unknown obtained on the ground steel and mass of the unknown on the Parafilm coating. The unknown oligonucleotide was later disclosed as having the sequence 5'-GGAGAGTGATTGGTAGTGTGG-3' with a calculated $(M+H)^+$ mass of 6638.2. Both the sample on the ground steel and the Parafilm gave an *m/z* of approximately 6640, indicating that the external standards functioned sufficiently well for obtaining mass data. In addition, the accuracy obtained with the use of external standards appears equal to the accuracy obtained on the ground steel although resolution of the spectra obtained on the Parafilm coating is once again superior (Figure 30A and B).

Lastly, the use of external standards was examined when analysing the more labile B[a]P adducted oligonucleotides. Table 2 shows a summary of the results obtained when two 16-mer and two 18-mer oligonucleotides, containing either the (+) or (-)-trans B[a]P adducts, were analyzed on the Parafilm coating utilizing external standards. The masses obtained correspond very well to the predicted $(M+H)^+$ peaks of the oligonucleotides. The error associated with the molecular masses was generally greater with the external standards than with the internal standards, however the average error was still under 1.1 *m/z* units

Table II. Summary of four B[a]P adducted oligonucleotides analyzed using MALDI-TOF MS on a Parafilm-coated plate utilizing external standards.

Oligonucleotide	Calculated $(M+H)^+$ Mass	Measured $(M+H)^+$ Mass	% Error	FWHM	S:N Ratio
(-)-Trans B[a]P 16mer	5013.43	5014.53	2.19E-04	7.565	42057.5
(+)-Trans B[a]P 16mer	5013.43	5014.023	1.18E-04	7.451	34948.4
(-)-Trans B[a]P 18mer	5621.826	5622.122	5.27E-05	9.199	16365.9
(+)-Trans B[a]P 18mer	5621.826	5623.932	3.75E-04	8.513	31092.1

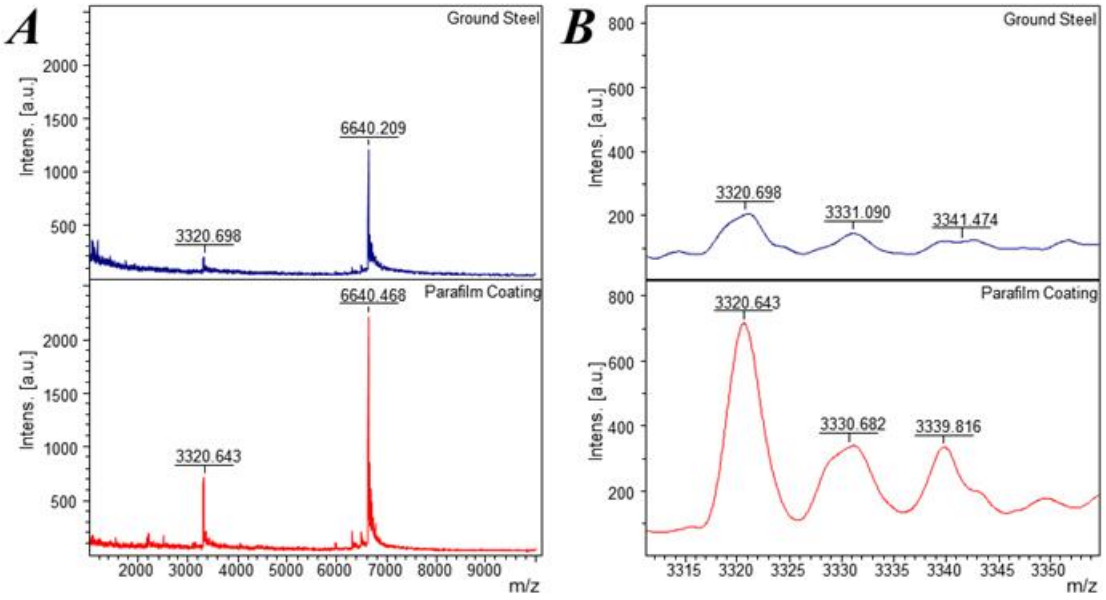

Figure 30. Comparison of MALDI-TOF mass spectrum using external standards for calibration on a steel plate and a Parafilm-coated steel plate. (A) Mass spectra of a 21-mer sample calculated using external standards (16-mer and 21-mer) on both ground steel (top) and Parafilm (bottom). The calculated mass of the oligonucleotide analyzed (5'-GGAGAGTGATTGGTAGTGTGG-3') was 6637.2 Daltons. (B) Expanded views of the $(M+2H)^{2+}$ peak range and corresponding salt peaks.

III. Surface Plasmon Resonance

A. Unmodifed DNA

Previous studies have looked at the effects various nucleotides have on polymerases. We have chosen to conduct our studies into dNTP selection using surface plasmon resonance (SPR) for two chief reasons: 1) SPR allows the re-use of the same DNA substrate for multiple binding studies conducted with various nucleotides and 2) multiple flow cells of the instrument allow concurrent experiments to be run in tandem. These two facets of SPR allow a direct comparison between varying the identity of nucleotides, and concurrently examining these changes on different DNA substrates. This setup provides a means to examine the dNTP effects others have noted previously, chiefly the stabilization achieved upon binding of the next correct dNTP, and a destabilizing effect an incorrect dNTP bestows upon the ternary complex. It has been conclusively shown that the sharp decrease in dissociation constants measured in the presence of the next correct dNTP correlate with a transition to a closed conformation (*24*). We have devised a binding experiment that clearly shows the gain or loss of stability upon dNTP binding, which correlates with conformational dynamics previously reported. We also examined polymerase binding to mismatched primer templates to determine how a misincorporation event placing a mismatch at the postinsertion site would affect dNTP selection.

i. Streptavidin Binding

We employed a streptavidin-biotin coupling to capture three different DNA primer-template duplexes (Figure 18) on three of the four flow cells of a CM5 sensorchip.

Initially all flow cells were bound with 1000 ± 100 RU of streptavidin using amine coupling to the carboxymethylated dextran matrix and the Biacore immobilization wizard.

The typical sensorgram attained when performing immobilization of streptavidin is shown in Figure 31. The initial injection is a test injection of streptavidin to measure the pre-concentratoin effects. The streptavidin is dissolved in pH 5.0 sodium acetate, giving it a positive attraction towards the matrix at this pH. This attraction process allows a low concentration of streptavidin to be used, which effectively concentrates the protein at the surface. The pH 5.0 sodium acetate and a 35 μg/mL solution of streptavidin provided a good pre-concentration effect, generating slopes of approximately 300 RU/min, which is sufficient for binding of 1000 RU of protein.

After ensuring the streptavidin solution concentrates properly to the matrix a mixture of EDC and NHS is injected, which activates the carboxylic acid residues on the dextran matrix surface. The EDC NHS provides an activated surface (Figure 32A) that the protein may then bind in a subsequent reaction (Figure 32B). Following activation, repeated injections of streptavidin are completed until the baseline shift indicates the desired level of protein is bound. Following a solution of ethanolamine is injected to quench any remaining reactive species.

ii. DNA Binding

One flow cell was used for a reference to allow subtraction of any non-specific interactions, or changes in the bulk refractive index of solution during injections of polymerase. DNA templates contained a 3'-biotin for capture on the streptavidin coated

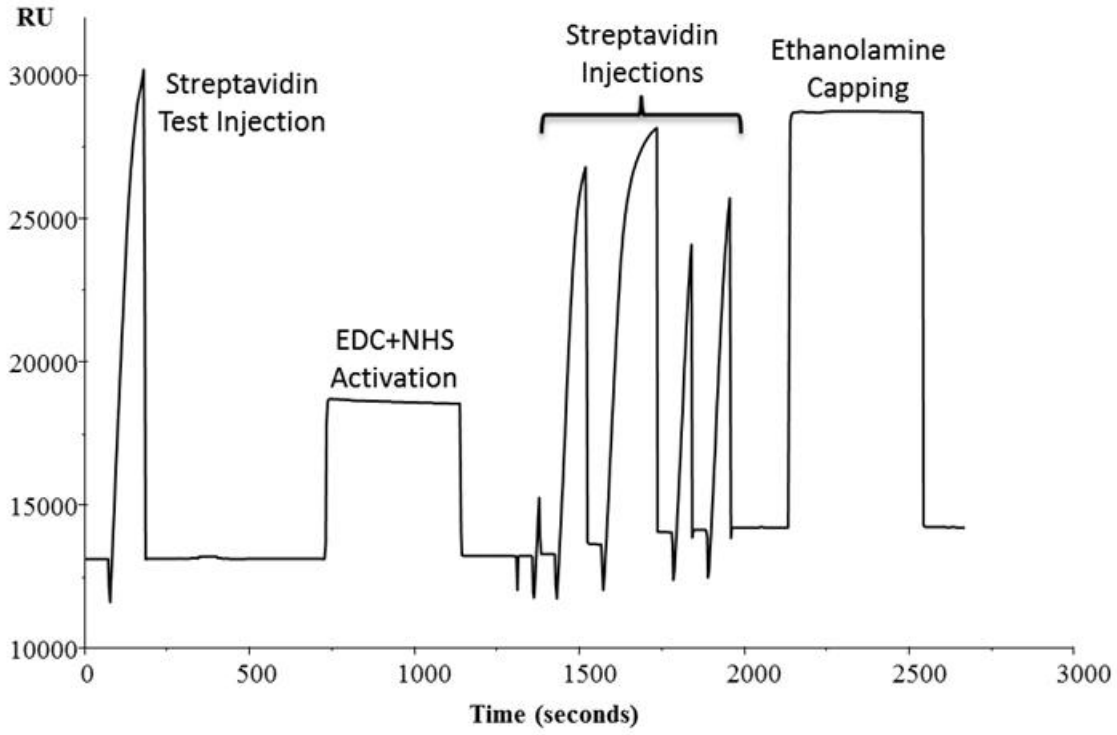

Figure 31. . Binding of Streptavidin to the dextran matrix surface. The surface is first tested with an injection of streptavidin to check for appropriate pre-concentration effects. Then the surface is activated with a mixture of EDC and NHS (see figure 32 for chemistry). After activation repeted injections of streptavidin are performed to attain binding levels of 1000 RU. Afterwards an injection of ethanolamine serves to quench the remaining reactive species, thereby preventing further binding.

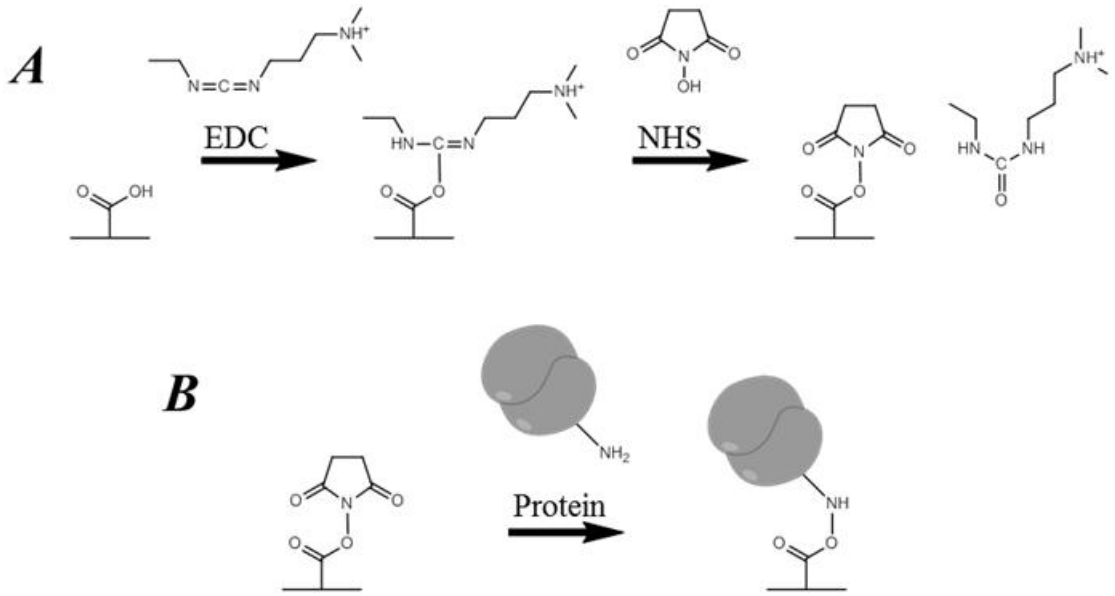

Figure 32. EDC NHS activation of CM5 sensor surface. (A) EDC and NHS activate the carboxylic acid residues of the carboxymethylated dextran surface. (B) The activated surface can be reacted with solvent exposed amines of proteins to provide covalent attachment of the protein to the surface.

surface. A 3'-biotinylated template versus a 5'-biotinylated primer was chosen so that future experiments using costly template-modified DNA could take advantage of using the template as the limiting oligonucleotide during duplex formation. Low levels of DNA, ~90 RU, were bound to limit any effects from mass transfer. Low concentrations of DNA primer-templates provided a good means of achieving low binding levels while being able to precisely control the quantity of DNA bound. Figure 33 shows a typical DNA binding sensorgram. In this instance, 3 separate injections of duplexed DNA are injected to achieve the desired 90 RU of duplex bound. DNA constructs shown in Figures 18A, B and C, were bound in flow cells 2, 3, and 4, respectively, for unmodified DNA experiments. Oligonucleotide duplexes shown in Figure 20A, B, and C were bound in flow cells 2, 3, and 4, respectively, for (-)-*trans*-*anti*-B[a]P-N^2-dG studies.

iii. Influence of Dideoxy Termination and Sequence on Klenow Fragment Binding

A sensorchip was created to compare binding related sequence effects, along with changes to the 3' OH of the primer-template terminus. For this experiment, DNA oligonucleotides shown in Figure 34A, B, and C were bound in flow cells 2, 3, and 4 respectively. This allows comparison of dideoxy and deoxy terminated primers, as well as a 22mer deoxy primer, with that of a 23mer deoxy primer. The binding levels and rates of association and dissociation were the same for both deoxy and dideoxy terminated primer-templates (Figure 35, green and red curves). This agrees with multiple other studies that show that dideoxy termination of primers has no effect on Klenow fragment binding properties.

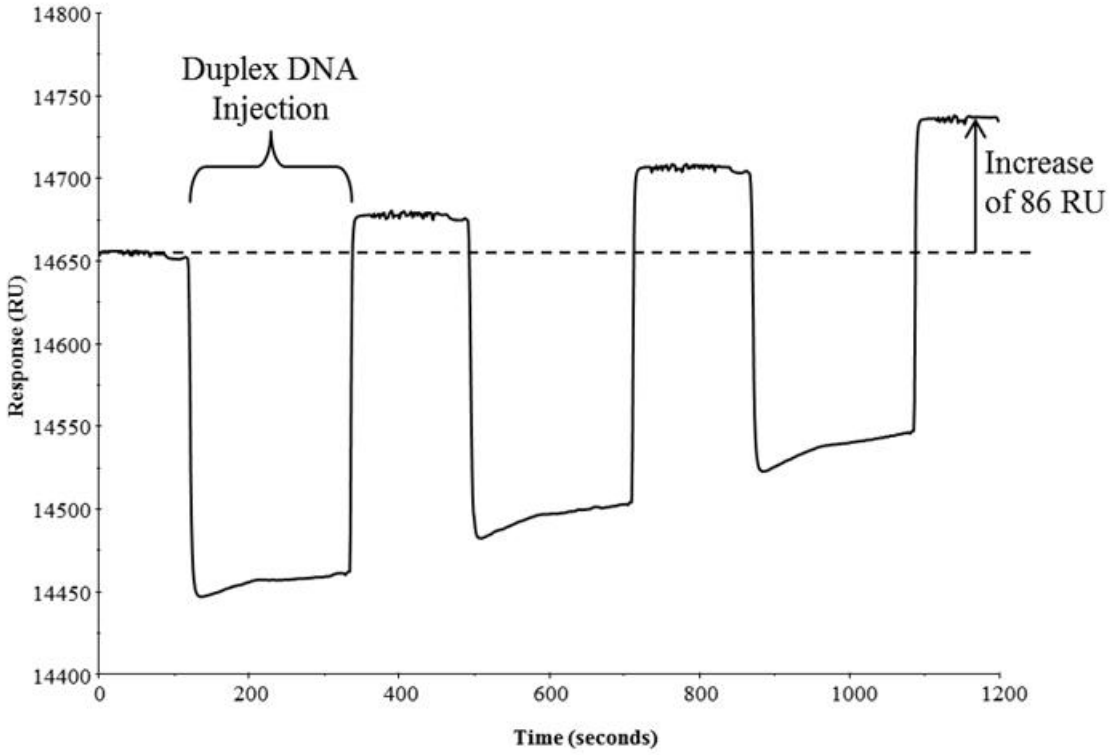

Figure 33. Representative sensorgram showing DNA capture onto streptavidin coated sensor surface. Surface is coated with streptavidin and templates contain a 3'-biotin. In this sensorgram three injections of duplex DNA were injected at 5 uL/min to achieve a binding level of approximately 86 response units. 2-4 injections were typically required to achieve binding levels of ~90 RU.

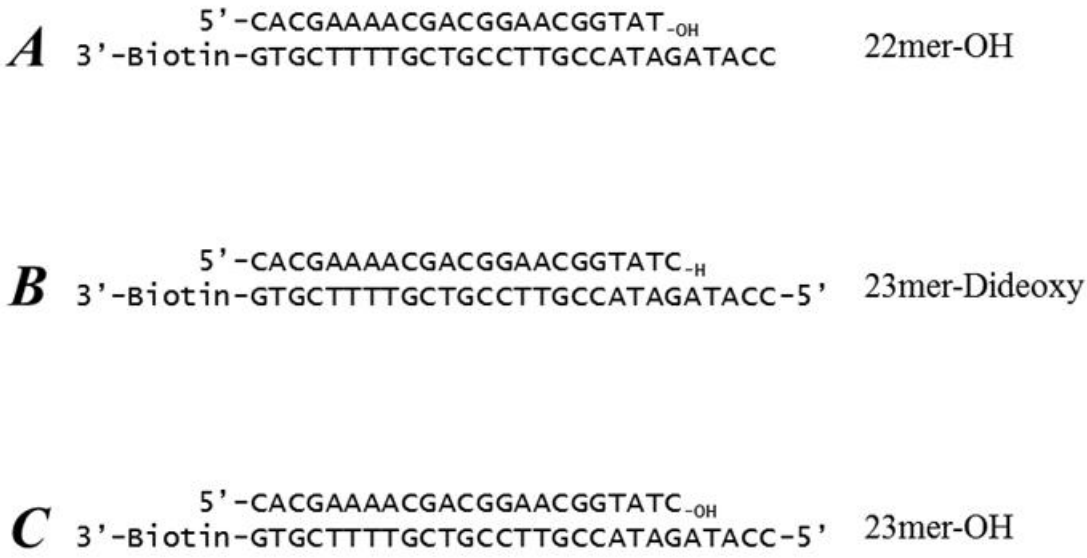

Figure 34. DNA Primer-template duplexes used in SPR dideoxy/deoxy experiments. (A) Duplex with a 22mer primer containing a native 3'-OH at the primer terminus. (B) Duplex with a 23mer primer containing a dideoxy terminated primer terminus. (C) Duplex with a 23mer primer containing a native 3'-OH at the primer terminus.

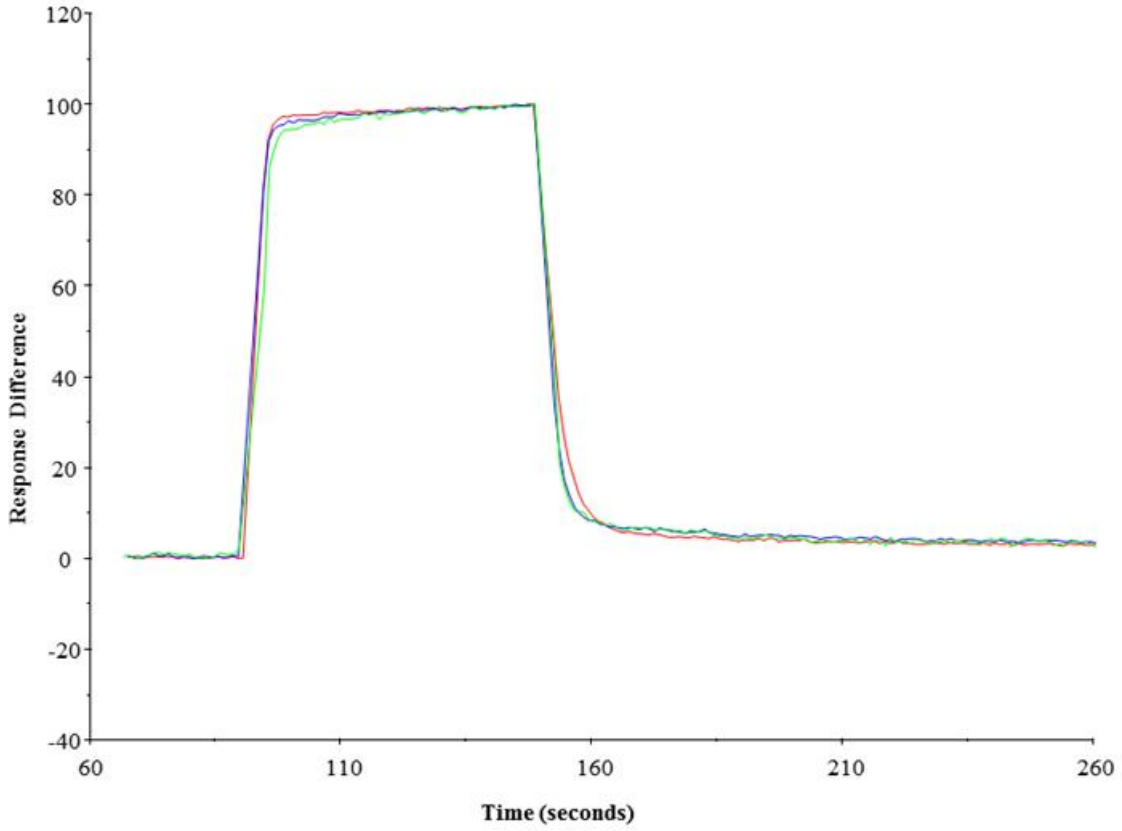

Figure 35. Effect of dideoxy termination and sequence on KF binding. Sensorgram showing the injection of 100 nM KF over DNA substrates in figure 34. Dideoxy terminated 23mer primer (blue) shows the same binding properties as non-dideoxy terminated 23mer primers (green). Changing the sequence by using a non-dideoxy terminated primer (red) has a very small, but noticeable effect on KF binding.

In addition, the sequence affect was monitored by using another 22mer primer that was non-terminated. The binding to this substrate was almost identical to the 23mers; however, there was a small but noticeable difference in the binding. The 22mer contains a terminal A:T base pair, whereas the 23mers contain terminal G:C base pairs. It is possible that this subtle change in sequence causes the small change in binding properties. Regardless, any changes noted were very small, and most importantly, dideoxy termination of primers showed no effect on binding.

iv. Klenow Fragment Binding Curves

The association rate of Klenow fragment to the DNA was very rapid, reaching equilibrium quickly (Figure 36), even on mismatched primer-templates. Previously others using different methods have found the association rate to be near diffusion limitations, consistent with our observations (*125*). The rapid rate at which equilibrium is achieved allowed short injections at high flow rates. Due to the complex nature of the polymerase binding mechanism, and the near-diffusion limited association rate, we are not reporting kinetic fits of our data and instead have chosen an equilibrium fitting method. Sufficient kinetic fits were obtained for this data, showing results consistent with a significantly simpler equilibrium analysis. The maximum binding capacity of the relative binding curves are accurately determined by curve fitting using non-linear regression to Equation 1. The calculated R_{max} for the binding curves were compared with the theoretical R_{max} that was calculated based upon the levels of DNA bound. The theoretical R_{max} and the calculated R_{max} were in good agreement. This allows accurate fitting of binding curves despite not reaching 100% saturation. In addition, this approach was verified with

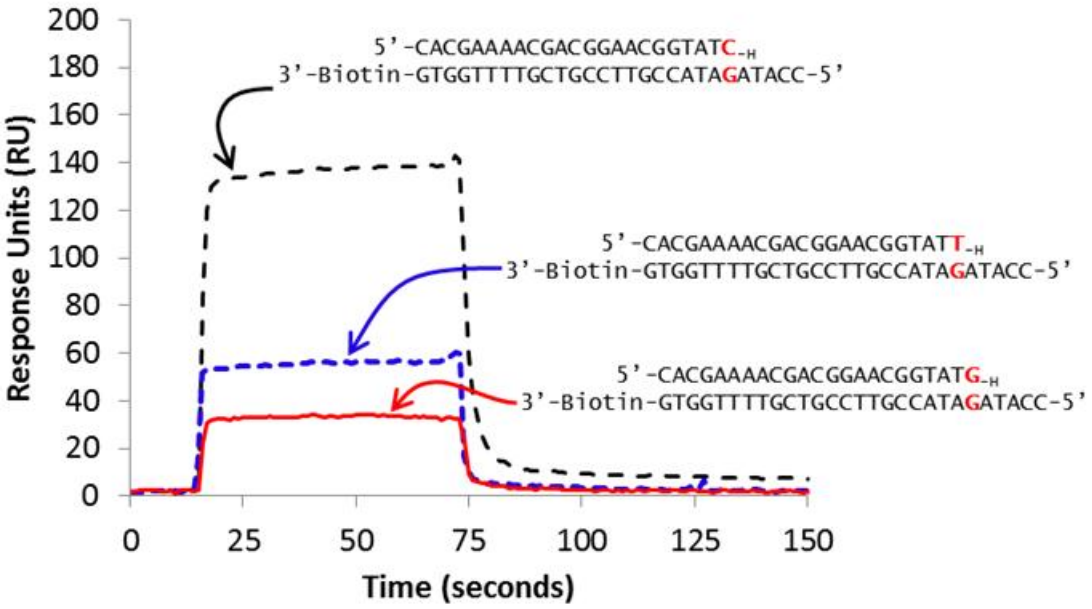

Figure 36. SPR sensorgrams showing 100 nM KF injection and binding to mismatched and correctly paired duplexes. Correctly paired duplex (long dashed line) shows the tightest Klenow fragment binding and a slightly longer dissociation phase than either a T:G mismatch (short dashed line), or a G:G mismatch (solid line). Faster dissociation is either caused by faster dissociation from the exonuclease site or by weaker KF-DNA interactions caused by a distorted structure.

injections that do reach 100% saturation, as in the case of the correct base pair with the next correct dNTP, where the calculated and theoretical values for R_{max} were very similar (< 10% difference).

v. Effects of NaCl on Klenow Fragment Binding in the Presence and Absence of dNTPs

Sensorgrams obtained in the absence and presence of 150 mM NaCl are shown in Figure 37A and Figure 37B, respectively. In general, in the absence of NaCl the binding is tighter and the dissociation rates are slower. The equilibrium binding levels do not increase in the presence of the next correct dNTP (dTTP), however the overall rate of dissociation does decrease. The presence of an incorrectly pairing dNTP (dGTP) leads to a lower equilibrium level, and a faster rate of dissociation.

The use of buffer containing NaCl shows a weaker binding, however the selection of correct vs. incorrect dNTP is greater than in the absence of NaCl. The inclusion of the next correct dNTP (dTTP) greatly increases the equilibrium binding levels and shows a slow rate of dissociation. The inclusion of an incorrectly base pairing dNTP (dGTP) greatly decreases the equilibrium binding levels, and leads to a rapid rate of dissociation. are shown to have an effect on polymerase binding.

The presence of NaCl has an effect on the binding of Klenow fragment to DNA. We examined this by measuring the equilibrium levels obtained with various concentrations of NaCl, in the presence and absence of correct or incorrect dNTPs. Figure

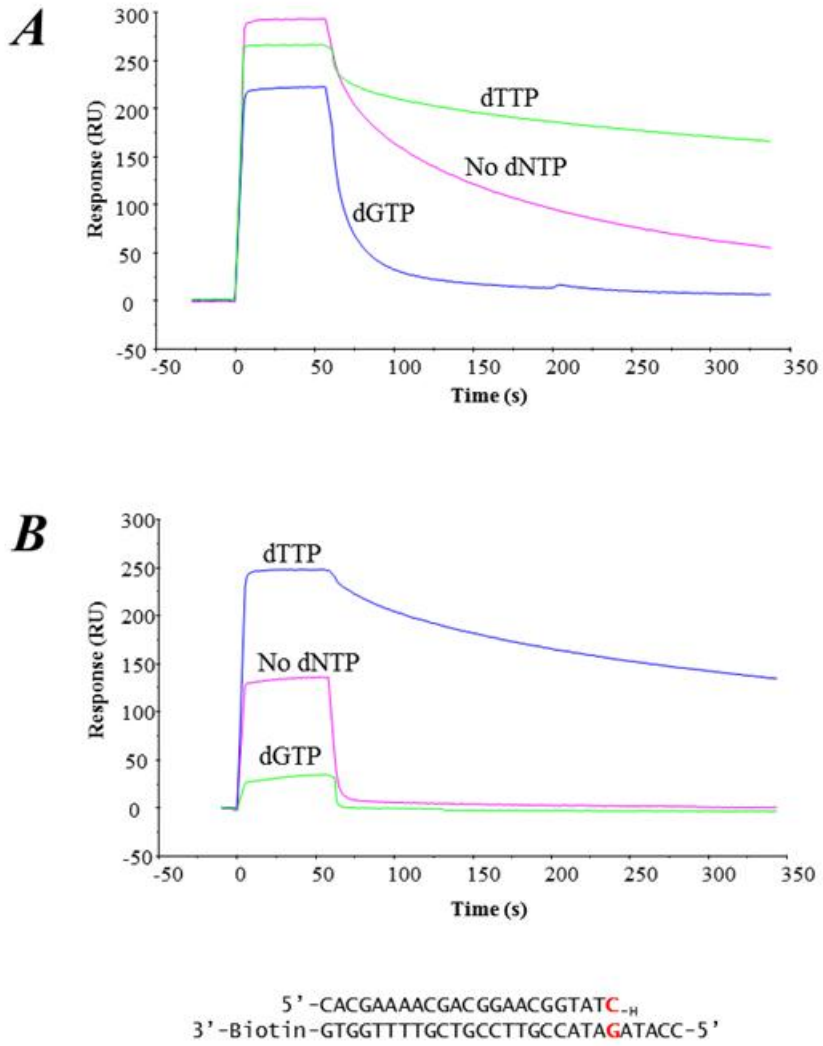

Figure 37. SPR sensorgrams showing KF injection and binding to correctly paired duplex in the presence or absence of 150 mM NaCl, in the presence of either dTTP, dGTP, or no dNTP. (A) 100 nM KF injections without NaCl. The presence of dTTP causes a slower dissociation, however the equilibrium level does not increase above that for no dNTP. dGTP shows a lower equilibrium level and a faster dissociation. (B) 100 nM KF injections with NaCl. The presence of dTTP causes a strong stabilization of KF binding during the equilibrium phase, and a slower dissociation. An incorrect dGTP causes a strong destabilization and a rapid dissociation.

38 shows the results of such an experiment. A NaCl concentration dependent decrease in polymerase binding is noted for all measured substrates. Interestingly, the rate of change for inclusion of dTTP, dGTP, or no dNTP is different. At low NaCl concentrations the binding levels of Klenow fragment in the presence of dTTP do not dramatically differ from the binding levels in the absence of dNTP. Conversely, at high concentrations of NaCl the binding levels of Klenow fragment in the presence of dGTP do not significantly differ from the binding levels in the in the absence of dNTP. However, at a NaCl concentration of approximately 150 mM, the difference in binding between all substrates is largest. Thus all experiments were thus conducted in the presence of 150 mM NaCl to observe the largest fold changes in binding with different dNTPs.

Overall the inclusion of 150 mM NaCl gave slightly weaker binding with higher dissociation constants than those found in typical solution based assays, but nevertheless exhibited larger differences between binding affinities of the measured substrates. The results are reported as apparent K_Ds and all conclusions drawn are based on relativistic changes of the values rather than their absolute quantity.

vi. Native and Mismatched Primer-Templates in the Absence of dNTPs.

A mismatch located at the -1 position places the misaligned structure at the post-insertion site (-1 position, see Figure 18A). We placed either a pyrimidine-purine (T:G, Figure 1A) or a purine-purine (G:G, Figure 18C) mismatch at the -1 position to compare with polymerase binding to a native primer-template (Figure 18B). Figure 38 shows a typical sensorgram that is obtained when a 100 nM Klenow fragment solution is injected over these substrates. The flow cells containing mismatched oligonucleodies contain

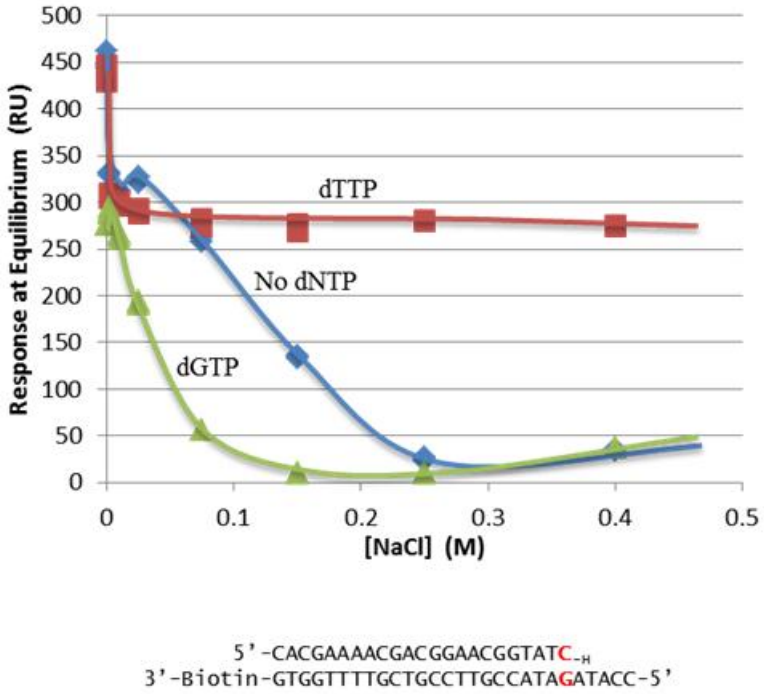

Figure 38. NaCl effects on polymerase binding. As NaCl concentration is increased, the binding equilibrium binding levels of Klenow fragment in the presence or absence of dNTPs decreases. At a concentration of 150 mM NaCl the largest difference in binding between no dNTP, correct dTTP, and incorrect dGTP is observed.

slightly higher levels of bound DNA, yet exhibit lower KF-DNA binding levels than the correctly aligned primer-template. Examining the dissociation phase reveals that the mismatched oligonucleotides induce a faster rate of dissociation of the polymerase than the correctly pair DNA substrates. Table 3 shows the dissociation constants for equilibrium fits to obtained data. Differences visually noted in the sensorgrams are confirmed in the dissociation constants. The dissociation constant for binding to a single mismatch is approximately 2.8-3.6 fold weaker binding than to a correctly paired primer-template.

vii. Correct vs. Incorrect dNTPs on Native Primer-Templates

The influence of correct vs. incorrect dNTPs is well established in solution-based assays (*3, 24, 38-40*). Our data illustrates that similar changes are evident in our SPR experiments. At Klenow fragment concentrations above 400 nM two polymerases begin binding each primer-template (Figure 39), so polymerase concentrations were kept at and below 200 nM. Others have reported similar results at high concentrations (*80, 126*). Below Klenow fragment concentrations of 200 nM the data fits well to a 1:1 Langmuir model. To generate these binding curves multiple concentrations of KF were injected over the sensor surfaces (Figure 40A). The equilibrium levels were then plotted as a function of the concentration of Klenow fragment used for the injection to generate binding curves (Figure 40B-D). Figure 40B shows Langmuir binding isotherms of correctly paired primer-templates in the presence of the next correctly pairing dTTP, incorrectly pairing dNTPs, or rNTPs. A correctly pairing dTTP caused approximately a 20-fold enhancement in binding over the absence of nucleotide (Table 3). This is

Table III. Dissociation constants for binding of Klenow fragment to various primer-templates in the presence or absence of 2'-deoxy- or ribo-nucleotide-5'-triphosphates.[a]

	Dissociation Constants, K_D (nM)[c]						
Primer-Templates[b]	No NTP	dTTP	dATP	dCTP	dGTP	rUTP	rATP
C:G Correct BP	163 ± 1	8 ± 1	990 ± 40	450 ± 10	1800 ± 100	441 ± 3	1370 ± 10
T:G Mismatch	580 ± 30	2300 ± 400	3900 ± 700	2400 ± 400	4200 ± 700	1400 ± 50	2000 ± 80
G:G Mismatch	450 ± 10	2810 ± 20	6200 ± 100	2530 ± 20	6100 ± 100	1370 ± 30	2900 ± 70

[a] The equilibrium dissociation constant values (K_D) were determined as described under materials and methods.
[b] The sequences used to form the primer-template duplexes are depicted in figure 18 (T:G mismatch, C:G correct BP, and G:G mismatch are A, B, and C respectively).
[c] Values represent averages of triplicates ± standard error

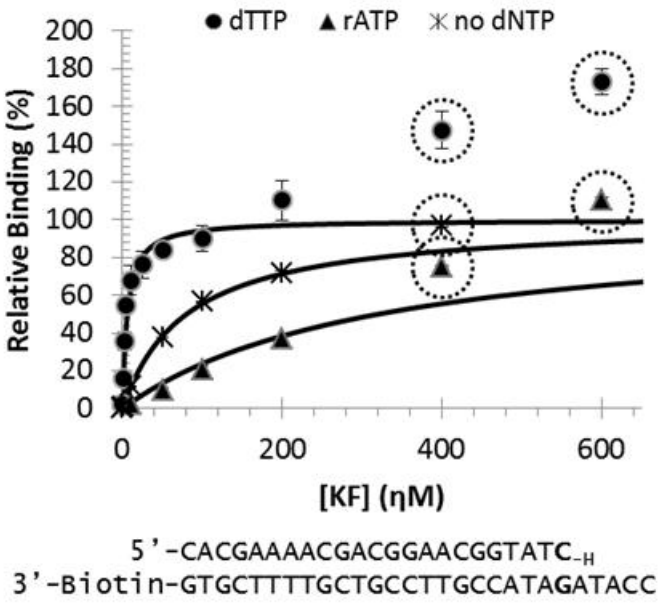

Figure 39. KF-DNA binding curves derived from SPR data at equilibrium levels (in HSM buffer). Data points are indicated as follows: no dNTP(×), dTTP (●), dATP (♦). Binding curves show that at concentrations of Klenow fragment above 200 nM two polymerases begin to bind the DNA primer-templates

consistent with formation of a closed ternary complex, causing an enhancement in binding (*24*). Conversely, the addition of an incorrectly WC-pairing dNTP causes a destabilizing effect, and a 2.8- to 11-fold increase in the dissociation constant. Similarly, the presence of a rNTP causes a destabilization of 2.7- to 8.4-fold. However, a correctly base-pairing and smaller rUTP causes less destabilization than the corresponding larger rATP. The influence of Klenow fragment binding follows the order dTTP >> no dNTP >> rUTP > dCTP > dATP > rATP > dGTP.

viii. Effect of dNTPs and rNTPs on Mismatched Primer-Templates

We investigated the ability of Klenow fragment to undergo a conformational change when a mismatch is positioned at the -1 position. The binding isotherms obtained with either a terminal T:G mismatch (Figure 40C), or a terminal G:G mismatch (Figure 40D), show that a destabilizing effect occurs in the presence of any NTP, deoxy or ribo. Unlike properly base-paired primer-templates, the dissociation constants reveal that polymerase binding to the T:G mismatch is destabilized approximately 2.4- to 7.2-fold by the presence of any NTP. Similarly, addition of any NTP to a G:G mismatch at the -1 position causes significant destabilization. On average, the destabilization seen with the G:G mismatched primer-template is greater than that observed with the T:G mismatched DNA construct in the presence of NTPs. Incorrectly pairing dATP and dGTP show the largest change, up to a 13.7 fold decrease in binding. A correctly base-pairing dTTP or rUTP show a smaller 3- to 6.2- fold decrease in binding. However, it is undetermined if this is simply a size exclusion in which the smaller dTTP or rUTP cause less distortion to the already crowded G:G mismatched terminus, or due to hydrogen-bonding interactions.

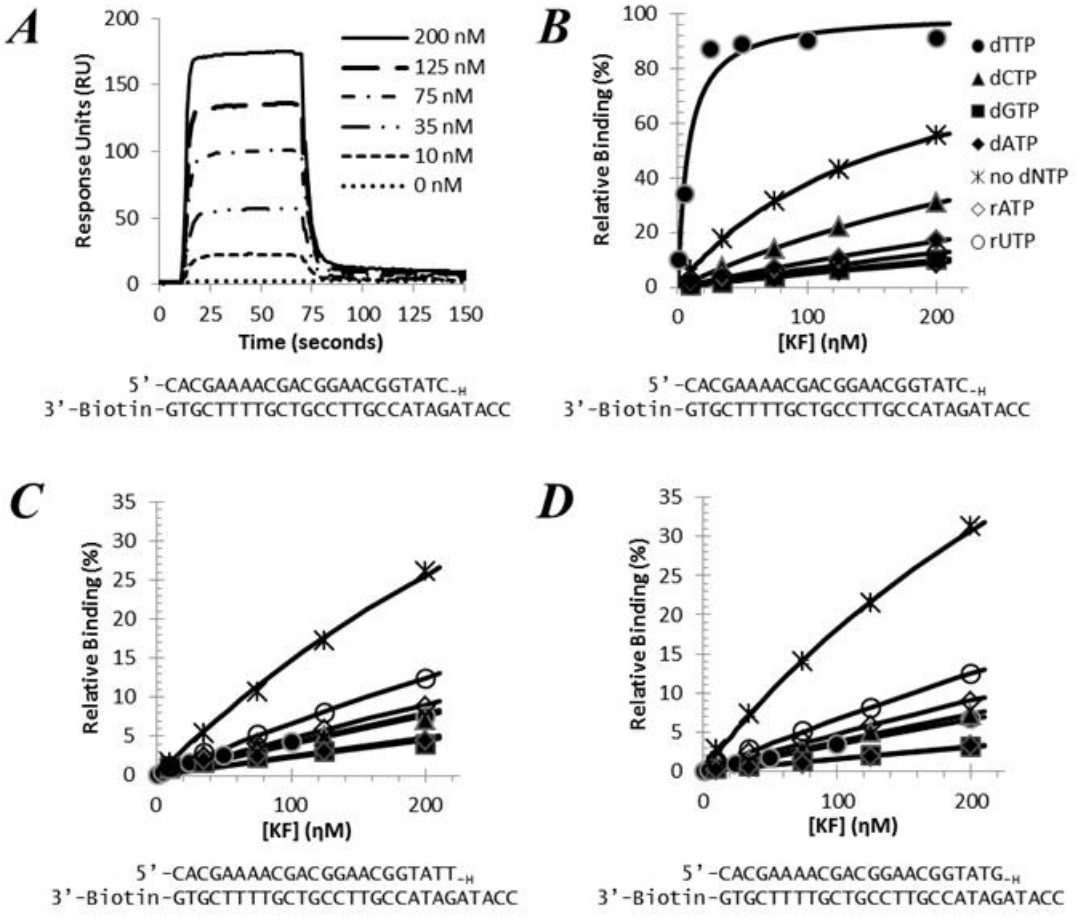

Figure 40. KF-DNA binding curves used to determine apparent dissociation constants (K_D). (A) KF concentration series. Plotting equlibirum levels vs concentration of KF and using non-linear regression of a 1:1 Langmuir binding isotherm to data points gives C-D. (B) Binding curves for correctly paired primer-template (Figure 18B). The presence of the next correct dNTP causes an increase in binding, whereas the presence of incorrect dNTPs or an rNTP causes a decrease in the measured binding. (C) Binding curves attained on T:G mismatched templates (Figure 18A). Here the presence of any dNTP or rNTP causes a decrease in binding. (D) Binding curves attained on G:G mismatched templates (Figure 18C). Once again, the presence of any dNTP or rNTP causes a decrease in binding. Data points are indicated as follows: no dNTP(×), dTTP (●), dATP (♦), dGTP (■), dCTP (▲), rUTP (○), rATP (□).

It is interesting to note that rATP causes less destabilization than dATP on the G:G mismatched primer-template. It is possible that the unique structure of this mismatch doesn't allow the larger rATP access to the active site, thereby limiting it to have a smaller destabilizing effect due to its inability to bind.

ix. Direct Measurement of Gain or Loss of Stability

Previous results show a clear correlation with the identity of a dNTP and either a gain or loss of stable polymerase binding (*24*). By examining the change in equilibrium binding while keeping the concentration of Klenow fragment constant and changing the concentration of the dNTP, we were able to directly show the gain or loss of KF-DNA stability as influenced by various dNTPs. Figure 41 displays the results of such an experiment. A baseline of zero would indicate that the inclusion that dNTP would have no effect on the KF-DNA complexes formed. An increase in the relative binding above zero with an increase in concentration of dNTP would indicate that the dNTP causes an increase in binding over the binary KF-DNA complex, and a negatively deflected curve with an increase in concentration of dNTP would indicate that dNTP decreases binding. As expected, inclusion of a correctly base-pairing dTTP on a correctly paired primer-template has a profound enhancing effect on the polymerase binding (Figure 41A and B, solid circles). The binding level increases rapidly with dTTP concentration, maxing out near the theoretical maximum DNA binding limit. Conversely, the inclusion of any incorrectly pairing dNTP causes a concentration-dependent decrease in binding. To quantify this, a modified version of the Hill equation (Equation 4) was fit to the data (Figure 41, black lines). This allows two important variables to be deduced: 1) the E_{max},

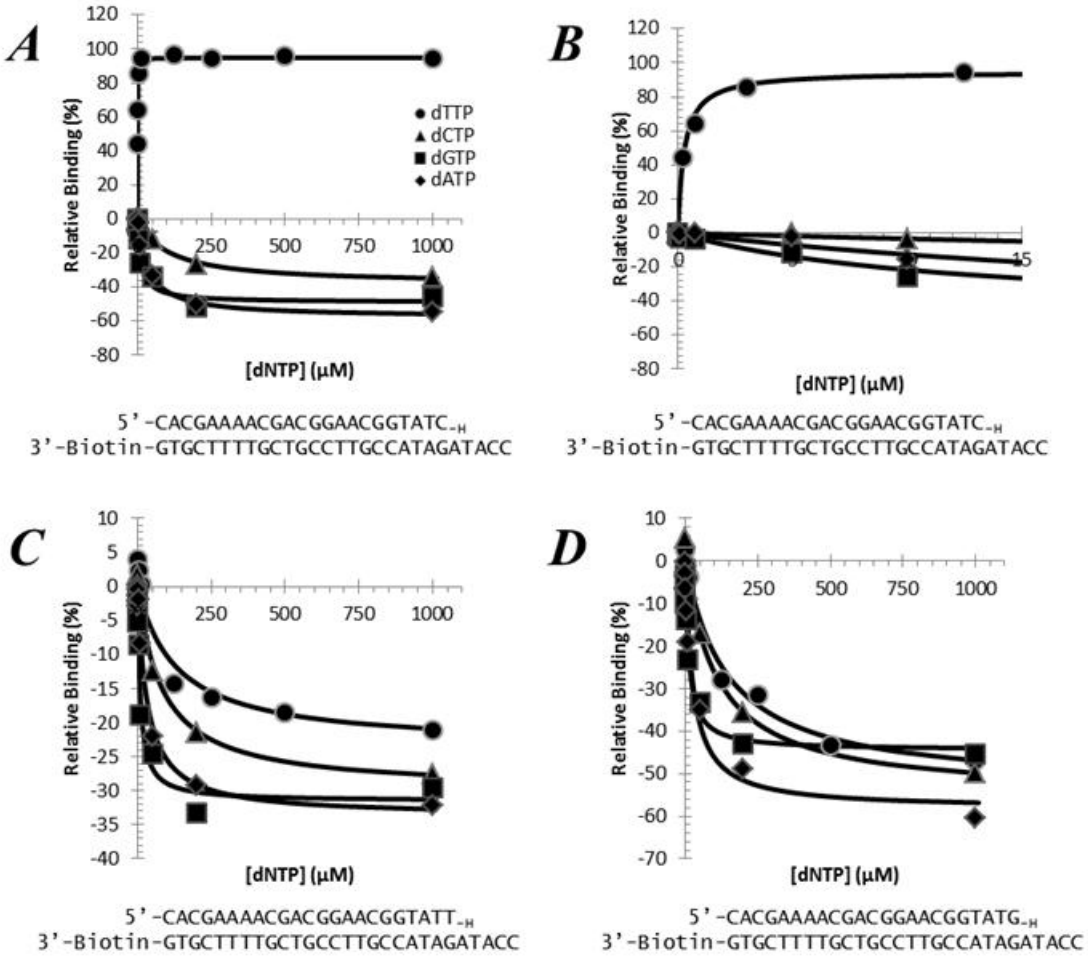

Figure 41. Results for dNTP selectivity assay. Data points are indicated as follows: dTTP (●), dCTP (▲), dATP(♦), dGTP(■). Solid lines represent fits of data points to equation 4. A) Influence of various dNTPs attained for Klenow fragment binding to correctly paired primer templates. Only the presence of dTTP causes an increase in the amount of KF-DNA complexes, and all other dNTPs cause a decrease in KF-DNA complexes. B) Zoomed in view of (A) showing more clearly the dTTP binding curve at low concentrations. Small amounts of dTTP induce a rapid increase in the levels of DNA bound Klenow fragment complexes, whereas incorrect dNTPs require a greater concentration to achieve their affect. This is evident when examining the Sf value in table 2. C) Curves attained for a T:G mismatched primer-template. Similar to the previous results, the presence of any dNTP causes a decrease in binding below formation of the binary complex alone. D) Results for binding to a G:G mismatched primer template. Here the presence of any dNTP causes a concentration dependent decrease in binding. Data points are averages of triplicates and error bars reflect the standard deviations of the averaged data points.

which represents the maximal effect the dNTP can cause, ranging from increasing binding to 100% of the available DNA substrate, or completely destabilizing all binding (-100%); or 2) a selectivity factor S_f, which represents the concentration of dNTP required to reach half of the E_{max}. High values of S_f would indicate that high concentration of the dNTP would be required to achieve the effect dictated by the E_{max}. Table 4 displays the results of this data set. For instance, dTTP shows a sharp rise in the curve, giving a low selectivity factor, indicating that dTTP reaches its maximal affect at a very low concentration. Conversely, the destabilizing dNTPs have a much greater selectivity factor, 47- to 380-fold higher than dTTP, and require a much higher concentration to reach their maximal destabilizing effect. In terms of destabilization, dCTP causes the smallest maximal effect and requires the highest concentration to achieve half this value, meaning it is the least destabilizing dNTP for this correctly base-paired substrate (Figure 41A).

The results for measurements with T:G mismatched and G:G mismatched primer-templates are shown in Figure 41C and 41D respectively. Similar to the equilibrium binding data, the selectivity experiment shows that the inclusion of any dNTP, even the next correctly base-pairing dTTP, causes a destabilizing effect in a concentration dependent manor. In the case of the T:G mismatched primer-template, dTTP has the least destabilizing effect followed by dCTP. Both dATP and dGTP cause the largest destabilization. The maximum destabilizing effect (E_{max}) of all four dNTPs are relatively similar, however, dTTP and dCTP show less destabilization at a lower concentration. Again consistent with the dissociation constants, a G:G mismatch shows a greater degree

Table IV. Computed values of E_{max} and S_f based upon fits of equation 4 to data presented in figure 39.[a]

	dTTP		dATP		dCTP		dGTP	
Primer-Templates[b]	E_{max} (%)	S_f (uM)	E_{max} (%)	S_f (uM)	E_{max} (%)	S_f (uM)	E_{max} (%)	S_f (uM)
C:G Correct BP	+94.9 ± 5.8	0.27 ± 0.04	-57.6 ± 1.9	35.7 ± 2.4	-38.3 ± 1.0	104 ± 25	-48.9 ± 1.4	12.7 ± 1.8
T:G Mismatch	-23.6 ± 1.3	131 ± 95	-33.8 ± 1.4	32.4 ± 11.8	-30.0 ± 3.4	83.2 ± 47.3	-31.6 ± 1.8	9.1 ± 2.5
G:G Mismatch	-53.7 ± 4.8	146 ± 43	-58.3 ± 4.2	26.1 ± 5.6	-55.4 ± 5.1	112 ± 23	-44.5 ± 4.3	12.0 ± 7.5

[a] E_{max} and S_f values were determined as described under materials and methods. All values represent averages of triplicates.
[b] The sequences used to form the primer-template duplexes are depicted in figure 18 (T:G mismatch, C:G correct BP, and G:G mismatch are Fig. 2 A, B, and C respectively).

of destabilization in the presence of any dNTP than observed on the T:G mismatch. There is also a lower degree of destabilization noted with dTTP and dCTP at a lower concentration, than with dATP or dGTP. Lastly, it should be noted that equilibrium binding experiments were conducted at dNTP concentrations of 400 μm, a dNTP concentration that generates large differences in polymerase binding based upon the identity of the dNTP.

x. Dissociation of Klenow Fragment Complexes in the Presence and Absence of dNTPs

Typically experiments are conducted so the injection of enzyme and any co-factors are only present during the association phase, while the dissociation phase typically is composed of only buffer. Injections of Klenow fragment mixed with various dNTPs were conducted, followed by dissociation with only buffer (Figure 42A). Figure 42A shows the results obtained for such an experiment on a properly paired C:G substrate. The inclusion of dTTP causes an increase in the equilibrium levels of KF-DNA binding above that obtained in the absence of dNTP. The dissociation phase also shows a slightly slower rate of dissociation than for the absence of dNTP. Conversely, the addition of dGTP to the association phase only results in a decrease in equilibrium binding followed by a rapid dissociation with buffer. To contrast this, and test the ability of Klenow fragment to sample dNTPs while remaining bound to the DNA we conducted experiments in which we placed dNTPs not only in the association phase (mixed with KF) but also into the dissociation phase (Figure 42B). The results obtained here are similar to those state above with two exceptions: 1) when a correctly base-pairing dTTP

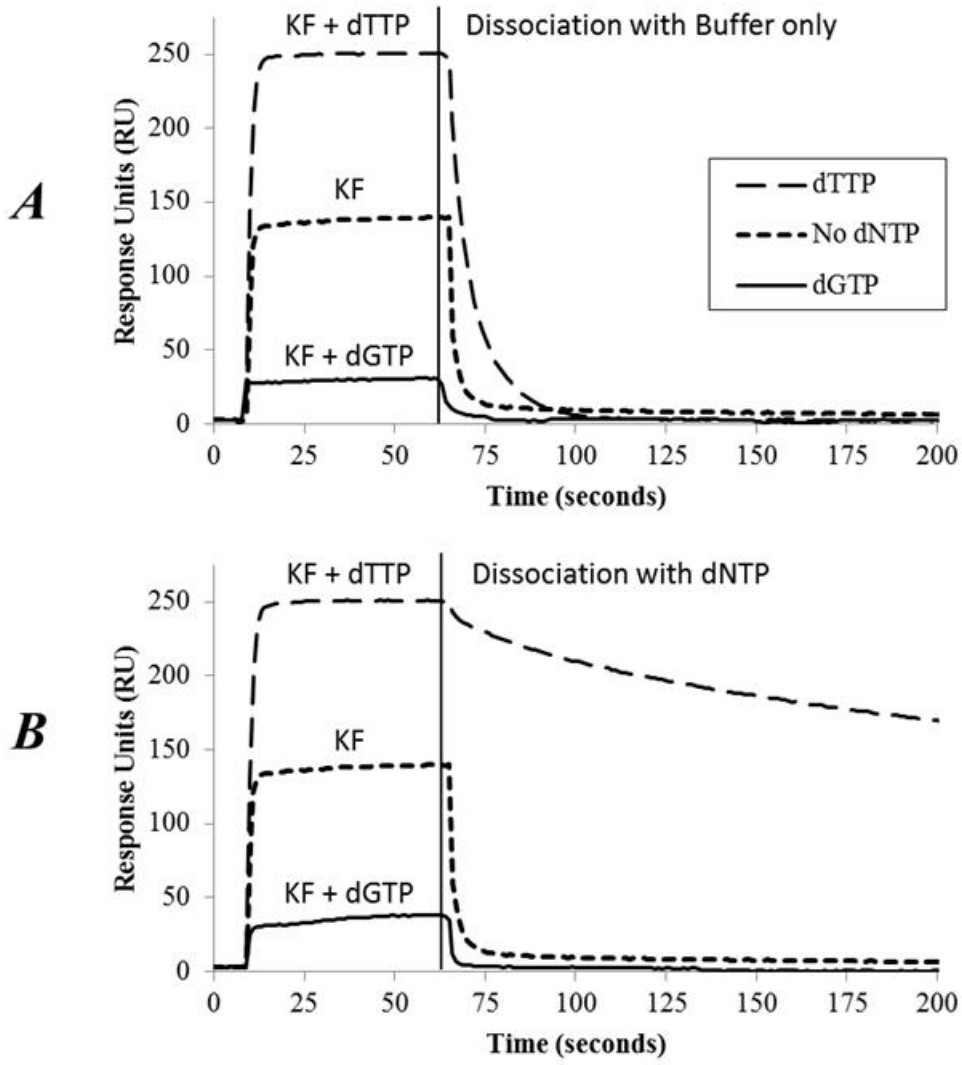

Figure 42. Sensorgrams depicting cycling of dNTP during Klenow fragment binding on proper C:G base paired primer-templates (Figure 18B). Sensorgrams are obtained by injection 100 nM Klenow fragment in the presence or absence of dNTPs. A) After equilibrium is established the injection of Klenow fragment is stopped (vertical solid black line) and buffer is flowed over the surface. This results in the dissociation of bound Klenow fragment. Klenow fragment bound with a correctly base pairing dTTP show a slower dissociation, most likely due to the formation of a closed ternary complex. B) After equilibrium is established the injection of Klenow fragment is stopped and buffer containing either dTTP, no dNTP, or dGTP is flowed over the surface. The inclusion of dTTP in the dissociation buffer results in a very slow dissociation of Klenow fragment. This is due to the Klenow fragment re-cycling dTTP as it opens and closes repeatedly.

was included into the dissociation buffer the dissociation rate of the complex was dramatically reduced; 2) the inclusion of a mismatching dGTP in the dissociation buffer resulted in a more rapid rate of dissociation than in buffer alone. The slower dissociation with dTTP in the buffer indicates that polymerase is capable of cycling the nucleotides prior to dissociation from the DNA. When equilibrium is established and the closed complex formed, if this was a stagnant complex the inclusion of dTTP during the dissociation phase would have no effect. However, because a large increase in binding is noted, a significant portion of the bound polymerase must be fluctuating between the open and closed conformation, even in the presence of the next correct dNTP.

B. Benzo[a]pyrene Studies

Previous surface plasmon resonance experiments show that Klenow fragment binding to a correctly paired unmodified primer-template in the presence of a correctly pairing dNTP causes a significant drop in the dissociation constant, and a much slower rate of dissociation. We again chose surface plasmon resonance to conduct studies to investigate the effects of a (-)-*trans*-*anti*-B[a]P-N^2-dG adduct on Klenow fragment binding. SPR allows the concomitant measurement of polymerase binding to three different DNA primer-template substrates. The ability to measure binding on multiple substrates allows a direct comparison between the three primer-templates listed in Figure 20. In addition, the same surface is utilized for multiple injections, again allowing a direct comparison between various injections, in this case the effect measured by the presence of various dNTPs and rNTPs. We have used an equilibrium type analysis as opposed to a kinetic fit of our sensorgrams. Sufficient kinetic fits were obtained for this data; however,

we find the overall conclusions attained are the same as with a significantly simpler equilibrium analysis.

i. Sensorgrams and Binding Curves

CM5 sensorchips were immobilized first with 1000 ± 50 RU of streptavidin in all flow cells using standard Biacore amine coupling procedures. Typically other experiments capture DNA employing a 5'-biotinylated primer duplexed to template. This type of setup using a 5'-biotinylated primer would require the template to be in excess upon duplex formation to ensure all primer was duplexed. We instead chose to utilize DNA templates which contain a 3'-biotin for capture. This allows limiting quantities of template to be used with a vast excess of easily purified primer upon duplex formation. This is the same strategy employed with previous unmodified DNA studies and again worked well here.

ii. Correctly Paired and Mismatched (-)-trans-anti-B[a]P-N2-dG Primer-Templates in the Absence of dNTPs

Injections of Klenow fragment onto the (-)-*trans-anti*-B[a]P-N^2-dG modified surfaces produce sensorgrams that display rapid association rates (Figure 43). All primer template structures, correctly base paired or containing terminal mismatches, display similar association phases. This is similar to the results noted in unmodified DNA studies. This indicates that the (-)-*trans-anti*-B[a]P-N^2-dG must not interfere significantly with the association of Klenow fragment to the duplex. However, where unmodified DNA shows the largest extent of binding to a correctly paired C:G substrate, Klenow fragment shows the greatest binding to a mismatched G:G-B[a]P primer-template (Figure 43). In

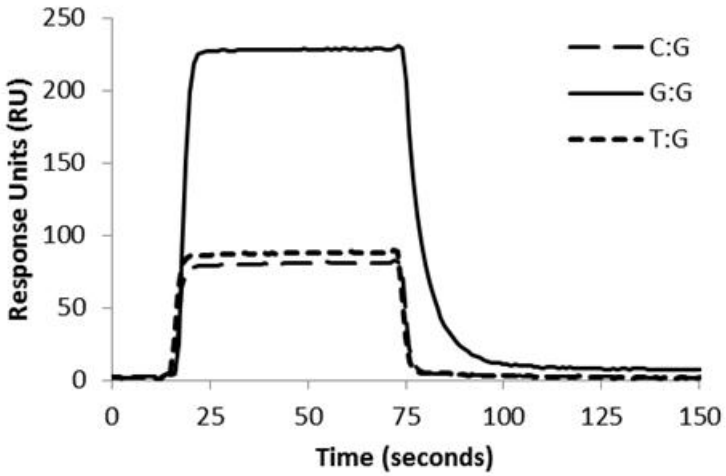

Figure 43. SPR response obtained when Klenow fragment is injected onto templates shown in figure 20. Binding to a G:G-B[a]P base pair is significantly stronger than to a correctly base paired C:G-B[a]P primer-template or a mismatched G:G-B[a]P primer-template. A longer dissociation phase is also evident from a G:G-B[a]P primer-template.

Figure 43 the quantities of immobilized DNA are within ± 5% of each other and would yield similar values of R_{max}. However, it is apparent that the binding of KF to a C:G-B[a]P substrate is much weaker. Also, unmodified DNA also showed a substantial decrease in binding of KF to a T:G mismatch relative to a C:G correct base pair. Here a T:G-B[a]P mismatch shows approximately the same levels of binding as a C:G-B[a]P correct base pair. Furthermore, the dissociation phase of the sensorgram for binding to a G:G-B[a]P appears to be slower than that observed for the T:G-B[a]P duplex or the C:G-B[a]P duplex. Again, this is opposite to the observations on unmodified DNA in which the dissociation phase for binding to a correctly paired C:G primer-template is the slowest and dissociations from mismatches are more rapid. This unexpected result with G:G-B[a]P primer-tempates was repeated multiple times on several sensorchips, under varying buffer conditions, and different levels of immobilized DNA, always giving the same trends.

To further probe this result, multiple injections of KF ranging in concentration from 0 nM to 200 nM were performed (representative series in Figure 45A). As the concentration of Klenow fragment increases, the equilibrium levels of the association phase increases. Generating a plot of the average equilibrium value versus the concentration of KF used for the injections allows the generation of binding curves (Figure 6 B-D). Fitting of a 1:1 Langmuir binding isotherm (Equation 1) allows determination of dissociation constants (K_D) (Table 5). It should be noted that these experiments include 150 mM NaCl within the buffer. We have conducted experiments both with and without salt and concluded that the inclusion of salt in the buffer allows a

Table V. Dissociation constants for binding of Klenow fragment to various B[a]P labeled primer-templates in the presence or absence of 2'-deoxy- or ribo-nucleotide-5'-triphosphates.[a]

	Dissociation Constants, K_D (nM)[c]						
Primer-Templates[b]	No NTP	dTTP	dATP	dCTP	dGTP	rUTP	rATP
C:G-B[a]P Correct BP	810 ± 10	1720 ± 10	2770 ± 20	1650 ± 10	2090 ± 10	2720 ± 20	3940 ± 40
T:G-B[a]P Mismatch	820 ± 10	3270 ± 30	5500 ± 100	2280 ± 20	6300 ± 100	3840 ± 30	7400 ± 100
G:G-B[a]P Mismatch	120 ± 10	492 ± 3	690 ± 10	306 ± 2	1030 ± 10	870 ± 20	1800 ± 50

[a] The equilibrium dissociation constant values (K_D) were determined as described under materials and methods.
[b] The sequences used to form the primer-template duplexes are depicted in figure 20 (T:G mismatch, C:G correct BP, and G:G mismatch are A, B, and C respectively).
[c] Values represent averages of triplicates ± standard error

larger-fold change to be observed upon addition of correct or incorrect dNTPs on unmodified DNA; however, inclusion of salt results in significantly higher dissociation constants. The results are thus reported as apparent K_Ds and all conclusions drawn are based on relativistic changes of the values rather than their absolute quantity. Examination of the equilibrium binding constants in table 5 in the absence of dNTPs show that the binding of KF to a G:G-B[a]P is approximately 7 fold tighter than to a T:G-B[a]P or a C:G-B[a]P substrate. This confirms the observations noted above upon visual examination of the sensorgrams. Conversely, unmodified DNA previously showed tightest binding to correctly paired C:G substrates, with a 3- to 4-fold decrease in binding to T:G and G:G mismatched substrates.

iii. Correct vs. Incorrect NTPs on Correctly Paired C:G-B[a]P Substrates

Klenow fragment is known to undergo a conformational change to a closed complex upon binding of the next correct dNTP. SPR experiments conducted with unmodified DNA show a substantial 20-fold increase in binding in the presence of the next correct dNTP. Conversely, the presence of an incorrectly pairing dNTP or any rNTP causes a destabilization by 3-11 fold, with the smaller pyrimidines causing less destabilization. Table 5 shows the binding constants determined in the presence of various dNTPs and rNTPs from fitting of a 1:1 Langmuir binding isotherm to data presented in Figure 44. Unlike unmodified DNA, (-)-*trans*-*anti*-B[a]P-N^2-dG modified DNA shows no increase in binding upon addition of any dNTP or rNTP. Instead, inclusion of any nucleotide results in a large destabilization. This is indicative of the (-)-*trans*-*anti*-B[a]P-N^2-dG adduct preventing the Klenow fragment from forming a closed

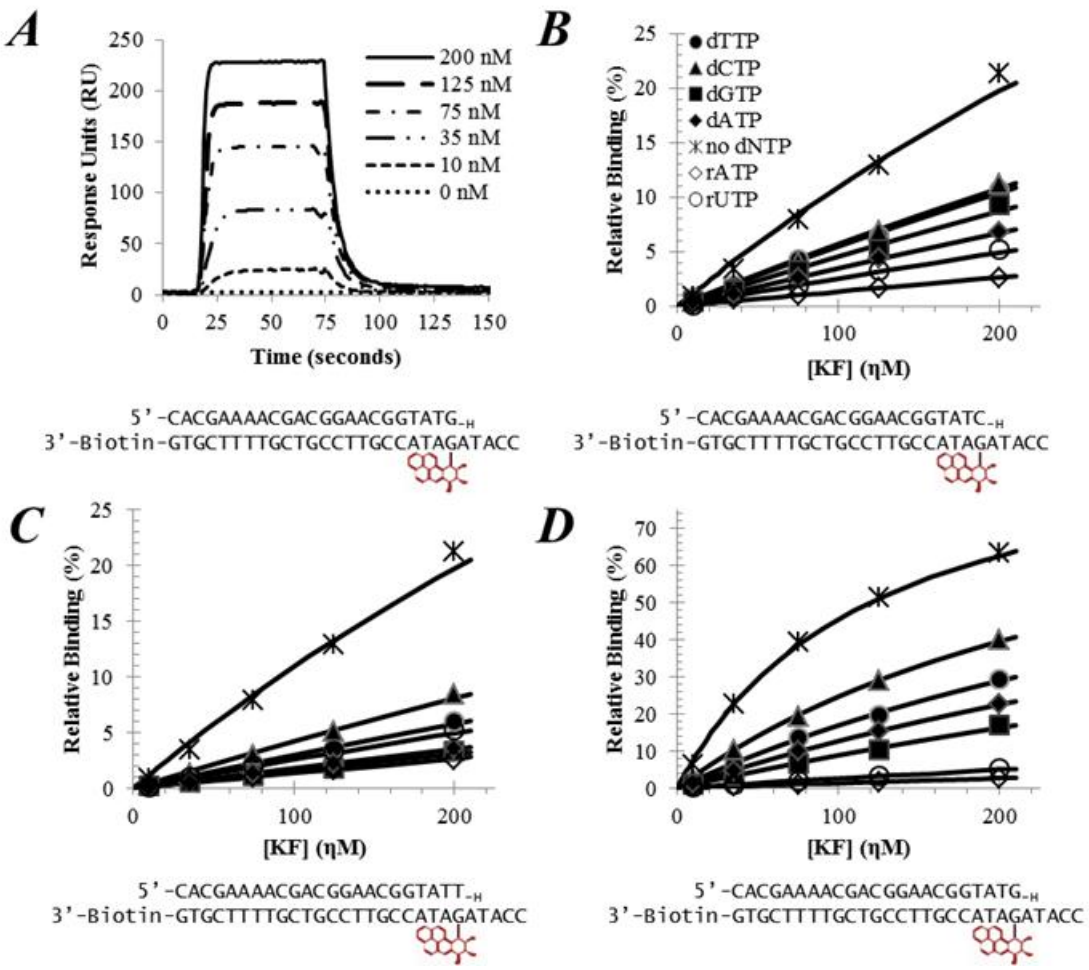

Figure 44. Determination of equilibrium binding constants from Langmuir binding isotherms. (A) Representative sensorgrams of concentration series showing KF binding to a G:G-B[a]P primer-template. (B) Isotherms for KF binding to a correctly base paired C:G-B[a]P primer-template. (C) Isotherms for KF binding to a mismatched base paired T:G-B[a]P primer-template. (D) Isotherms for KF binding to a mismatched base paired G:G-B[a]P primer-template. Data points are indicated as follows: no dNTP(×), dTTP (●), dATP (♦), dGTP(■), dCTP(▲), rATP(◊), and rUTP(○).

ternary complex in the presence of a correctly pairing dNTP. The active site is most likely so distorted by the large adduct that even properly base-pairing dNTPs are interpreted as incorrect. However, the binding of dNTP must still occur because its presence leads to a measureable destabilization. This is similar to gel shift binding experiments examining (-)-*trans*-*anti*-B[a]P-N^2-dG modified templates that show no net stabilization from the addition of any dNTP, but instead a destabilizing effect was noted (*64*). Yet, similar to unmodified DNA, (-)-*trans*-*anti*-B[a]P modified templates show less destabilization in the presence of smaller incorrectly pairing pyrimidines that larger bulky mispairing purines.

iv. Effect of NTPs on Mismatched (-)-trans-anti-B[a]P-N2-dG Primer-Templates

Positioning of a mismatch at the -1 position on unmodified DNA resulted in an inability for the KF to undergo a conformational transition to the closed complex upon addition of any dNTP or rNTP. Similarly, positioning of a T:G-B[a]P or a G:G-B[a]P at the -1 position caused the polymerase to become destabilized upon addition of any dNTP or rNTP. The T:G-B[a]P substrate showed a 4- to 8-fold decrease in stabilization upon addition of any dNTP. Similarly, the tighter binding G:G-B[a]P complex also underwent a 3-9 fold decrease in binding upon addition of any dNTP. This is in very similar to the 3-13 fold decrease seen with unmodified DNA mismatches at the -1 position. In addition, the smaller pyrimidines once again exhibited smaller levels of destabilization than the larger purine nucleotide triphosphates.

v. Dissociation Rates from (-)-trans-anti-B[a]P Primer-Templates

Visual examination of the sensorgrams revealed that the G:G-B[a]P complex undergoes slower rates of dissociation than properly paired C:G-B[a]P or T:G-B[a]P substrates. Figure 45 shows fitting of a single exponential decay (Equation 2) to C:G-B[a]P, T:G-B[a]P, and G:G-B[a]P substrates. Single exponential decays provided good fits to the data. Table 6 shows the determined k_{off} values for the various experiments. The same trends noted above are once again noted upon examination of the dissociation rates. The G:G-B[a]P mismatch shows the slowest off rate, approximately 3- to 4-fold slower than for C:G-B[a]P, or T:G-B[a]P substrates. The addition of any dNTP or rNTP to any of the (-)-*trans*-*anti*-B[a]P-N^2-dG DNA substrates resulted in an increase in the k_{off} by approximately 2- to 4-fold.

Table VI. Dissociation rates for release of Klenow fragment from various B[a]P labeled primer-templates in the presence or absence of 2'-deoxynucleotide-5'-triphosphates.[a]

	Dissociation rates, K_d (s^{-1})[c]				
Primer-Templates[b]	No NTP	dTTP	dATP	dCTP	dGTP
C:G-B[a]P Correct BP	0.53 ± 0.04	1.09 ± 0.03	1.37 ± 0.14	0.89 ± 0.06	1.42 ± 0.11
T:G-B[a]P Mismatch	0.61 ± 0.09	1.13 ± 0.2	1.26 ± 0.16	0.84 ± 0.14	1.54 ± 0.05
G:G-B[a]P Mismatch	0.17 ± 0.01	0.48 ± 0.02	0.63 ± 0.12	0.38 ± 0.02	0.72 ± 0.23

[a] The dissociation rates (K_d) were determined as described under materials and methods.
[b] The sequences used to form the primer-template duplexes are depicted in figure 20 (T:G mismatch, C:G correct BP, and G:G mismatch are A, B, and C respectively).
[c] Values represent averages of global fits to triplicate data ± standard deviation

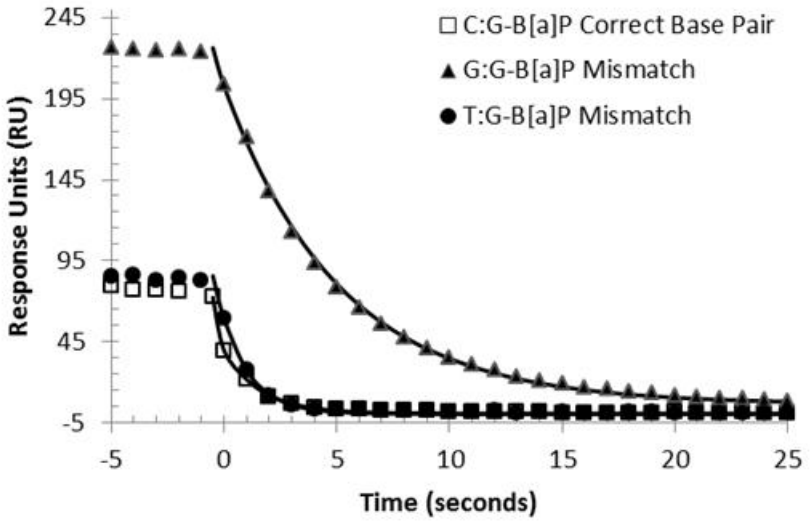

Figure 45. Representative dissociation phase for Klenow fragment binding in the absence of dNTPs. Data points are shown as points and fits are shown as solid lines. Data points are indicated as follows: C:G-B[a]P correct base pair (□),T:G-B[a]P mismatch (●), G:G-B[a]P mismatch (▲).

CHAPTER IV: DISCUSSION

I. MALDI-TOF Method Development

It has been established by prior work that hydrophobic surfaces can enhance the resolution of MALDI-TOF mass spectra and aid in the ability of obtaining sample spots with high levels of crystalline matrix suitable for laser vaporization (*111, 112*). We have developed methods for preparing a uniform hydrophobic surface made up of a thin and very uniform layer of Parafilm that not only provides these advantages, but also allows the use of external standards and provides low levels of background signal.

Our hydrophobic coating is easy to apply, inexpensive, and the materials are readily available in almost all labs. The very thin hydrophobic layer produces a true non-wetting surface that minimizes the contact surface area of the liquid to the coating. This is beneficial because the volume to surface area ratio is minimized by placing hydrophilic buffers on non-wetting surfaces. Because the volume to surface area ratio of the sample spots are larger on the hydrophobic surface as compared with the ground steel, the spots dry more slowly. As the samples dry they maintain a spherical shape while shrinking in diameter whereas the sample spots on the steel tend to flatten out and remain widespread. This compact nature of the sample makes it much easier upon sample crystallization to find areas with crystals that give good spectra. Further, this action concentrating action also lowers the limits of detection for samples. This is in agreement with result others have found using different hydrophobic surfaces (*111, 112*).

Quite often the most difficult part of MS is locating sample that gives good signal. On the Parafilm layer this is not difficult because of the wealth of usable signal. This has

also previously been noted by other researchers utilizing similar hydrophobic surfaces (*111, 112*). This effect is thought to occur due to the concentration of sample into a smaller area. This effectively raises the amount of sample vapourized (and subsequently traveling to the detector) with each shot of the laser. Our results indicate about a 20 times higher likelihood of obtaining similar spectra on parafilm coated surfaces than on ground steel. This implies that if one were to randomly shoot at the crystal one would be about 20 times more likely to hit a high quality area for crystals grown on the Parafilm coating than on the ground steel. This increase in area that gives high quality signals on the Parafilm coating dramatically cuts down on the time needed to locate regions within the crystal that are usable. In addition, the number of samples spotted that do not give any usable signal also drops significantly. Virtually all samples spotted gave usable signal.

Not only does the Parafilm layer greatly increase the usable sample area for analysis, but also results in improved resolution. The spectra obtained tend to be of superior quality, and have clearer peaks. As a result less smoothing is required upon processing of spectra. The clearer spectra containing usable additional salt peaks provide further points for calibration when shooting standards, and provide more peaks to confirm the identity of unknown sample masses. In addition, the spectra obtained on ground steel tend to lack M+2H peaks in comparison to spectra obtained on Parafilm. The lack of these peaks reduces the utility of internal standards since these calibration points are often missing. Spectra obtained on the hydrophobic coating consequently allow mass calibration over a wider range, extending their usefulness. Adding to this is the lower background noise obtained at low mass ranges on the Parafilm layer. This becomes useful

when spectra over a large mass range are being obtained. For instance, when performing exonuclease digests of DNA and subsequently utilizing the MALDI-TOF for sequencing analysis, the introduction of noise in the low mass range interferes with identifying lower mass fragments (*103*). As a result exonuclease digests must be performed in both the 5' to 3' and 3' to 5' directions. The use of this Parafilm coating may help reduce the aberrant noise found in the lower mass range, which will aid in obtaining a more complete mass spectrum of the exonuclease digest.

Prior studies had shown that when utilizing coatings on plates it is difficult to employ external standards due to variances in the thickness of the deposited coating (*112*). These variations in film thickness create shorter and longer time of flights that introduce error into the associated masses. The prior experiments indicated that the variances in the mass spectral data prior to processing were minimal. This high reproducibility between subsequent spots on the Parafilm-coated plate implied that the variances in the Parafilm thickness may be negligible. Microscopic examination of the Parafilm layer revealed that its thickness was smaller than the thickness of most crystals. As a result we chose to examine the possibility of utilizing external standards with the Parafilm coating. Our results suggest that the use of the Parafilm coating allows accurate mass determination even when utilizing external standards. The accuracy obtained with the Parafilm coating when using external standards served to further confirm the ability for this thin, homogenous layer to improve on currently used MALDI-TOF methods. Overall the time saving and ease at which excellent spectra are obtained make this method valuable to mass spectrometry.

II. Surface Plasmon Resonance

A. Unmodified DNA

Replication could not proceed without a method for proper dNTP selection. Numerous studies have identified various intermediate states describing a relatively linear mechanistic pathway (*27*). With the exception of partitioning to the exonuclease domain, the current mechanism of polymerization is in fact a linear path (Figure 4). Mismatches represent misincorporation events that have already occurred. In the case of our results, mismatches placed at the primer terminus, at the -1 position, cause a destabilizing effect as depicted by their increased dissociation constants relative to correctly base paired primer-templates. This reduced binding can be easily described along the linear polymerization path. The forward rate of step 1 (Figure 4) could be decreased due to unfavourable interactions of the non-Watson Crick DNA structure, restricting polymerase binding. Alternatively, the reverse dissociation rate could be increased due to an unstable conformation the DNA adopts within the polymerase upon binding. Polymerases with exonuclease domains have also been shown to increase the partitioning to the exonuclease domain upon binding mismatches, and that the dissociation rate from this domain is different than that from the polymerase domain (*30, 31, 127*). Regardless, the observed effects of terminal mismatches in the absence of dNTPs are readily accounted for in the current mechanistic model.

Similarly, the increase in binding noted in the presence of the next correct dNTP can also be accounted for in the linear model. Addition of a correctly pairing dNTP causes a conformational change of the polymerase into a ternary closed complex (Step 3)

(*24*). This sequestering of enzyme and DNA in this closed conformation effectively shifts the equilibrium to the right, de-populating the binary complex and causing free DNA and enzyme to bind in order to fill the void. Such a shift results in more KF-DNA complex which is measured as an increase in binding. This result is also neatly validated in the linear mechanistic pathway.

However, the addition of an incorrectly pairing dNTP has experimentally been shown to decrease the level of binding below that of simply binary complex formation (in this study and in (*80, 89*)). It is of importance to note that any DNA bound by enzyme, whether in a binary, open ternary, or closed ternary complex, will show up as "binding" on many experiments such as gel shift, or in this case SPR experiments. With the current linear model as seen in Figure 4 this destabilization result simply cannot be explained. For example, if the dNTP was an incompatible fit and subsequently did not undergo transition to the closed ternary complex but instead remained populated within the open ternary complex, the relative populations of the binary and open ternary complex will still exceed that of the binary complex in the absence of nucleotide. Taken one step further, the worst case example would be if the dNTP was completely restricted from forming the ternary complex at all, the mechanism remaining would be that up to binary complex formation. Even in this worst case dNTP binding situation, it is impossible for the level of enzyme-DNA binding to fall below that of binary complex alone, meaning that experiments showing a decrease in KF-DNA binding below levels of experiments conducted without dNTPs cannot be explained using this linear model. The linear mechanism simply cannot account for this result.

To explain this abnormality, we propose a new path along the mechanism that is capable of accounting for this result, as well as providing a new selection pathway along which dNTPs can be continually sampled without the necessary dissociation of the polymerase. Figure 46 shows our modified mechanism. Here, an open ternary complex is formed, from dNTP binding the open binary complex, followed by one of two states; 1) in the case of a correct dNTP the polymerase may form the closed ternary complex followed by catalysis, or 2) in the case of an incorrect dNTP, the polymerase may form a destabilized ternary complex followed by rejection of the dNTP to form a destabilized binary complex, following with either direct dissociation from the DNA or reforming the open binary complex. This evacuation pathway provides several key intermediates and resolves the problem of the current model to account for destabilization caused by incorrect dNTPs. The resolution comes from the fact that once this destabilized complex is formed, the enzyme-DNA complex may directly dissociate to free enzyme and DNA. This provides a second route to free the enzyme from the DNA, and importantly, this allows the measured levels of KF-DNA complexes to fall below the levels of KF-DNA achieved during binary complex formation in the absence of dNTPs. This is because the formation of some ternary complex could potentially lead back to free enzyme and DNA without having to reform the binary complex. The dissociation from the destabilized binary complex may be brought about by decreased KF-DNA interactions following release of the incorrect dNTP.

Direct evidence for this destabilized state of the polymerase has already been experimentally determined, yet unaccounted for in the polymerase mechanism. In 2006

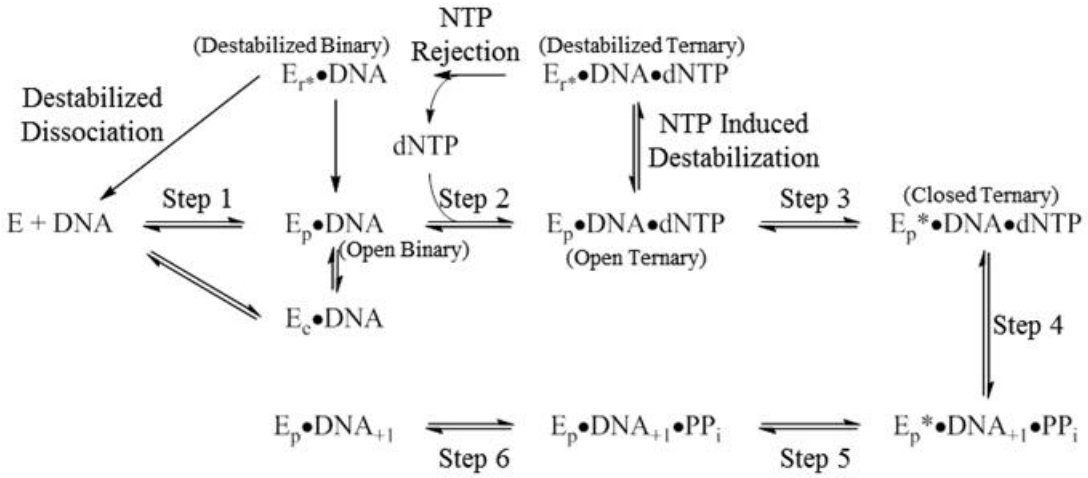

Figure 46. Novel proposed mechanism for DNA synthesis reflecting a dNTP selection cycle. Schematic representation of various states achieved during synthesis. The newly proposed mechanism includes a conformational change to a destabilized ternary complex (Er●DNA●dNTP) where the enzyme exists in a conformational state that promotes the rapid rejection of the dNTP. Following release of the dNTP the Er polymerase conformation may reform the native binary conformation or dissociate directly to free enzyme and DNA. This dissociation from the Er●DNA complex may be brought about by decreased KF-DNA interactions following release of the incorrect dNTP. Inclusion of this step provides a mechanism by which a decrease in stability may be measured during experiments such as the SPR binding assays.

Johnson *et al.* suggested that binding of an incorrect dNTP may use some of the binding energy to actively misalign catalytic residues of the polymerase (*39*). We propose that this misalignment is in fact the polymerase actively rejecting the dNTP in an attempt to speed up synthesis by finding a correctly pairing dNTP. This provides the polymerase a method to increase the dissociation of incorrect dNTPs and increase the binding of correct dNTPs as is seen with measurements of ground state dNTP binding (unpublished results). Johnson *et. al.* also stated that the resting polymerase may be in a partially closed state and that the presence of an incorrect dNTP causes the polymerase to populate the fully open state. We feel that the resting polymerase is in an open state defined by our model, and that the presence of an incorrect dNTP induces formation of a destabilized state. Joyce *et al.* have recently confirmed the existence of such a destabilized state (*38*). Using fluorescence resonance energy transfer (FRET) with two fluorophores positioned on the polymerase, they were able to show that an incorrect dNTP evokes a fluorescent state that is different from either the open binary, or the closed ternary complex. Their results fit very well into our model in which the novel fluorescent state they measured is direct evidence for either the destabilized binary or destabilized ternary complexes.

Our results also show that rNTPs undergo destabilization of the KF-DNA complexes. Because of this, we feel that rNTPs, mispairing or correctly pairing, will fall along the same pathway as mispairing dNTPs. Again, the only way to explain a destabilization effect exceeding that of forming the binary complex alone is through an alternate pathway. This is again supported by Joyce *et. al.* where it was noted that the presence of rNTPs caused the formation of the same FRET state as the incorrect dNTPs.

Also, the relative partitioning between returning from the open ternary complex to the binary complex versus preceding through the destabilized pathway may account for rate differences observed between various rNTPs versus dNTPs. For instance, the mismatched G:G primer-template shows a larger destabilization from addition of dATP than for rATP. This could indicate that the ability of rATP to bind in the open ternary complex is not as easy as for the dATP. If the rATP is incapable of forming the open ternary complex due to steric interactions, then the destabilized ternary complex cannot form. This is observed only with mismatches, possibly owning to their more confined active sites not allowing competent binding of the rATP.

In addition to simply forming a destabilized complex followed by dissociation of the polymerase, we have included a step whereby the destabilized binary complex may transition back to an open binary complex, and feel this is the preferred path for several reasons. This step ensures that each time the polymerase incurs a mismatched dNTP or an rNTP within the active site it will not necessarily lead to dissociation of the entire complex. We feel that the preferred route for an incorrect NTP is the cyclic path: 1) incorrect dNTP binding to form an open ternary complex, 2) dNTP-induced polymerase misalignment forming destabilized ternary complex, 3) dissociation of the incorrect dNTP to form a destabilized open complex and 4) reforming of the open binary complex to which new dNTP may bind. This pathway provides the polymerase a method to cycle actively the nucleotides in a rapid and efficient effort to find a correct match. Figure 47 shows a representation of how the DNA synthesis pathway overlaps with what we term the dNTP selection loop. This process can occur without dissociation of the polymerase;

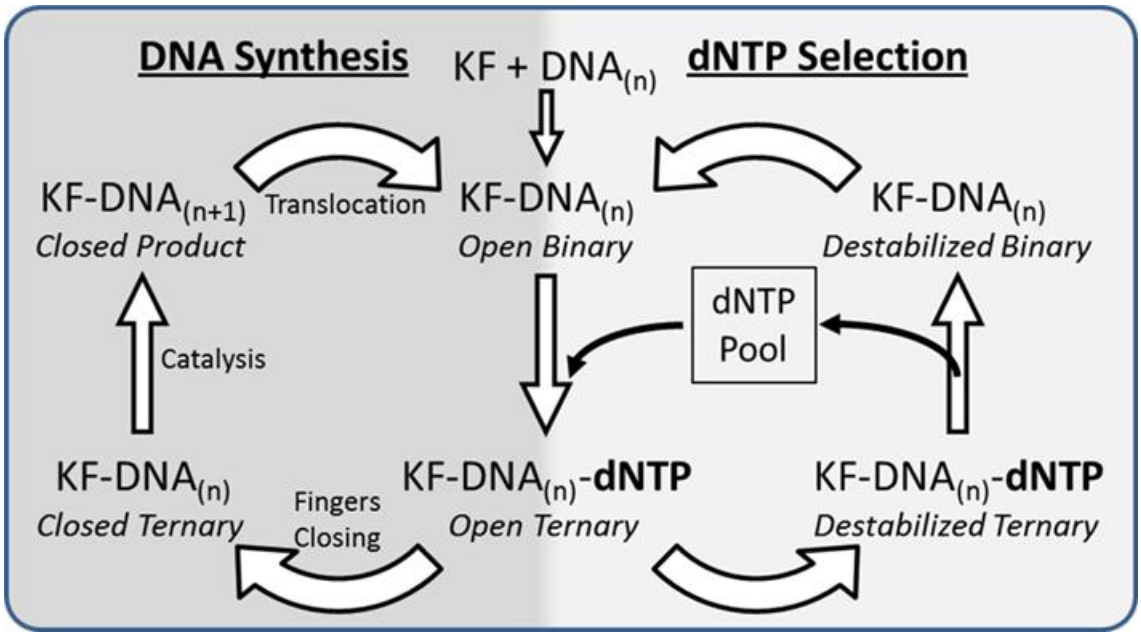

Figure 47. dNTP selection cycle. Cartoon depiction showing how the DNA synthesis cycle may be coupled to the dNTP selection cycle. After formation of an open ternary complex the polymerase will transform into one of two conformational states that is driven by the nature of the template-dNTP interactions. Incorrectly pairing dNTPs will be rejected reforming the open binary complex and allowing a new dNTP from the pool to be sampled and correct dNTPs will undergo synthesis into the growing primer chain.

however, the destabilized binary complex does possess the ability to dissociate to free enzyme, giving the polymerase an advantage on non-native templates such as carcinogenic adducts. For instance, if a polymerase stalls at a location due to an altered or non-native template base, the polymerase may cycle in multiple attempts to find a correct dNTP match, followed by an increased rate of dissociation from existing in the destabilized state. This dissociation will allow another polymerase, possibly a lesion bypass polymerse in the case of DNA adducts, to complete the synthesis. Similar to this example, repetitive bombardment of mispairing dNTPs is seen in experiments such as ours in which only the incorrect dNTP is present, and no correct match can be found. Here even a small contribution to this repetitive loop by directly dissociating from the destabilized binary complex to free enzyme can contribute to equilibrium binding levels that fall below that of binary complex formation alone.

This cycle also predicts that a great deal of nucleotide selectivity must occur in the open state. The proverbial fork in the pathway exists after formation of the open ternary complex. Previous reports have argued that a great deal of the dNTP selection process must occur within the open ternary complex (*2*). Our model agrees with this, in which the resulting mechanistic path that is chosen based upon whether the current dNTP within the polymerase was deemed correct or not; however, it should be noted that the forked point may be downstream of the open ternary complex falling after another intermediate, but must still remain prior to formation of the closed ternary complex. That is to say that step 3 may be broken into several smaller steps, and the formation of the destabilized state will lay at some step prior to conformational closing (*27*).

Our selectivity assay correlates well with this novel cycle in the mechanism. The stabilization measured in the presence of a correctly base-pairing dTTP on the correct substrate indicates formation of the closed ternary complex. The destabilization measured with any other dNTPs is due to formation of the destabilized ternary complex which eventually leads to direct dissociation of the destabilized binary complex. The mismatched primer-templates also showed the ability to form destabilized complexes although they did not form any stabilizing complexes. This result indicates that with these mismatched substrates the polymerase are still capable of forming a ternary complex; however, it transitions primarily to a destabilized ternary complex and not to a closed ternary complex. The mismatch at the post insertion site most likely forms a conformation the polymerase interprets as incorrect, inhibiting formation of a closed ternary complex. However, the polymerase must not block the formation of the destabilized ternary complex because we are still capable of measuring destabilization above and beyond formation of the binary complex alone. This dissociation would be advantageous to the cell to allow other enzymes to repair the damaged DNA bases prior to re-initiating synthesis.

Our results shown in Figure 42B also illustrate the process by which dNTPs are sampled without dissociation of the polymerase. The equilibrium KF-DNA binding levels obtained prior to initiating dissociation will populate the various states defined by the mechanism. During dissociation, when a dNTP is not present, the population of Klenow fragment in the closed ternary complex quickly re-opens to form the open ternary complex followed eventually by dissociation from the DNA, which is seen as a fast

dissociation phase. Conversely, when a correctly pairing dNTP is added during the dissociation phase, the polymerase remains bound significantly longer. The explanation for this comes from the polymerase being able to open and exchange dNTPs without dissociation from the DNA. In the case of no dNTP present during dissociation, the closed ternary complexes formed during equilibrium will have no dNTP to exchange when it reopens to form the binary complex. On the other hand, the dissociation phase containing free correct dNTP affords the polymerase the ability to open, releasing the dNTP followed by binding of a new dNTP and reforming the closed complex. If this exchange of dNTP was not possible the results for Figure 42A and 42B would be expected to be the same or very similar.

In our mechanism the transition from open ternary to destabilized ternary may be reversible, but the direction the equilibrium lies will be determined by the identity of the dNTP. We have also assigned single direction arrows to three particular steps of the mechanism. We feel these steps represent one-way steps in which we predict the reverse rates will be extremely slow in any situation. The transition from a destabilized ternary complex to a destabilized binary complex should not occur in reverse. Once the dNTP has dissociated, the following steps are most likely rapid and energetically favoured. The dissolution of the destabilized binary complex to either the free enzyme or the binary complex is also considered a one-way step. Similar to what was proposed by Johnson *et al.*, the binding energy of the mismatched dNTP is required to transition to the destabilized state (*39*). Direct transitions from the open binary complex to a destabilized binary complex would be energetically expensive and an unlikely occurrence given no

driving energy is available for the process. The use of the dNTP binding energy to cause the polymerase to change conformation is not a new idea (*39*). The energy of binding can be used to drive the conformational change noted in the presence of a correct dNTP. Likewise, if an incorrect dNTP is present, the conformation of the polymerase may be altered into what we call the rejection conformation (E_{r*}). Formation of the rejection conformation will similarly use dNTP binding energy, and will result in a complex that has a weaker affinity for the dNTP. This correlates with studies that have shown the equilibrium dissociation constants for binding of incorrect dNTPs are higher than correct dNTPs. We also suggest that there may possibly be alternative conformations of the DNA formed during this process. This is a possibility, although we feel it is unlikely. The direct dissociation of the rejection conformation would be due to weaker KF-DNA interactions induced by changes in polymerase conformations rather than DNA conformational alterations.

DNA polymerases have had a great deal of time to evolve and perfect their mechanism of DNA synthesis. It appears unlikely that through evolution polymerases would miss an opportunity to actively expedite the process of dNTP selection. Our proposed model incorporates a new cyclic pathway whereby the polymerase actively undergoes dNTP selection that can take place without dissociation of the enzyme, thereby allowing an increase in the rate at which a polymerase finds a correct dNTP. Inclusion of this novel pathway is obligatory to understanding the way polymerases function. We feel that this minimal reaction mechanism should currently be examined when interpreting results. In addition, other enzymes that use a similar process of selection, for instance

RNA polymerases, may also benefit from including such a selection step in their mechanisms. Lastly, our mechanism predicts states that should hopefully be detectible in future assays.

B. Benzo[a]pyrene

The ability of DNA polymerases such as Klenow fragment to accurately choose the correct dNTP for incorporation into the primer is of prime significance in determining the accuracy of DNA replication. A mistake during DNA synthesis can have disastrous outcomes for the cell. Most DNA polymerases have the extraordinary ability to correctly choose dNTPs on native undamaged DNA in a repeated and rapid process (*128*). However, when a carcinogenic adduct is positioned on the same template the results are often quite different (*129*). We previously utilized surface plasmon resonance to investigate the mechanism of DNA replication, specifically to study what happens when Klenow fragment is in the presence or absence of either a correctly pairing deoxy- or ribo-NTP or a mismatched deoxy- or ribo-NTP, on both correctly paired primer-templates and mismatched primer-templates. Using this approach we identified a novel process in the mechanism of DNA replication that selects for a correct dNTP. The addition of a correctly pairing dNTP on native correctly matched substrates results in the formation of a closed ternary complex that is productive in catalyzing the addition of the dNTP to the growing primer stand. Conversely, addition of a mismatched dNTP, or any rNTP, causes a destabilizing effect in which a destabilized ternary complex is formed followed by rejection of the nucleotide to form a destabilized binary complex (Figure 46). This destabilized complex can then dissociate from the DNA at a rate that exceeds the

reverse of step 1, binary complex formation, leading to a net decrease in measured binding levels. Using a similar approach, we have investigated how polymerase binding to a a (-)-*trans*-*anti*-B[a]P-N^2-dG adduct fits into this new step of the polymerase mechanism.

In this study, we positioned a (-)-*trans*-*anti*-B[a]P-N^2-dG adduct at the -1 position, paired with either a correctly base-pairing cytosine on the 5' end of the primer, or a mismatched thymine or guanine. Extension assays have shown that this is the location that stalls predominantly occur, with the polymerase being able to extend up to and across from a B[a]P adduct (Figure 25) (*62, 130*). Measuring the binding of Klenow fragment at this stalling position allowed us to examine what occurs during the pivitol moment when polymerases fail, and determine how misparing at this location affects polymerase binding. Similar SPR experiments on unmodified DNA showed that Klenow fragment prefers to bind to correctly base-paired primer-template terminus, with the binding to mismatched T:G and G:G primer termini being weaker. This weaker binding is due to incompatible primer-template termini that disrupt the polymerase-DNA interactions. Interestingly, our (-)-*trans*-*anti*-B[a]P-N^2-dG adducted template showed the strongest binding when a G:G-B[a]P was positioned at the -1 position. Whereas the binding to properly C:G-B[a]P and mismatched T:G-B[a]P was weaker. This implies that the structures of C:G-B[a]P and T:G-B[a]P are adopting conformations that are not conducive to the binding of the polymerase. Most likely the B[a]P moiety is adopting a conformation within the primer-template and polymerase active site that causes significant steric clashes with either the protein, or disrupts the DNA to the extent that the

polymerase is no longer capable of forming normal alignments with the primer-template terminus. The result of either would be a weakened binding to these substrates. The G:G-B[a]P mismatch may have an increased level of binding due to hydrophobic interactions of the pyrene moiety with the polymerase that is exacerbated by the G:G mismatch. Alternatively, the orientation of the pyrene moiety may be such that the adduct is positioned interacting with the DNA resulting in the mismatched guanine on either the primer or the template being positioned into a hydrophobic pocket of the polymerase. In either case, the polymerase retains a tighter affinity to the G:G-B[a]P mismatch that is unique to this structure.

The increase in binding to a G:G-B[a]P over C:G-B[a]P and T:G-B[a]P substrates indicates that the G:G-B[a]P is adopting a conformation that promotes the interactions of Klenow fragment with the substrate. Yet, despite the increased affinity, the complex is still not capable of forming productive alignments to form a closed ternary complex. The addition of the next correctly base-pairing dTTP does not induce tighter binding, but conversely diminishes binding. On all substrates tested, the inclusion of any dNTP or rNTP decreased the levels of polymerase binding lower than those obtained in the absence of dNTPs or rNTPs. The inability of the polymerase to undergo a conformational transition to a closed ternary complex indicates that NTPs are not capable of productively binding the complex. The blocking of the conformational transition to the closed complex can again be attributed to the conformations adopted by the B[a]P adducted primer-template termini. The already tight constraints of the polymerase active site, now further crowded by the presence of the adduct, interferes with the proper geometric alignment of

residues that are responsible for testing the fit of the incoming dNTP. Relating this to the polymerization mechanism, the conformational closing motion (step 3) is inhibited (Figure 48). The build-up of the open ternary complex will now cause a higher proportion of complexes to occupy the destabilized ternary complex, resulting in a measureable destabilizing effect.

Y family polymerases are able to accommodate such lesions due to their more open active site (Figure 14). The open active site will preclude the insertion of the pyrene moiety into hydrophobic pockets of the enzyme, and will free up more room for dNTPs to productively align. Members of the Y family of bypass polymerases, such as human pol K, are capable of bypassing a (-)-*trans*-*anti*-B[a]P-N^2-dG adduct by correctly inserting a C (*131*). Another study examined which polymerases are specifically responsible for non-mutagenic bypass of these adducts (*132*). Here it was found that non-mutagenic bypass of the (+)-*trans*-*anti*-B[a]P-dG was accomplished by DNA polymerase IV and V, whereas non-mutagenic bypass of the (-)-*trans*-*anti*-B[a]P-dG was accomplished by DNA polymerase IV alone. This variation in polymerase for non-mutagenic bypass illustrates the importance stereochemistry and the conformations that these adducts adopt within the polymerease. It has yet to be determined whether bypass polymerases undergo the same kinetic mechanism as regular replicative polymerases, but it would appear that they are less susceptible to undergoing re-arrangements to a destabilized ternary complex due to their open active sites.

In summary, the positioning of a bulky (-)-*trans*-*anti*-B[a]P-N^2-dG adduct at the -1 position causes Klenow fragment to be unable to efficiently undergo a conformational

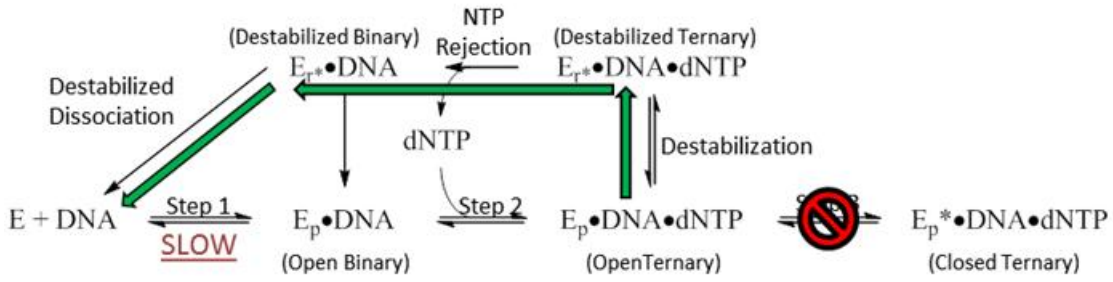

Figure 48. Mechanism of DNA replication. The presence of a (-)-*trans*-*anti*-B[a]P-N^2-dG adduct inhibits the formation of the ternary closed complex, resulting in a greater partitioning to the destabilized ternary complex, and a faster rate of dissociation from the DNA.

rearrangement to a closed ternary complex in the presence of dNTPs or rNTPs. This results in the population of destabilized ternary complex and rapid dissociation of the polymerase from the DNA. In addition a G:G-B[a]P mismatch forms a unique structure that yields a tightly bound complex that is also incapable of forming a normal closed ternary complex. Taken together, this suggests that the structures of these various primer-templates are different within the polymerase.

III. Conclusions and Future Directions

A. Unmodified DNA

Using surface plasmon resonance and an assay that directly examines the impact of the identity of the incoming dNTP on formation of KF-DNA complexes; we have shown evidence for the formation of a stabilized complex in the presence of correctly pairing dNTPs, and formation of a destabilized complex in the presence of incorrectly pairing dNTPs. The formation of a closed ternary complex has been previously accounted for in the minimal reaction pathway. However, the minimal reaction pathway cannot account for the destabilizing effect an incorrect dNTP bestows upon the complex. We have accounted for this by including a destabilized dissociation pathway into the minimal reaction scheme. Furthermore, inclusion of the destabilized complex into the minimal mechanism of DNA polymerization reveals a selection cycle by which polymerases may choose a correctly pairing substrate for incorporation into the growing primer strand. This minimal reaction pathway predicts particular intermediates that may be probed in future studies. For example, single molecule studies may be able to directly measure formation of the various destabilized states, and directly monitor the destabilizing effect in real

time. In particular, measurements capable of visualizing either the destabilized ternary, or the destabilized binary complex, would supply further evidence for this pathway.

Our reaction pathway also predicts a dNTP selection cycle. This selection cycle shows how polymerases aid in the removal of mispairing dNTPs from their active sites in an effort to seek a correctly pairing dNTP for catalysis. Future experiments can utilize combinations of dNTPs, both correct and incorrect, at varying levels to examine the ability of polymerase to sample the substrates. By examining the concentration dependence and ratio of these substrates to the binding of Klenow fragment, insight can be gained into how the polymerase can cycle through various dNTP substrates.

Our experiments examining mismatches revealed that an incorporation event that places a mismatch into the post-insertion site creates a substrate where the polymerase is incapable of sufficiently determining the next correct dNTP to be incorporated. This terminal mismatch presumably forms an incompatible substrate with our tested mismatches. To further examine the effects of mismatches, an A:G mismatch can be compared with the G:G and T:G mismatches used in this study. Also, examination of mismatches in other sequence contexts may reveal a sequence dependence effect whereby some mismatches can be accommodated in some sequence contexts. Further, similar experiments can be performed with different classes of polymerases, such as the bypass polymerase Polη, to determine how they cope with the presence of mismatches and how they are capable of determining nucleotide selectivity on these DNA substrates.

B. Benzo[a]pyrene

Bulky DNA adducts such as benzo[a]pyrene interfere with replication by forming structures within the polymerase that preclude the productive binding of dNTPs, and/or inhibit the conformational change. We studied the effect various dNTPs have upon Klenow fragment binding to several (-)-*trans*-anti-B[a]P-N^2-dG adducted primer-templates. The presence of the (-)-*trans*-*anti*-B[a]P-N^2-dG adduct interferes with the formation of a stable closed ternary complex. Unlike unmodified DNA, the addition of any dNTP favoured formation of a destabilized ternary complex that rapidly dissociates to free polymerase and DNA. In addition, Klenow fragment shows tighter binding to a mismatched G:G-B[a]P adducted primer-template than either a correctly base paired C:G-B[a]P or mismatched T:G-B[a]P primer template. The G:G-B[a]P structure was also inhibited from forming the closed ternary complex, yet dissociation rates from this complex were slower than for the correctly base paired C:G-B[a]P or mismatched T:G-B[a]P primer template. This result indicates that the conformation adopted by the G:G-B[a]P within the active site of the polymerase is unique to this structure.

It is unclear whether this increased binding is a result of the G:G-B[a]P mismatch alone, or also dictated by the surrounding sequence. Future experiments can examine the same G:G-B[a]P mismatch positioned within different sequence contexts to make this determination. In addition, experiments can be conducted where the similar (+)-*trans*-*anti*-B[a]P-N^2-dG adduct is placed within the same sequence. The mutagenic profile for the (-)-*trans*-*anti*-B[a]P-N^2-dG adduct is different from that of the (+)-*trans*-*anti*-B[a]P-N^2-dG adduct, and we would predict that this adduct would not form the same types of

structures (*133*). Also, the study can be furthered by examining the (-)-*cis*-*anti*-B[a]P-N^2-dG and (+)-cis-*anti*-B[a]P-N^2-dG adducts. Again, it is expected that each of these adducts will produce a different binding pattern than the (-)-*trans*-*anti*-B[a]P-N^2-dG adduct due to differences in their mutagenic profiles (*7*). Further, binding of various polymerases such as the bypass polymerase Polη can be examined to note any differences as compared to replicative polymerases.

REFERENCES

1. Watson, J. D., and Crick, F. H. (1953) The structure of DNA, *Cold Spring Harb Symp Quant Biol 18*, 123-131.
2. Joyce, C. M., Potapova, O., Delucia, A. M., Huang, X., Basu, V. P., and Grindley, N. D. (2008) Fingers-closing and other rapid conformational changes in DNA polymerase I (Klenow fragment) and their role in nucleotide selectivity, *Biochemistry 47*, 6103-6116.
3. Dzantiev, L., Alekseyev, Y. O., Morales, J. C., Kool, E. T., and Romano, L. J. (2001) Significance of nucleobase shape complementarity and hydrogen bonding in the formation and stability of the closed polymerase-DNA complex, *Biochemistry 40*, 3215-3221.
4. Wuite, G. J., Smith, S. B., Young, M., Keller, D., and Bustamante, C. (2000) Single-molecule studies of the effect of template tension on T7 DNA polymerase activity, *Nature 404*, 103-106.
5. Kapitulnik, J., Levin, W., Conney, A. H., Yagi, H., and Jerina, D. M. (1977) Benzo[a]pyrene 7,8-dihydrodiol is more carcinogenic than benzo[a]pyrene in newborn mice, *Nature 266*, 378-380.
6. Gupta, P. K., Johnson, D. L., Reid, T. M., Lee, M. S., Romano, L. J., and King, C. M. (1989) Mutagenesis by single site-specific arylamine-DNA adducts. Induction of mutations at multiple sites, *J Biol Chem 264*, 20120-20130.
7. Loechler, E. L. (1995) How are potent bulky carcinogens able to induce such a diverse array of mutations?, *Mol Carcinog 13*, 213-219.

8. Denissenko, M. F., Pao, A., Tang, M., and Pfeifer, G. P. (1996) Preferential formation of benzo[a]pyrene adducts at lung cancer mutational hotspots in P53, *Science 274*, 430-432.

9. Ibanez, R., Agudo, A., Berenguer, A., Jakszyn, P., Tormo, M. J., Sanchez, M. J., Quiros, J. R., Pera, G., Navarro, C., Martinez, C., Larranaga, N., Dorronsoro, M., Chirlaque, M. D., Barricarte, A., Ardanaz, E., Amiano, P., and Gonzalezi, C. A. (2005) Dietary intake of polycyclic aromatic hydrocarbons in a Spanish population, *Journal of food protection 68*, 2190-2195.

10. Kornberg, A. (1957) Enzymatic synthesis of deoxyribonucleic acid, *Harvey Lect 53*, 83-112.

11. Shlomai, J., and Kornberg, A. (1980) A prepriming DNA replication enzyme of Escherichia coli. I. Purification of protein n': a sequence-specific, DNA-dependent ATPase, *J Biol Chem 255*, 6789-6793.

12. Klenow, H., and Overgaard-Hansen, K. (1970) Proteolytic cleavage of DNA polymerase from Escherichia Coli B into an exonuclease unit and a polymerase unit, *FEBS Lett 6*, 25-27.

13. Klenow, H., and Henningsen, I. (1970) Selective elimination of the exonuclease activity of the deoxyribonucleic acid polymerase from Escherichia coli B by limited proteolysis, *Proc Natl Acad Sci U S A 65*, 168-175.

14. Derbyshire, V., Grindley, N. D., and Joyce, C. M. (1991) The 3'-5' exonuclease of DNA polymerase I of Escherichia coli: contribution of each amino acid at the active site to the reaction, *EMBO J 10*, 17-24.

15. Ollis, D. L., Brick, P., Hamlin, R., Xuong, N. G., and Steitz, T. A. (1985) Structure of large fragment of Escherichia coli DNA polymerase I complexed with dTMP, *Nature 313*, 762-766.

16. Korolev, S., Nayal, M., Barnes, W. M., Di Cera, E., and Waksman, G. (1995) Crystal structure of the large fragment of Thermus aquaticus DNA polymerase I at 2.5-A resolution: structural basis for thermostability, *Proc Natl Acad Sci U S A 92*, 9264-9268.

17. Beese, L. S., Derbyshire, V., and Steitz, T. A. (1993) Structure of DNA polymerase I Klenow fragment bound to duplex DNA, *Science 260*, 352-355.

18. Li, Y., Korolev, S., and Waksman, G. (1998) Crystal structures of open and closed forms of binary and ternary complexes of the large fragment of Thermus aquaticus DNA polymerase I: structural basis for nucleotide incorporation, *EMBO J 17*, 7514-7525.

19. Arai, K., Arai, N., Shlomai, J., and Kornberg, A. (1980) Replication of duplex DNA of phage phi X174 reconstituted with purified enzymes, *Proc Natl Acad Sci U S A 77*, 3322-3326.

20. Kiefer, J. R., Mao, C., Braman, J. C., and Beese, L. S. (1998) Visualizing DNA replication in a catalytically active Bacillus DNA polymerase crystal, *Nature 391*, 304-307.

21. Doublie, S., Tabor, S., Long, A. M., Richardson, C. C., and Ellenberger, T. (1998) Crystal structure of a bacteriophage T7 DNA replication complex at 2.2 A resolution, *Nature 391*, 251-258.

22. Pelletier, H., Sawaya, M. R., Kumar, A., Wilson, S. H., and Kraut, J. (1994) Structures of ternary complexes of rat DNA polymerase beta, a DNA template-primer, and ddCTP, *Science 264*, 1891-1903.

23. Li, Y., Kong, Y., Korolev, S., and Waksman, G. (1998) Crystal structures of the Klenow fragment of Thermus aquaticus DNA polymerase I complexed with deoxyribonucleoside triphosphates, *Protein Sci 7*, 1116-1123.

24. Dzantiev, L., and Romano, L. J. (2000) A conformational change in E. coli DNA polymerase I (Klenow fragment) is induced in the presence of a dNTP complementary to the template base in the active site, *Biochemistry 39*, 356-361.

25. Doublie, S., Sawaya, M. R., and Ellenberger, T. (1999) An open and closed case for all polymerases, *Structure 7*, R31-35.

26. Brown, J. A., Fiala, K. A., Fowler, J. D., Sherrer, S. M., Newmister, S. A., Duym, W. W., and Suo, Z. (2010) A novel mechanism of sugar selection utilized by a human X-family DNA polymerase, *J Mol Biol 395*, 282-290.

27. Joyce, C. M., and Benkovic, S. J. (2004) DNA polymerase fidelity: kinetics, structure, and checkpoints, *Biochemistry 43*, 14317-14324.

28. Dahlberg, M. E., and Benkovic, S. J. (1991) Kinetic mechanism of DNA polymerase I (Klenow fragment): identification of a second conformational change and evaluation of the internal equilibrium constant, *Biochemistry 30*, 4835-4843.

29. Datta, K., Johnson, N. P., and von Hippel, P. H. (2010) DNA conformational changes at the primer-template junction regulate the fidelity of replication by DNA polymerase, *Proc Natl Acad Sci U S A 107*, 17980-17985.

30. Donlin, M. J., Patel, S. S., and Johnson, K. A. (1991) Kinetic partitioning between the exonuclease and polymerase sites in DNA error correction, *Biochemistry 30*, 538-546.

31. Beechem, J. M., Otto, M. R., Bloom, L. B., Eritja, R., Reha-Krantz, L. J., and Goodman, M. F. (1998) Exonuclease-polymerase active site partitioning of primer-template DNA strands and equilibrium Mg2+ binding properties of bacteriophage T4 DNA polymerase, *Biochemistry 37*, 10144-10155.

32. Trincao, J., Johnson, R. E., Escalante, C. R., Prakash, S., Prakash, L., and Aggarwal, A. K. (2001) Structure of the catalytic core of S. cerevisiae DNA polymerase eta: implications for translesion DNA synthesis, *Mol Cell 8*, 417-426.

33. Ling, H., Boudsocq, F., Woodgate, R., and Yang, W. (2001) Crystal structure of a Y-family DNA polymerase in action: a mechanism for error-prone and lesion-bypass replication, *Cell 107*, 91-102.

34. Goodman, M. F., and Tippin, B. (2000) The expanding polymerase universe, *Nat Rev Mol Cell Biol 1*, 101-109.

35. Patel, S. S., Wong, I., and Johnson, K. A. (1991) Pre-steady-state kinetic analysis of processive DNA replication including complete characterization of an exonuclease-deficient mutant, *Biochemistry 30*, 511-525.

36. Wong, I., Patel, S. S., and Johnson, K. A. (1991) An induced-fit kinetic mechanism for DNA replication fidelity: direct measurement by single-turnover kinetics, *Biochemistry 30*, 526-537.

37. Astatke, M., Ng, K., Grindley, N. D., and Joyce, C. M. (1998) A single side chain prevents Escherichia coli DNA polymerase I (Klenow fragment) from incorporating ribonucleotides, *Proc Natl Acad Sci U S A 95*, 3402-3407.

38. Santoso, Y., Joyce, C. M., Potapova, O., Le Reste, L., Hohlbein, J., Torella, J. P., Grindley, N. D., and Kapanidis, A. N. (2010) Conformational transitions in DNA polymerase I revealed by single-molecule FRET, *Proc Natl Acad Sci U S A 107*, 715-720.

39. Tsai, Y. C., and Johnson, K. A. (2006) A new paradigm for DNA polymerase specificity, *Biochemistry 45*, 9675-9687.

40. Luo, G., Wang, M., Konigsberg, W. H., and Xie, X. S. (2007) Single-molecule and ensemble fluorescence assays for a functionally important conformational change in T7 DNA polymerase, *Proc Natl Acad Sci U S A 104*, 12610-12615.

41. Christian, T. D., Romano, L. J., and Rueda, D. (2009) Single-molecule measurements of synthesis by DNA polymerase with base-pair resolution, *Proc Natl Acad Sci U S A 106*, 21109-21114.

42. Pott, P. (1775) *Reprinted in Natl. Cancer Inst. Mono. 10*, 7-13.

43. Bell, J. (1876) *Edinburgh Med. J. 22*, 135-137.

44. Passey, R. D. (1922) *Brit. Med. J. 2*, 1112-1116.

45. Cook, J., Hewett, C. L., and Heiger, I. (1933) *J. Chem. Soc.*, 398-405.

46. Phillips, D. H. (1983) Fifty years of benzo(a)pyrene, *Nature 303*, 468-472.

47. Zedeck, M. S. (1980) Polycyclic aromatic hydrocarbons: a review, *Journal of environmental pathology and toxicology 3*, 537-567.

48. Wood, A. W., Chang, R. L., Levin, W., Yagi, H., Thakker, D. R., Jerina, D. M., and Conney, A. H. (1977) Differences in mutagenicity of the optical enantiomers of the diastereomeric benzo[a]pyrene 7,8-diol-9,10-epoxides, *Biochem Biophys Res Commun 77*, 1389-1396.

49. Lee, M. L., Prado, G. P., Howard, J. B., and Hites, R. A. (1977) Source identification of urban airborne polycyclic aromatic hydrocarbons by gas chromatographic mass spectrometry and high resolution mass spectrometry, *Biomedical mass spectrometry 4*, 182-185.

50. Hattemer-Frey, H. A., and Travis, C. C. (1991) Benzo-a-pyrene: environmental partitioning and human exposure, *Toxicol Ind Health 7*, 141-157.

51. Simon, R., Palme, S., and Anklam, E. (2006) Single-laboratory validation of a gas chromatography-mass spectrometry method for quantitation of 15 European priority polycyclic aromatic hydrocarbons in spiked smoke flavourings, *Journal of chromatography 1103*, 307-313.

52. Pandey, M. K., Yadav, S., Parmar, D., and Das, M. (2006) Induction of hepatic cytochrome P450 isozymes, benzo(a)pyrene metabolism and DNA binding following exposure to polycyclic aromatic hydrocarbon residues generated during repeated fish fried oil in rats, *Toxicology and applied pharmacology 213*, 126-134.

53. Santodonato, J., Howard, P., and Basu, D. (1981) Health and ecological assessment of polynuclear aromatic hydrocarbons, *Journal of environmental pathology and toxicology 5*, 1-364.

54. Hecht, S. S. (1999) Tobacco smoke carcinogens and lung cancer, *Journal of the National Cancer Institute 91*, 1194-1210.

55. Boyland, E. (1947) *Yale J. Med. Biol. 20*, 321-341.

56. Brookes, P., and Lawley, P. D. (1964) Reaction Of Some Mutagenic And Carcinogenic Compounds With Nucleic Acids, *J Cell Physiol 64*, SUPPL 1:111-127.

57. Geacintov, N. E., Yoshida, H., Ibanez, V., and Harvey, R. G. (1981) Non-covalent intercalative binding of 7,8-dihydroxy-9,10-epoxybenzo(a)pyrene to DNA, *Biochem Biophys Res Commun 100*, 1569-1577.

58. Weinstein, I. B., Jeffrey, A. M., Jennette, K. W., Blobstein, S. H., Harvey, R. G., Harris, C., Autrup, H., Kasai, H., and Nakanishi, K. (1976) Benzo(a)pyrene diol epoxides as intermediates in nucleic acid binding in vitro and in vivo, *Science 193*, 592-595.

59. Geacintov, N. E., Cosman, M., Hingerty, B. E., Amin, S., Broyde, S., and Patel, D. J. (1997) NMR solution structures of stereoisometric covalent polycyclic aromatic carcinogen-DNA adduct: principles, patterns, and diversity, *Chem Res Toxicol 10*, 111-146.

60. Pradhan, P., Jernstrom, B., Seidel, A., Norden, B., and Graslund, A. (1998) Induced circular dichroism of benzo[a]pyrene-7,8-dihydrodiol 9,10-epoxide

stereoisomers covalently bound to deoxyribooligonucleotides used to probe equilibrium distribution between groove binding and intercalative adduct conformations, *Biochemistry 37*, 4664-4673.

61. Kozack, R. E., and Loechler, E. L. (1999) Molecular modeling of the major adduct of (+)-anti-B[a]PDE (N2-dG) in the eight conformations and the five DNA sequences most relevant to base substitution mutagenesis, *Carcinogenesis 20*, 85-94.

62. Alekseyev, Y. O., and Romano, L. J. (2000) In vitro replication of primer-templates containing benzo[a]pyrene adducts by exonuclease-deficient Escherichia coli DNA polymerase I (Klenow fragment): effect of sequence context on lesion bypass, *Biochemistry 39*, 10431-10438.

63. Zhuang, P., Kolbanovskiy, A., Amin, S., and Geacintov, N. E. (2001) Base sequence dependence of in vitro translesional DNA replication past a bulky lesion catalyzed by the exo- Klenow fragment of Pol I, *Biochemistry 40*, 6660-6669.

64. Alekseyev, Y. O., Dzantiev, L., and Romano, L. J. (2001) Effects of benzo[a]pyrene DNA adducts on Escherichia coli DNA polymerase I (Klenow fragment) primer-template interactions: evidence for inhibition of the catalytically active ternary complex formation, *Biochemistry 40*, 2282-2290.

65. Shlomai, J., and Kornberg, A. (1980) An Escherichia coli replication protein that recognizes a unique sequence within a hairpin region in phi X174 DNA, *Proc Natl Acad Sci U S A 77*, 799-803.

66. Santella, R. M., and Zhang, Y. J. (2011) Immunologic detection of benzo(a)pyrene-DNA adducts, *Methods Mol Biol 682*, 271-278.

67. Eger, B. T., and Benkovic, S. J. (1992) Minimal kinetic mechanism for misincorporation by DNA polymerase I (Klenow fragment), *Biochemistry 31*, 9227-9236.

68. Washington, M. T., Carlson, K. D., Freudenthal, B. D., and Pryor, J. M. (2010) Variations on a theme: eukaryotic Y-family DNA polymerases, *Biochim Biophys Acta 1804*, 1113-1123.

69. Dzantiev, L., and Romano, L. J. (1999) Interaction of Escherichia coli DNA polymerase I (Klenow fragment) with primer-templates containing N-acetyl-2-aminofluorene or N-2-aminofluorene adducts in the active site, *J Biol Chem 274*, 3279-3284.

70. Miller, H., and Grollman, A. P. (1997) Kinetics of DNA polymerase I (Klenow fragment exo-) activity on damaged DNA templates: effect of proximal and distal template damage on DNA synthesis, *Biochemistry 36*, 15336-15342.

71. Dzantiev, L., and Romano, L. J. (2000) Differential effects of N-acetyl-2-aminofluorene and N-2-aminofluorene adducts on the conformational change in the structure of DNA polymerase I (Klenow fragment), *Biochemistry 39*, 5139-5145.

72. Lone, S., and Romano, L. J. (2003) Mechanistic insights into replication across from bulky DNA adducts: a mutant polymerase I allows an N-acetyl-2-

aminofluorene adduct to be accommodated during DNA synthesis, *Biochemistry 42*, 3826-3834.

73. Bell, J. B., Eckert, K. A., Joyce, C. M., and Kunkel, T. A. (1997) Base miscoding and strand misalignment errors by mutator Klenow polymerases with amino acid substitutions at tyrosine 766 in the O helix of the fingers subdomain, *J Biol Chem 272*, 7345-7351.

74. Romano, L. J., and Richardson, C. C. (1979) Requirements for synthesis of ribonucleic acid primers during lagging strand synthesis by the DNA polymerase and gene 4 protein of bacteriophage T7, *J Biol Chem 254*, 10476-10482.

75. Dutta, S., Li, Y., Johnson, D., Dzantiev, L., Richardson, C. C., Romano, L. J., and Ellenberger, T. (2004) Crystal structures of 2-acetylaminofluorene and 2-aminofluorene in complex with T7 DNA polymerase reveal mechanisms of mutagenesis, *Proc Natl Acad Sci U S A 101*, 16186-16191.

76. Irimia, A., Zang, H., Loukachevitch, L. V., Eoff, R. L., Guengerich, F. P., and Egli, M. (2006) Calcium is a cofactor of polymerization but inhibits pyrophosphorolysis by the Sulfolobus solfataricus DNA polymerase Dpo4, *Biochemistry 45*, 5949-5956.

77. Rodriguez, H., and Loechler, E. L. (1993) Mutational specificity of the (+)-anti-diol epoxide of benzo[a]pyrene in a supF gene of an Escherichia coli plasmid: DNA sequence context influences hotspots, mutagenic specificity and the extent of SOS enhancement of mutagenesis, *Carcinogenesis 14*, 373-383.

78. Richardson, C. C., Romano, L. J., Kolodner, R., LeClerc, J. E., Tamanoi, F., Engler, M. J., Dean, F. B., and Richardson, D. S. (1979) Replication of bacteriophage T7 DNA by purified proteins, *Cold Spring Harb Symp Quant Biol 43 Pt 1*, 427-440.

79. Tebbs, R. S., and Romano, L. J. (1994) Mutagenesis at a site-specifically modified NarI sequence by acetylated and deacetylated aminofluorene adducts, *Biochemistry 33*, 8998-9006.

80. Gill, J. P., and Romano, L. J. (2005) Mechanism for N-acetyl-2-aminofluorene-induced frameshift mutagenesis by Escherichia coli DNA polymerase I (Klenow fragment), *Biochemistry 44*, 15387-15395.

81. Strauss, B. S. (1992) The origin of point mutations in human tumor cells, *Cancer Res 52*, 249-253.

82. Meng, E. C., Pettersen, E. F., Couch, G. S., Huang, C. C., and Ferrin, T. E. (2006) Tools for integrated sequence-structure analysis with UCSF Chimera, *BMC Bioinformatics 7*, 339.

83. Pettersen, E. F., Goddard, T. D., Huang, C. C., Couch, G. S., Greenblatt, D. M., Meng, E. C., and Ferrin, T. E. (2004) UCSF Chimera--a visualization system for exploratory research and analysis, *J Comput Chem 25*, 1605-1612.

84. Verhofstad, N., van Oostrom, C. T., Zwart, E., Maas, L. M., van Benthem, J., van Schooten, F. J., van Steeg, H., and Godschalk, R. W. (2011) Evaluation of benzo(a)pyrene-induced gene mutations in male germ cells, *Toxicol Sci 119*, 218-223.

85. Gelhaus, S. L., Harvey, R. G., Penning, T. M., and Blair, I. A. (2011) Regulation of benzo[a]pyrene-mediated DNA- and glutathione-adduct formation by 2,3,7,8-tetrachlorodibenzo-p-dioxin in human lung cells, *Chem Res Toxicol 24*, 89-98.

86. Kuchta, R. D., Benkovic, P., and Benkovic, S. J. (1988) Kinetic mechanism whereby DNA polymerase I (Klenow) replicates DNA with high fidelity, *Biochemistry 27*, 6716-6725.

87. Washington, M. T., Prakash, L., and Prakash, S. (2001) Yeast DNA polymerase eta utilizes an induced-fit mechanism of nucleotide incorporation, *Cell 107*, 917-927.

88. Xu, C., Maxwell, B. A., Brown, J. A., Zhang, L., and Suo, Z. (2009) Global conformational dynamics of a Y-family DNA polymerase during catalysis, *PLoS Biol 7*, e1000225.

89. Vooradi, V., and Romano, L. J. (2009) Effect of N-2-acetylaminofluorene and 2-aminofluorene adducts on DNA binding and synthesis by yeast DNA polymerase eta, *Biochemistry 48*, 4209-4216.

90. Li, N., Luo, H. D., Jia, Y. Z., Zhou, N., and Li, Y. Q. (2011) Rapid determination of benzo(a)pyrene in processed meat and fish samples by second-derivative constant-energy synchronous fluorescence spectrometry, *Food Addit Contam Part A Chem Anal Control Expo Risk Assess 28*, 235-242.

91. Vogelstein, B., and Kinzler, K. W. (1992) Carcinogens leave fingerprints, *Nature 355*, 209-210.

92. Karas, M., Bachmann, D., and Hillenkamp, F. (1985) Influence of the wavelength in high-irradiance ultraviolet laser desorption mass spectrometry of organic molecules, *Analytical Chemistry 57*, 2935-2939.

93. Pasch, H., Schrepp, W. (2003) MALDI-TOF mass spectrometry of synthetic polymers reference, Springer, New York.

94. Puapaiboon, U., Jai-nhuknan, J., and Cowan, J. A. (2000) Rapid and direct sequencing of double-stranded DNA using exonuclease III and MALDI-TOF MS, *Anal Chem 72*, 3338-3341.

95. Smirnov, I. P., Roskey, M. T., Juhasz, P., Takach, E. J., Martin, S. A., and Haff, L. A. (1996) Sequencing oligonucleotides by exonuclease digestion and delayed extraction matrix-assisted laser desorption ionization time-of-flight mass spectrometry, *Anal Biochem 238*, 19-25.

96. Nordhoff, E., Luebbert, C., Thiele, G., Heiser, V., and Lehrach, H. (2000) Rapid determination of short DNA sequences by the use of MALDI-MS, *Nucleic Acids Res 28*, E86.

97. Kaetzke, A., and Eschrich, K. (2002) Simultaneous determination of different DNA sequences by mass spectrometric evaluation of Sanger sequencing reactions, *Nucleic Acids Res 30*, e117.

98. Petkovski, E., Keyser-Tracqui, C., Hienne, R., and Ludes, B. (2005) SNPs and MALDI-TOF MS: tools for DNA typing in forensic paternity testing and anthropology, *Journal of forensic sciences 50*, 535-541.

99. Bray, M. S., Boerwinkle, E., and Doris, P. A. (2001) High-throughput multiplex SNP genotyping with MALDI-TOF mass spectrometry: practice, problems and promise, *Human mutation 17*, 296-304.

100. Zhang, L., Kasif, S., and Cantor, A. C. (2007) Quantifying DNA-protein binding specificities by using oligonucleotide mass tags and mass spectroscopy, *Proc Natl Acad Sci U S A 104*, 3061-3066.

101. Marchand, C., Krajewski, K., Lee, H. F., Antony, S., Johnson, A. A., Amin, R., Roller, P., Kvaratskhelia, M., and Pommier, Y. (2006) Covalent binding of the natural antimicrobial peptide indolicidin to DNA abasic sites, *Nucleic Acids Res 34*, 5157-5165.

102. Qiao, Z., Udeochu, U., Jimerson, T., Fletcher, M., Bakare, O., and Hosten, C. M. (2006) Detection of benzopyrene-deoxyguanosine adducts by matrix-assisted laser desorption/ionization time-of-flight mass spectrometry, *Rapid Commun Mass Spectrom 20*, 487-492.

103. Tretyakova, N., Matter, B., Ogdie, A., Wishnok, J. S., and Tannenbaum, S. R. (2001) Locating nucleobase lesions within DNA sequences by MALDI-TOF mass spectral analysis of exonuclease ladders, *Chem Res Toxicol 14*, 1058-1070.

104. Park, S., Seetharaman, M., Ogdie, A., Ferguson, D., and Tretyakova, N. (2003) 3'-Exonuclease resistance of DNA oligodeoxynucleotides containing O6-[4-oxo-4-(3-pyridyl)butyl]guanine, *Nucleic Acids Res 31*, 1984-1994.

105. Yang, X., Wu, H., Kobayashi, T., Solaro, R. J., and van Breemen, R. B. (2004) Enhanced ionization of phosphorylated peptides during MALDI TOF mass spectrometry, *Anal Chem 76*, 1532-1536.

106. Zhang, Z., Zhou, L., Zhao, S., Deng, H., and Deng, Q. (2006) 3-Hydroxycoumarin as a new matrix for matrix-assisted laser desorption/ionization time-of-flight mass spectrometry of DNA, *Journal of the American Society for Mass Spectrometry 17*, 1665-1668.

107. Shahgholi, M., Garcia, B. A., Chiu, N. H., Heaney, P. J., and Tang, K. (2001) Sugar additives for MALDI matrices improve signal allowing the smallest nucleotide change (A:T) in a DNA sequence to be resolved, *Nucleic Acids Res 29*, E91.

108. Schuerenberg, M., Luebbert, C., Eickhoff, H., Kalkum, M., Lehrach, H., and Nordhoff, E. (2000) Prestructured MALDI-MS sample supports, *Anal Chem 72*, 3436-3442.

109. Yuan, X., and Desiderio, D. M. (2002) Protein identification with Teflon as matrix-assisted laser desorption/ionization sample support, *J Mass Spectrom 37*, 512-524.

110. Hung, K. C., Ding, H., and Guo, B. (1999) Use of poly(tetrafluoroethylene)s as a sample support for the MALDI-TOF analysis of DNA and proteins, *Anal Chem 71*, 518-521.

111. Hung, K. C., Rashidzadeh, H., Wang, Y., and Guo, B. (1998) Use of paraffin wax film in MALDI-TOF analysis of DNA, *Anal Chem 70*, 3088-3093.

112. Tannu, N. S., Wu, J., Rao, V. K., Gadgil, H. S., Pabst, M. J., Gerling, I. C., and Raghow, R. (2004) Paraffin-wax-coated plates as matrix-assisted laser desorption/ionization sample support for high-throughput identification of proteins by peptide mass fingerprinting, *Anal Biochem 327*, 222-232.

113. Wood, R. W. (1902) On a remarkable case of uneven distribution of light in a diffraction grating spectrum, *Philos Mag 4*, 396-402.

114. Wood, R. W. (1912) Diffraction gratings with controlled groove form and abnormal distribution of intensity, *Philos Mag 23*, 310-317.

115. Fano, U. (1936) Some Theoretical Considerations on Anomalous Diffraction Gratings, *Phys Rev 50*, 573.

116. Fano, U. (1941) The Theory of Anomalous Diffraction Gratings and of Quasi-Stationary Waves on Metallic Surfaces (Sommerfeld's Waves), *J Opt Soc Am 31*, 213-222.

117. Rayleigh, L. (1907) Note on the remarkable case of diffraction spectra described by Prof. Wood, *Philos Mag 14*, 60-65.

118. Kretschmann, E., and Reather, H. (1968) Radiative decay of non-radiative surface plasmons excited by light, *Z Naturforsch, Teil A 23*, 2135-2136.

119. Otto, A. (1968) Excitation of nonradiative surface plasma waves in silver by the method of frustrated total reflection, *Phys 216*, 398-410.

120. Leidberg, B., Nylander, C., and Lundstrom, I. (1983) Surface plasmon resonance for gas detection and biosensing, *Sens Actuators 4*, 299-304.

121. Schasfoort, R. B. M., and Tudos, A. J. (2008) *Handbook of surface plasmon resonance*, Royal Society of Chemistry, Cambridge.

122. Cantor, C. R., Warshaw, M. M., and Shapiro, H. (1970) Oligonucleotide interactions. 3. Circular dichroism studies of the conformation of deoxyoligonucleotides, *Biopolymers 9*, 1059-1077.

123. Mao, B., Margulis, L. A., Li, B., Ibanez, V., Lee, H., Harvey, R. G., and Geacintov, N. E. (1992) Direct synthesis and identification of benzo[a]pyrene diol epoxide-deoxyguanosine binding sites in modified oligodeoxynucleotides, *Chem Res Toxicol 5*, 773-778.

124. Arghavani, M. B., SantaLucia, J., Jr., and Romano, L. J. (1998) Effect of mismatched complementary strands and 5'-change in sequence context on the thermodynamics and structure of benzo[a]pyrene-modified oligonucleotides, *Biochemistry 37*, 8575-8583.

125. Rothwell, P. J., and Waksman, G. (2007) A pre-equilibrium before nucleotide binding limits fingers subdomain closure by Klentaq1, *J Biol Chem 282*, 28884-28892.

126. Bailey, M. F., Van der Schans, E. J., and Millar, D. P. (2007) Dimerization of the Klenow fragment of Escherichia coli DNA polymerase I is linked to its mode of DNA binding, *Biochemistry 46*, 8085-8099.

127. Joyce, C. M. (1989) How DNA travels between the separate polymerase and 3'-5'-exonuclease sites of DNA polymerase I (Klenow fragment), *J Biol Chem 264*, 10858-10866.

128. Kunkel, T. A., and Bebenek, K. (2000) DNA replication fidelity, *Annu Rev Biochem 69*, 497-529.

129. Kozack, R., Seo, K. Y., Jelinsky, S. A., and Loechler, E. L. (2000) Toward an understanding of the role of DNA adduct conformation in defining mutagenic mechanism based on studies of the major adduct (formed at N(2)-dG) of the potent environmental carcinogen, benzo[a]pyrene, *Mutat Res 450*, 41-59.

130. Lipinski, L. J., Ross, H. L., Zajc, B., Sayer, J. M., Jerina, D. M., and Dipple, A. (1998) Effect of single benzo[a]pyrene diol epoxide-deoxyguanosine adducts on the action of DNA polymerases in vitro, *Int J Oncol 13*, 269-273.

131. Zhang, Y., Yuan, F., Wu, X., Rechkoblit, O., Taylor, J. S., Geacintov, N. E., and Wang, Z. (2000) Error-prone lesion bypass by human DNA polymerase eta, *Nucleic Acids Res 28*, 4717-4724.

132. Seo, K. Y., Nagalingam, A., Miri, S., Yin, J., Chandani, S., Kolbanovskiy, A., Shastry, A., and Loechler, E. L. (2006) Mirror image stereoisomers of the major benzo[a]pyrene N2-dG adduct are bypassed by different lesion-bypass DNA polymerases in E. coli, *DNA Repair (Amst) 5*, 515-522.

133. Dong, H., Bonala, R. R., Suzuki, N., Johnson, F., Grollman, A. P., and Shibutani, S. (2004) Mutagenic potential of benzo[a]pyrene-derived DNA adducts positioned in codon 273 of the human P53 gene, *Biochemistry 43*, 15922-15928.

ABSTRACT

NEW INSIGHTS INTO THE MECHANISM OF DNA REPLICATION ON UNMODIFIED AND BENZO[A]PYRENE MODIFIED TEMPLATES USING SURFACE PLASMON RESONANCE

by

RICHARD G. FEDERLEY

May 2011

Advisor: Dr. Louis J. Romano

Major: Chemistry (Biochemistry)

Degree: Doctor of Philosophy

DNA polymerase has had a great deal of time to evolve efficient strategies to perform synthesis. Critical to this process is the selection of a correctly base pairing dNTP to become incorporated into the primer strand. A variety of effects are induced by the identity of the incoming dNTP and its ability to effectively base pair with the templating base. The presence of the next correct dNTP is known to induce a conformational change of the polymerase and lead to an increase in KF-DNA binding. Conversely, the presence of an incorrect dNTP is shown to lead to a destabilization and reduction in the levels of KF-DNA complexes formed. Using surface plasmon resonance and an assay that directly examines the impact of the identity of the incoming dNTP on formation of KF-DNA complexes, we present evidence for the formation of a destabilized complex in the presence of incorrectly pairing dNTPs. We present and discuss the implications of a new model for DNA synthesis that involves a dNTP selection cycle. This selection cycle shows how polymerases aid in the removal of

mispairing dNTPs from their active sites in an effort to seek a correctly pairing template-dNTP for catalysis. Polymerases have evolved to utilize efficiently this method of dNTP selection to speed up dNTP selection.

Bulky DNA adducts such as benzo[a]pyrene interfere with replication by forming structures within the polymerase that preclude the productive binding of dNTPs, and/or inhibiting the conformational change. Surface plasmon resonance was used to study the effect various dNTPs have upon Klenow fragment binding to several (-)-*trans*-anti-B[a]P-N^2-dG adducted primer-templates. Dissociation constants were determined for Klenow fragment binding to primer templates containing either a correctly paired C:G-B[a]P, mismatched T:G-B[a]P, or mismatched G:G-B[a]P positioned at the -1 position, in the presence and absence of various dNTPs and rNTPs. The presence of the (-)-*trans*-*anti*-B[a]P-N^2-dG adduct interferes with the formation of a stable closed ternary complex. Moreover, the addition of any dNTP favoured formation of a destabilized ternary complex that rapidly dissociates to free polymerase and DNA. In addition, Klenow fragment shows tighter binding to a mismatched G:G-B[a]P adducted primer-template than either a correctly base paired C:G-B[a]P or mismatched T:G-B[a]P primer template. The G:G-B[a]P structure was also inhibited from forming the closed ternary complex, yet dissociation rates from this complex were slower than for the correctly base paired C:G-B[a]P or mismatched T:G-B[a]P primer template. This result indicates that the conformation adopted by the G:G-B[a]P within the active site of the polymerase is unique to this structure.

AUTOBIOGRAPHICAL STATEMENT

Richard G. Federley

Education

Ph. D. in Biochemistry 2004-2011
Wayne State University, Detroit MI
Distributed minor in Analytical, Organic and Biophysical Chemistry
Advisor: Dr. Louis J. Romano
Dissertation Title: "*New Insights Into the Mechanism of DNA Replication On Unmodified and Benzo[a]pyrene Modified Templates Using Surface Plasmon Resonance*"

B.S. in Biology 2000-2004
Lake Superior State University, Sault Ste. Marie MI
Minor in Chemistry
Advisor: Dr. R. Marshall Werner
Thesis Title: "*Assay Development and Large Scale Purification of Thiaminase*"

Awards

Graduate School Citation for Excellence in Teaching May, 2006
- Wayne State University, Detroit MI

Undergraduate Research Grant May, 2002
- Lake Superior State University, Sault Ste. Marie MI

Board of Trustees Ontario Academic Scholarship May, 2000
- Lake Superior State University, Sault Ste. Marie MI

Papers and Publications

Federley, R. G.; Romano, L. J., "DNA Polymerase: Structural Homology, Conformational Dynamics, and the Effects of Carcinogenic DNA Adducts", *Journal of Nucleic Acids*, vol. 2010, 2010.

O'Toole, M.; Federley, R. G.; Werner, M., "Thiaminase: Progress Toward a Novel Fluorescent Microplate Assay", *Biochemistry*, 2002.

Federley, R. G.; Romano, L. J., "DNA Polymerase Actively Rejects Mispairing dNTPs during DNA Synthesis: Evidence for a New Cycle in the DNA Polymerase Mechanism", *Manuscript finished*

Federley, R. G.; Romano, L. J., "A (-)-Trans Benzo[a]pyrene Labelled Guanine-Guanine Mismatch at the Primer Terminus Forms a Distinct Complex when bound to Klenow Fragment", *Manuscript finished*

Acknowledgements

Salim, N.N.; Feig, A.L., "An Upstream Hfq Binding Site in the fhlA mRNA Leader Region Facilitates the OxyS-fhlA Interaction". *PLoS ONE*, 2010.